



# Kent Academic Repository

**Barber, Jack (2019) *Growth, assembly and fragmentation mechanisms in the molecular life cycle of Sup35NM prion and alpha-synuclein amyloid particles*. Master of Research (MRes) thesis, University of Kent,.**

## Downloaded from

<https://kar.kent.ac.uk/79539/> The University of Kent's Academic Repository KAR

## The version of record is available from

## This document version

Other

## DOI for this version

## Licence for this version

UNSPECIFIED

## Additional information

## Versions of research works

### Versions of Record

If this version is the version of record, it is the same as the published version available on the publisher's web site. Cite as the published version.

### Author Accepted Manuscripts

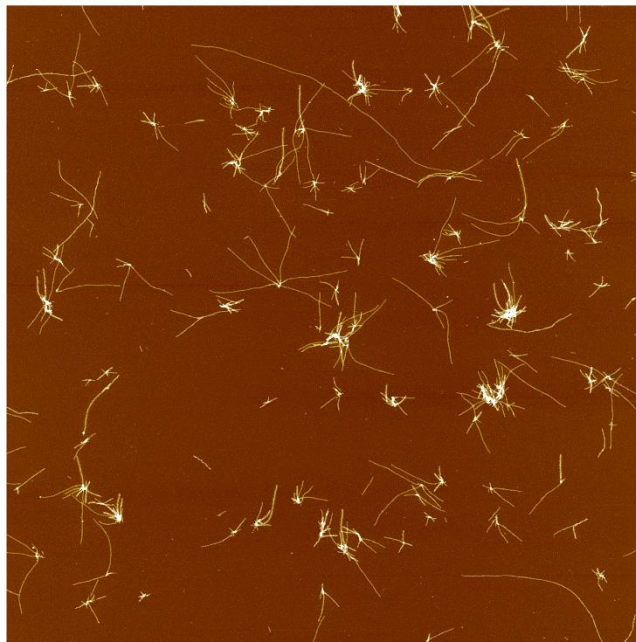
If this document is identified as the Author Accepted Manuscript it is the version after peer review but before type setting, copy editing or publisher branding. Cite as Surname, Initial. (Year) 'Title of article'. To be published in *Title of Journal*, Volume and issue numbers [peer-reviewed accepted version]. Available at: DOI or URL (Accessed: date).

## Enquiries

If you have questions about this document contact [ResearchSupport@kent.ac.uk](mailto:ResearchSupport@kent.ac.uk). Please include the URL of the record in KAR. If you believe that your, or a third party's rights have been compromised through this document please see our [Take Down policy](https://www.kent.ac.uk/guides/kar-the-kent-academic-repository#policies) (available from <https://www.kent.ac.uk/guides/kar-the-kent-academic-repository#policies>).

Growth, Assembly and Fragmentation  
Mechanisms in the Molecular Life cycle of  
Sup35NM Prion and  $\alpha$ -Synuclein Amyloid  
Particles

Jack Barber



University of  
**Kent**

## Declaration

No part of this thesis has been submitted in support of any other application for a degree or qualification of the University of Kent or any other University or institution of learning.

Jack Barber

August 2019

## Acknowledgements

Firstly, I would like to thank my supervisor Dr Wei-Feng Xue for the opportunity of this research project and his assistance over the last year. Thanks must also go to all members of the Kent Fungal Group who have supported me constantly throughout my time working with them. This is especially true for Tracey Purton, Liisa Lutter, Liam Aubrey and Dave Beal, who have made me very welcome in the WFX lab.

Lastly, I would like to thank my friends and family for their continued support that made this possible.

## Table of Contents

Declaration.....	2
Acknowledgements.....	3
Table of Contents.....	4
Abbreviations.....	7
Abstract.....	8
1. Introduction.....	10
1.1 Amyloid Overview.....	10
1.1.1 Definition of Amyloid.....	10
1.1.2 Amyloid structure.....	11
1.1.3 Structural polymorphisms.....	13
1.1.4 Definition of Prions.....	14
1.1.5 Functional amyloid.....	15
1.1.6 The amyloid life cycle.....	16
1.1.7 Transmissibility.....	18
1.2 Species, processes and kinetics of the amyloid life cycle.....	20
1.2.1 Amyloid species.....	20
1.2.2 Amyloid growth and kinetics.....	22
1.3 Amyloid in Biology.....	24
1.3.1 Disease association.....	24
1.3.2 Functional amyloid.....	25
1.4 The main processes of the amyloid life cycle.....	26
1.4.1 Overview.....	26
1.4.2 Primary processes.....	27
1.4.3 Secondary processes.....	28
1.5 Experimental and modelling approaches to characterise the amyloid life cycle.....	29
1.5.1 Overview.....	29
1.5.2 Thioflavin T and Congo red staining.....	30
1.5.3 Visualising amyloid.....	31
1.6 Model systems for studying amyloid and prions.....	33
1.6.1 Sup35.....	33
1.6.2 $\alpha$ -synuclein.....	34
1.7 Concluding remarks: Questions and challenges.....	35

2. Materials and Methods.....	37
2.1 Materials .....	37
2.1.1 Lysogeny Broth Media .....	37
2.1.2 Sup35NM Protein Purification Buffer Composition.....	38
2.1.3 Sup35NM AKTA Buffer Composition.....	39
2.1.4 Sup35NM Fibril Formation Buffer .....	40
2.1.5 $\alpha$ -synuclein Protein Purification Buffer Composition .....	41
2.1.6 $\alpha$ -synuclein AKTA Buffer Composition .....	41
2.1.7 $\alpha$ -synuclein Fibril Formation Buffer .....	42
2.1.8 Sup35NM C-terminal Hexa-His <i>E. coli</i> strain .....	43
2.1.9 $\alpha$ -synuclein <i>E. coli</i> strain .....	44
2.2 Protein expression .....	44
2.2.1 Sup35NM C terminal hexa-His expression.....	44
2.2.2 $\alpha$ -synuclein expression.....	45
2.3 Protein purification .....	46
2.3.1 Sup35NM C terminal hexa-His purification .....	46
2.3.2 $\alpha$ -synuclein purification .....	47
2.4 Thioflavin T assays.....	48
2.4.1 Sup35NM well and assay preparation .....	48
2.4.2 Sup35NM ThT kinetic assay .....	50
2.4.3 $\alpha$ -synuclein well and assay preparation.....	51
2.4.4 $\alpha$ -synuclein ThT kinetic assay.....	53
2.4.5 Thioflavin T analysis .....	54
2.5 Seed generation .....	54
2.5.1 Sup35NM seed generation .....	54
2.5.2 $\alpha$ -synuclein seed generation.....	55
2.6 Seeded Thioflavin T assays.....	55
2.6.1 Sup35NM seeded growth assays .....	55
2.6.2 $\alpha$ -synuclein seeded growth assays.....	56
2.7 Time-dependent growth assays.....	56
2.7.1 Sup35NM time-dependent growth imaging assay .....	56
2.7.2 $\alpha$ -synuclein time-dependent growth imaging assay.....	57
2.8 Atomic force microscopy imaging.....	58
2.8.1 Mica disk preparation .....	58
2.8.2 Sup35NM sample preparation.....	59
2.8.3 $\alpha$ -synuclein sample preparation .....	59

2.8.4 AFM imaging .....	59
2.8.5 AFM image analysis.....	60
3. Results .....	61
3.1 Sup35NM C terminal Hexa-His tag.....	61
3.1.1 Protein expression and purification .....	61
3.1.2 <i>De novo</i> fibril formation .....	63
3.1.3 Fragmentation and quantifiable seed production .....	66
3.1.4 Use of seeding to explore elongation .....	69
3.1.5 Time-dependent imaging assay .....	76
3.2 $\alpha$ -synuclein .....	78
3.2.1 Protein expression and purification .....	78
3.2.2 <i>De novo</i> fibril formation .....	81
3.2.3 Fragmentation and quantifiable seed production .....	83
3.2.4 Seeded assay .....	84
3.2.5 Time-dependent imaging assay .....	86
3.3 Fibril morphology .....	88
3.3.1 Fibril width .....	88
3.3.2 Morphology observations .....	89
4. Discussion.....	91
4.1 <i>De novo</i> growth.....	91
4.2 Seeded growth .....	92
4.3 Fragmentation and stability .....	94
4.4 Elongation and growth.....	95
4.5 Morphology.....	97
5. Conclusions and Further research .....	100
6. References .....	105
7. Appendices.....	115

## Abbreviations

<b>αFFB</b>	α-synuclein Fibril Formation Buffer
<b>AFM</b>	Atomic Force Microscopy
<b>BSE</b>	Bovine Spongiform Encephalopathy
<b>CJD</b>	Creutzfeldt Jakob Disease
<b>E</b>	Elongation Assay
<b>E &amp; F</b>	Elongation & Fragmentation Combined Assay
<b>Gx</b>	Generation x, fibrils or seeds
<b>HET-s</b>	Heterokaryon Incompatibility Protein S
<b>LB</b>	Lysogeny Broth
<b>MLB</b>	Melki Lysis Buffer
<b>MLBG</b>	Melki Lysis Buffer Denaturing, G=guanidine
<b>MLBGE</b>	Melki Lysis Buffer Elution
<b>NCC</b>	Nucleated Conformational Conversion Model
<b>NP</b>	Nucleated Polymerisation Model
<b>PrP<sup>C</sup></b>	Cellular Prion Protein
<b>PrP<sup>Sc</sup></b>	Scrapie Prion Protein
<b>SFFB</b>	Sup35NM Fibril Formation Buffer
<b>SIM</b>	Structured Illumination
<b>STED</b>	Stimulated Emission Depletion
<b>TEM</b>	Transmission Electron Microscopy
<b>ThT</b>	Thioflavin T
<b>TSEs</b>	Transmissible Spongiform Encephalopathies



## Abstract

With devastating diseases like Alzheimer's disease and Parkinson's disease rising in numbers, amyloid and prion research is steadily increasing. However, there are many questions that have yet to be answered. One such question is how their life cycle relates to their transmissibility and hence nature of being an amyloid or prion, as well as how it relates to their disease association or beneficial functionality.

Through the use of ThT fluorescence curves and atomic force microscopy (AFM) imaging, this study compared the elongation and fragmentation rates in the life cycle of Sup35NM, a functional prion, to  $\alpha$ -synuclein, a prion-like amyloid associated with Parkinson's disease. Using sonication at a reduced amplitude as a method of mechanical perturbation, it was determined that fibrils formed by Sup35NM have a significantly lower stability to these conditions than those formed by  $\alpha$ -synuclein. Seeds produced during the fragmentation assays were then used to explore the initial rates of elongation. This allowed a striking difference in elongation rates to be imaged through the use of AFM, where Sup35NM fibrils elongated at an increased rate relative to  $\alpha$ -synuclein.

The increased stability and reduced elongation rate of  $\alpha$ -synuclein fibrils would suggest a slow growth of aggregated material and a reduced ability to fragment which would lower the ability to be transferred between cells of an individual. This would be biologically beneficial as would lower the spread and impact of any associated disease and hence could be the product of a biological drive to favour  $\alpha$ -synuclein to form fibrils that have these properties.

Sup35NM behaves in the reverse, with a low stability and high elongation rate. These would allow a large number of small seeds to be produced rapidly, which would facilitate the spread of aggregates between individual yeast cells and speed up their growth once they enter the cell. As a functional prion, these properties are desirable as would allow the rapid activation of their associated phenotype within an individual as well as its neighbours. This again could suggest that as these properties would be favoured they would be selected for.

## 1. Introduction

### 1.1 Amyloid Overview

#### 1.1.1 Definition of Amyloid

Due to their association with diseases, amyloid and prions have become the subject of a large amount of research that has grown over the past few decades. Amyloid have been associated with the devastating age-related Alzheimer's and Parkinson's diseases in particular (Irvine et al., 2008). While amyloid are suggested to have been first observed in 1639, they were not named until 1854 by Rudolf Virchow (Sipe and Cohen, 2000). The definition of amyloid has varied since and the definition proposed by the Nomenclature Committee of the International Society of Amyloidosis is a protein deposited as insoluble fibrils (Fig 1.1A). These fibrils bind Congo red and exhibit green birefringence when viewed by polarization microscopy and their sequence must have been unambiguously characterised by protein sequence analysis (Sipe et al., 2012). The modern biophysical definition is an unbranched protein fibril with repeating  $\beta$  strands running perpendicular to the axis of the fibril (Fig 1.1B), forming a cross- $\beta$  sheet (Greenwald and Riek, 2010; Westermark, 2005). This conformation can be shown by x-ray diffraction as will produce a distinctive cross- $\beta$  diffraction pattern, an example of which can be seen in Fig 1.1.C. This definition by structure has become the primarily used definition since its creation in the 1970s. It has also been suggested through *in vitro* studies using various proteins, including myoglobin and homopolymers, that forming an amyloid structure is a generic feature of all polypeptide chains (Dobson, 2003).

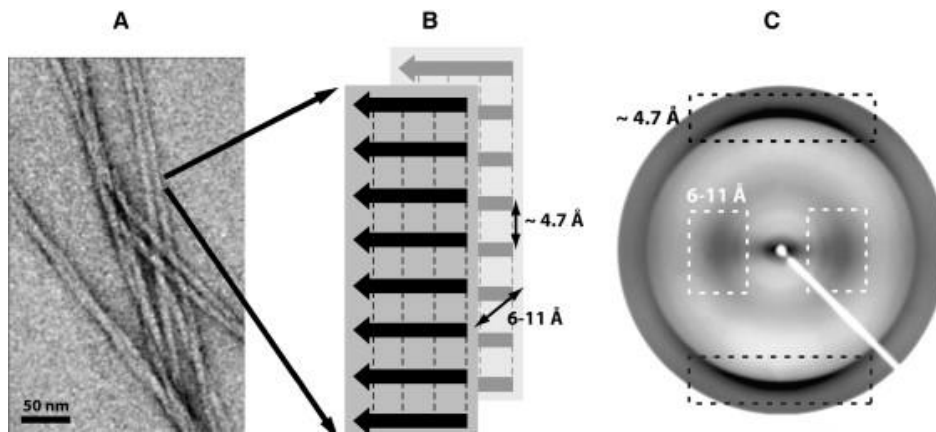


**Figure 1.1- Amyloid fibril structures.** (A) Image of mature amyloid fibrils viewed using electron microscopy. Amyloid aggregates form long thread-like fibrils as they elongate and mature. (B) Cross- $\beta$  sheet diagram showing the structure of multiple polypeptide chains (arrows) forming protofilaments with an  $\sim 4.7$  Å distance between the polypeptides. These protofilaments align and interact to form an amyloid fibril, where there is a 6-11 Å distance between the protofilaments. (C) Typical X-ray diffraction pattern for an amyloid fibril. The horizontal reflection at 6-11 Å corresponds to the interaction between the protofilaments and the vertical reflection at  $\sim 4.7$  Å corresponds to the interactions between the individual polypeptides within a protofilament. All images from Greenwald and Riek 2010.

### 1.1.2 Amyloid structure

The cross- $\beta$  sheet was first described by Astbury (1935) who suggested two intermolecular  $\beta$ -sheets with the strands of the sheets perpendicular to the fibril axis and the sheets running parallel to it. The characteristic cross- $\beta$  diffraction pattern has a strong reflection at 4.7 Å positioned parallel to the fibril axis and another of 6 to 11 Å positioned perpendicular to the fibril axis (Eisenberg and Jucker, 2012). When proteins have their amide N-H and C=O groups exposed, they can couple to form hydrogen bonds with other peptides that are “in register”, which is where the same regions of the peptides align, forming a  $\beta$ -sheet. This is the amyloid core which produces the 4.7 Å interaction as well as how the amyloid will template new

polypeptides to misfold into the same conformation, allowing them to aggregate with this growing structure during elongation (Soto, 2012). This  $\beta$ -sheet structure is termed a protofilament and is the most basic unit of the amyloid structure (Greenwald and Riek, 2010). The 6 to 11 Å reflection is produced by the interaction between protofilaments where their side chains will interact, becoming tightly interdigitated, like a zipper. This structure is known as a fibril and consists of varying numbers of protofilaments. The zipper motif (Fig 1.2) allows strong van der Waal interactions to occur between the side chains of adjacent protofilaments (Nelson et al., 2005). Hence this is known as the steric zipper model (Sawaya et al., 2007; Eisenberg and Jucker, 2012). Between both the sheets and the strands, water is excluded. Hereby creating a “dry interface” and maximising interactions between the peptides, especially the hydrogen bonding between the peptides within a protofilament. These strong interactions are in part why amyloid fibrils are very strong and stable structures that have a lower free energy than their associated globular forms (Nelson et al., 2005).

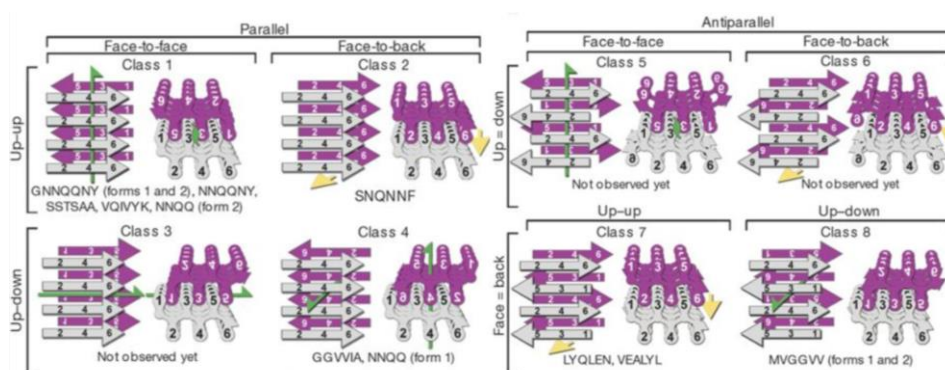


**Figure 1.2- The 8 proposed classes of steric zippers.** The classes are separated by the orientation of the faces, orientation of the strands and if they are parallel or antiparallel. The green arrows show two-fold screw axes and yellow arrows show translational symmetry. The amino acids below each diagram show protein segments that are listed to belong to that class. Image from Sawaya et al., 2007.

### 1.1.3 Structural polymorphisms

Amyloid structures can have various structural polymorphisms. These are local energy minima in the folds and assembly energy landscape, which may be sensitive to the environment, leading to various forms existing at the same time.

The first type of polymorphism is sequence polymorphism, which is when the amino acid sequence of the peptide changes, possibly caused by a change at the genetic level. This change in amino acids in the amyloid core will lead to changes in the other types of polymorphism. The remaining types of polymorphism can be classified under the grouping of assembly polymorphisms, resulting from assembly of precursors with identical sequences. Within assembly polymorphism, there are filament polymorphisms and the subclass of core polymorphisms, containing packing and segmental polymorphisms. Filament polymorphisms are where there are differences in the arrangement of protofilaments within a fibril and how they interact with each other. Core polymorphisms relate to differences in the amyloid core itself. Segmental polymorphisms arise from different sections of the polypeptide being used in the assembly of the amyloid core of the protofilaments. Packing polymorphisms are where the same section forms the amyloid core but are packed differently from each other (Lutter et al., 2019). For example, if the peptides of a protofilament follow the same direction (e.g. N to C and N to C), they will be parallel strands, but if they follow the opposite direction to the next strand (e.g. N to C and C and N), then they are anti-parallel strands. While the different types of polymorphism can be thought of as separate, they will interact with each other leading to other types to some degree. An example of this is that sequence polymorphisms can lead to alterations in the

assembly of the protofilament producing assembly polymorphisms which can then affect the overall filament, meaning filament polymorphisms are partially a culmination of the others (Greenwald and Riek, 2010). The variations in the fibrils caused by these polymorphisms mean amyloid fibrils of differing properties can be formed from a single protein.

#### 1.1.4 Definition of Prions

Prions like amyloid also have association with disease states, such as scrapie, kuru and Creutzfeldt Jakob disease, leading to them having biological and medical importance. Similar to amyloid, the definition of a prion has varied overtime, causing various definitions to still be in use alongside each other. The term prion was originally suggested by Prusiner (1982) to name “a small proteinaceous infectious particle which is resistant to inactivation by most procedures that modify nucleic acids”. Taking prions by this definition, it is suggested that any protein that can cause infection by itself would be a prion. A more modern definition is that prions are a subclass of amyloid in which the aggregation process has become self-perpetuating and infectious (Sabate, 2014). Prions are known to use a similar method as amyloid to template folding of the peptide into the prion protein form. For example PrP<sup>Sc</sup> (Scrapie prion protein) templates conversion of PrP<sup>C</sup> (cellular prion protein) into the PrP<sup>Sc</sup> form (Prusiner, 1998). Prions are suggested to fulfil all of Koch’s postulates for infectious agents, even given the differences with other known infectious agents (Soto, 2012). A key part of the amyloid and prion life cycle, known as fragmentation, is where amyloid will fragment and generate smaller oligomeric particles that can

template proteins and elongate into new aggregates. This mechanism is core to a prion's ability to be transmissible and infect other individuals. The definition used in this study will therefore be: a rarely spontaneously formed, self-propagating protein conformation that must replicate via templating themselves onto their non-prion form proteins and finally that they must spread to new hosts to find new substrate pools (Caughey et al., 2009).

#### 1.1.5 Functional amyloid

While Alzheimer's and Parkinson's diseases have been both previously mentioned, they are just a couple of the many possible biological consequences of amyloid formations. Since their discovery, traditionally amyloid have been associated with diseases such as the aforementioned. In recent years however, several functional amyloid that are part of normal cellular biology have been discovered. These include Curli in *Escherichia coli* which play an integral role in biofilm formation (Shewmaker et al., 2009).

There have also been studies suggesting the possibility that the formation of amyloid fibrils in neurodegenerative diseases is actually used to sequester more toxic oligomeric species (Silveira et al., 2005; Caughey and Lansbury, 2003; Balch et al., 2008). While they will have been optimised through evolution to gain an increased ability to aggregate in comparison to disease associated amyloid (Fowler et al., 2005), functional amyloid can still form different structural polymorphisms (Hu et al., 2011).



### 1.1.6 The amyloid life cycle

Amyloid and prions follow a 'life cycle' that explains their *de novo* formation and growth. A summary of this can be seen in Fig 1.3. There are four stages to the cycle, with the first being conversion. This is where the polypeptide will reversibly convert into a conformation that would allow it to template a region of this structure that will become the amyloid core. Once other peptides aggregate with this, they will become more stable and form primary nuclei. The second stage of the life cycle, elongation, can then begin and is the stage the majority of the aggregated material is produced. The amyloid core will template more peptides into the  $\beta$ -sheet structure allowing the corresponding protofilament to grow in length. These will interact to form a fibril, which will continue to grow from its exposed ends. These exposed ends are of high importance as these are where elongation, and hence most of the aggregation, will occur. Therefore, increasing the number of these will allow the rate of growth to increase significantly.

The third stage of the life cycle addresses this via two main routes, secondary nucleation and fragmentation. Secondary nucleation does not occur in all amyloid and involves the templating of nuclei off the side of existing fibrils, leading to apparent "branching". Fragmentation on the other hand is where fibrils break down into smaller species via various methods, such as mechanical perturbation or via assistance from chaperones. Due to these smaller species having exposed ends they become able to undergo elongation. This increase in number of exposed ends allows an increased growth of total amyloid aggregates, but the size reduction is also important for prions and prion-like amyloids as it allows propagation, a stage

characteristic to their life cycle, to occur. Propagation is where the species use their small size to aid in transferring into a new cell, prions and prion-like, or potentially a new individual, prions only. This is core to the prion characteristic of transmissibility. The processes of fragmentation and secondary nucleation are important to accelerating the growth of total amyloid content and lead to its exponential growth phase (Marchante et al., 2017; Hofmann and Vorberg, 2013).

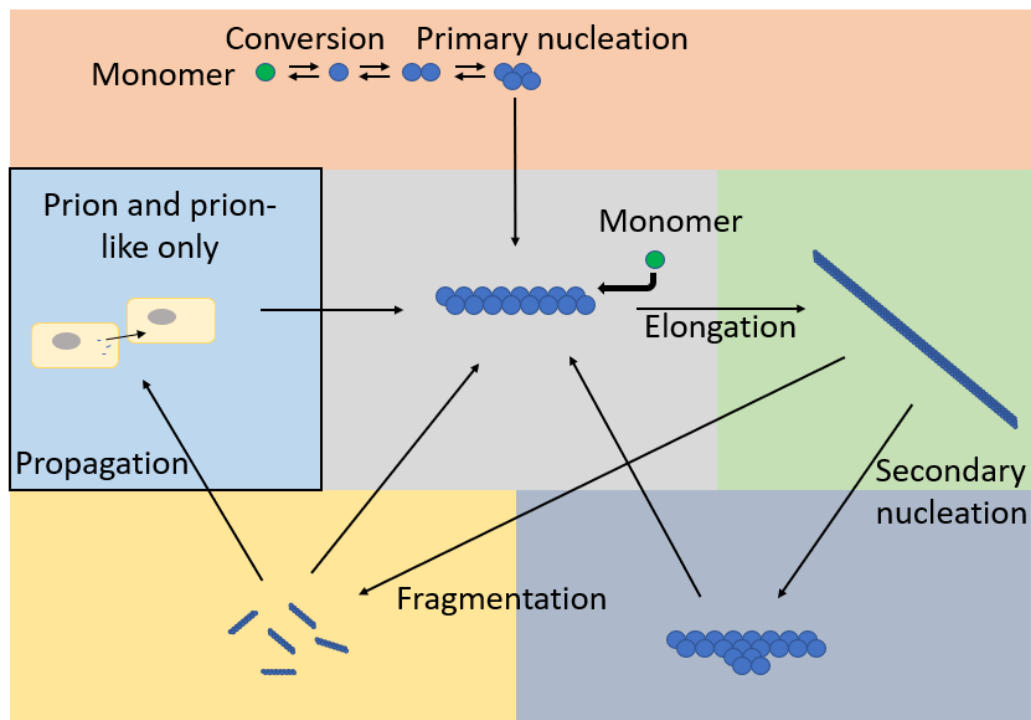


**Figure 1.3- Overview of the life cycle of prions and amyloid following the nucleation polymerisation model.** There are three stages to the amyloid life cycle: conversion, elongation and secondary nuclei formation. The primary processes of conversion and elongation lead to the de novo formation of an amyloid fibril. The secondary processes of fragmentation and secondary nucleation form secondary nuclei allowing the growth rate to become exponential. Prions and prion-like amyloids have an additional fourth stage of propagation occurring after fragmentation, where the smaller species formed can transfer between cells and in the case of prions are even able to transfer between organisms.

### 1.1.7 Transmissibility

The subject of transmissibility is an important one in relation to amyloid and prions, especially to do with their associated diseases. Completely non-transmissible amyloid would only be able to build up fibrils inside their host cell, while completely transmissible prions would have the ability to infect not just other nearby cells, but even new individuals they come into contact with. Research in recent years into neurodegenerative diseases, such as Alzheimer's, has suggested that transmissibility is not as straightforward as this. Amyloid-like proteins have been suggested to be able to spread between cells of a brain tissue and lead to the disease state in those cells (Sabate, 2014; Jaunmuktane et al., 2015). This suggests the possibility that while not all amyloid are prions, they can still possess a certain level of transmissibility. This makes transmissibility a sliding scale with non-transmissible amyloid at one end and prions at the other. Those amyloid that have some of the traits of prions, but still differ, would be in the middle of amyloid and prions and are suggested to be prion-like (Caughey et al., 2009). For example, they could only be capable of being transferred between neighbouring cells while prions in the strictest sense could even be transferred between individuals, such as ingestion or by access to wounds. This leaves the important question of what causes the differences in transmissibility between non-transmissible amyloid, prions and prion-like? The first point required to answer this question is what allows an aggregate particle to be transmissible. It has been suggested that the property that allows a particle to be transmissible is the size distribution of the particles formed, with there being an upper threshold that will prevent particles being transmissible (Derdowski et al., 2010). An example of such a threshold for Sup35NM is suggested to be a particle length of 200nm, where

particles smaller than this length can propagate into cells and those larger cannot (Marchante et al., 2017).

Accurate prediction of prions in comparison to amyloid is highly elusive, due to only a small number of amyloid being *bona fide* prions despite their significant overlap in conformational properties as well as the fact the sequence features that confer it are unknown. As yeast prions are the best characterised, their features have been analysed to find possible clues to this. Large domains that are unstructured in the native protein form have a high glutamine/asparagine (Q/N) content, which is suggested to be used to drive amyloid formation by becoming the amyloid core (Fernández et al., 2017). Further research has suggested requirements that must be met by a polypeptide sequence to form one of these Q/N prions. Firstly, an amyloid prone region must be able to form the amyloid core in a specific sequence dependent manner that leads to a high rate of aggregation as well as displaying brittleness to allow a high rate of fragmentation. These properties would allow the creation of a high number of species smaller than the size threshold so are capable of propagating, as well as increasing the number of nucleation events per cell that will occur post transmission. Secondly, the amyloid core needs to be in a structurally disordered section of the protein, allowing for easy conversion to the  $\beta$ -cross structure without a prior requisite of unfolding. This increases the aggregation rate during elongation while potentially increasing brittleness. Also, these intrinsically disordered regions increase the solubility of proteins and potentially have anti-aggregative effects (Graña-Montes et al., 2014), allowing more control over primary nucleation, which is important for the next rule. Thirdly, the amyloid core must possess a sequence that while conferring amyloid character in stress situations, must also allow a soluble form

in normal physiological conditions in order to maintain function as well as to control the prion phenotype (Sabate et al., 2015). One suggestion towards this end has been that the amyloid cores of prions are longer than normal which helps with reducing amyloid forming ability by primary nucleation whilst increasing the ability to form the soluble conformation as well as its brittleness once an amyloid has formed (Fernández et al., 2017). Together these requirements lead to N and Q being important in prion-forming domains due to their features of not only allowing amyloid formation, but they also favour disorder (Sabate et al., 2015).

## 1.2 Species, processes and kinetics of the amyloid life cycle

### 1.2.1 Amyloid species

There are different forms a of protein in relation to amyloid species. The smallest unit is a monomer, i.e. a single peptide that can be in solution in a folded or unfolded form, but can also refer to a single peptide within an aggregate. Aggregates are then defined as assemblies that contain multiple monomers. The main forms of aggregated species are nuclei, protofilaments, fibrils, oligomers and protofibrils. Mature amyloid fibrils are characterised by their cross- $\beta$  sheet structure that produces the typical x-ray diffraction pattern (Fig 1.1C). They are usually long and straight in appearance with a larger width than other species. There are two main models for how amyloid fibrils are formed: nucleated polymerisation (NP) and nucleated conformational conversion (NCC).

Nuclei are the first stage of the nucleated polymerisation model of fibril formation. They are formed by monomers reversibly aggregating into a species that can template its fold onto other monomers to elongate faster than it dissociates back into monomers. They also have the highest associated free energy and are the state that acts as the energy barrier between soluble monomers and amyloid fibrils (Arosio, Knowles and Linse, 2015). Elongation will lead to the formation of a protofilament by the addition of a single monomer to the exposed ends of the structure. A protofilament is a long thin structure consisting of a single layer of peptides where the aligned peptide chains forming the amyloid core interact. In this model multiple protofilaments will interact to form a mature fibril.

Oligomers are difficult to strictly define due to the wide range of aggregates the term is used for as can be used to refer to any small multimeric aggregate species which can include nuclei and can be formed transiently as well as be on pathway or off pathway to fibril formation (Linse, 2019). These species can be formed by primary and secondary nucleation processes and characterised by their antibody specificity as well as increased cytotoxicity (Laganowsky et al., 2012). They are also core to oligomer addition-based fibril formation, which differs from the standard monomer addition based nucleated polymerisation model. In this model multiple oligomers will aggregate into protofibrils which are shorter and thinner than mature fibrils and tend to be curlier. Protofibrils can then extend by the addition of oligomers to their ends and mature into fibrils (Modler et al., 2003).

### 1.2.2 Amyloid growth and kinetics

The *de novo* formation of a nucleus, i.e. primary nucleation, is the spontaneous generation of a nucleus from monomers in an unfavourable and reversible process, during the nucleation phase. This step of slow generation of nuclei is what limits amyloid formation, as further elongation once a nucleus has grown is rapid and will lead to the elongation phase (Wetzel, 2006). This is in part why amyloid fibrils display sigmoidal growth kinetics, leading to a lag phase, growth phase and a stationary phase (Fig 1.4). The lag phase is caused primarily by the aforementioned reversibility of nuclei formation and the duration it lasts is based off the probability of a nuclei forming and starting elongation, which is known as the lag time. During this phase the number of amyloid fibrils will be very low or zero. Once the elongation phase has started for some fibrils, fragmentation and secondary nucleation can occur. Fragmentation is the increase of fibril ends by fibrils fragmenting into smaller fibrils and secondary nucleation is where fibrils can be nucleated off of previously formed fibrils, leading to a new fibril being started. This increase in number of fibrils causes more fibril ends to be available, increasing the possible rate of increase in fibril yield, starting the exponential growth of the growth phase. Once monomer concentrations become limiting this rate will start to slow until all monomers have aggregated. This is the beginning of the stationary phase, where fibril yield will no longer change (Arosio, Knowles and Linse, 2015; Iadanza et al., 2018). The lag phase can alternatively be by-passed through the use of seeding. This is where a preformed amyloid fibril, or seed, is introduced allowing the elongation phase to start (Harper and Lansbury, 1997).

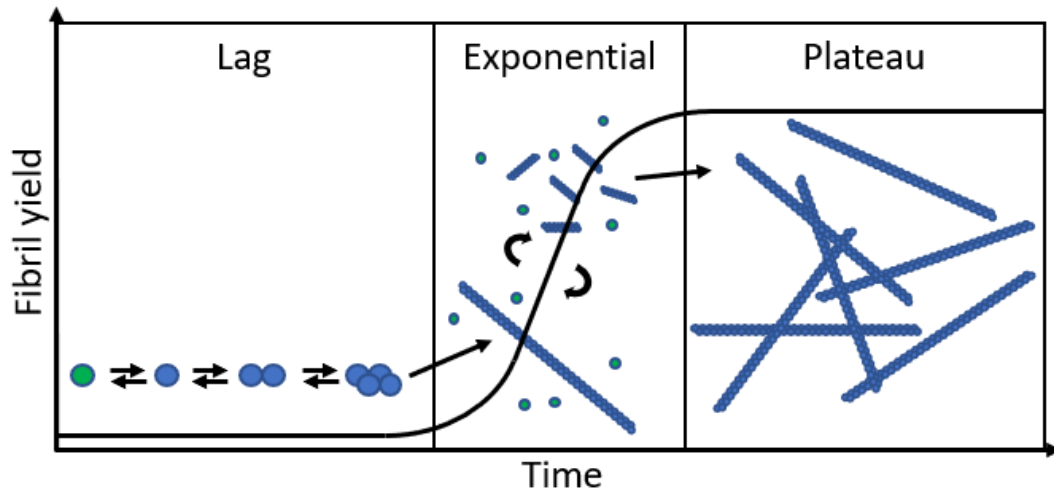


**Figure 1.4- A typical sigmoidal curve of amyloid aggregates produced using Thioflavin T fluorescence intensity.** The corresponding stage of amyloid growth are overlaid. The lag, or nucleation, phase corresponds to the reversible and unfavoured step of proteins folding into an amyloid conformation and then aggregating to form nuclei that will lead to oligomer formation. Once a critical amount of aggregated material has been formed, a cycle dominated by fragmentation and/or secondary nucleation, depending on the system and elongation will begin, increasing the number of fibrils and the yield will grow exponentially. Once the monomer concentrations become rate limiting, the growth will slow to a stop and the plateau phase will begin.

Amyloid fibrils have a lower free energy than their corresponding monomeric proteins making them not just more stable and resistance to losing their structure but also a more condensed form. Under normal physiological conditions, with chaperones working correctly, amyloid states are completely unfavoured relative to the monomeric state. However, under certain conditions, such as monomeric concentration being very high, amyloid aggregation will become more favoured (Nelson et al., 2005). Due to the significant barrier between the monomeric form and the amyloid form it can be presumed that under conditions where this energy barrier



can be crossed the more stable amyloid form can be attained. Due to the lower free energy of amyloid aggregates relative to the monomeric form they would be the thermodynamically favoured form of proteins. This can be one of the possible reasons that amyloid tend to be associated with age related diseases such as Alzheimer's where a longer time has elapsed allowing longer for this equilibration to occur as well as the possibility of abnormal cellular conditions.

### 1.3 Amyloid in Biology

#### 1.3.1 Disease association

Changing the fold of a soluble protein into an insoluble aggregated form does not just cause problems for the cell in the obvious way of the protein losing its function. As cells are cramped environments with a large number of cellular components in a small area, everything needs to fit together well. The size and insolubility of fibrils will therefore cause inappropriate interactions, leading to toxicity and interrupting proteostasis (Bucciantini et al., 2002). The actual amount of aggregated material deposited can also rise to large amounts, possibly kilograms, leading to all manner of issues inside of organs, these issues can include diseases such as Alzheimer's disease, Parkinson's disease and type II diabetes. The cytotoxic potential of an aggregate is suggested to have a negative correlation with fibril length as reduction in length enhances the ability of the aggregate to disrupt membranes, leading to oligomeric species being more toxic than fibrils. This is also in part due to the increased surface to volume ratio leading to the exposure of more hydrophobic side chains. These factors cause fibril fragmentation to raise the toxicity of amyloid aggregates by

reducing the number of relatively inert fibrils and producing a high number of potentially toxic oligomeric species (Xue et al., 2009). A possible reason many of these diseases are age-related is due to the mechanisms that protect us from protein misfolding and aggregation will decay with age as the processes become damaged. The proteins that are associated with neurodegenerative diseases are vulnerable to this as their levels become so high they are “super-saturated”, making aggregation more likely (Dobson, 2017).

Prions are associated with different diseases other than the aforementioned and in mammals cause a series of diseases called transmissible spongiform encephalopathies (TSEs). These include Bovine Spongiform Encephalopathies (BSE), also known as mad cow disease, kuru, Creutzfeldt-Jakob disease (CJD), and scrapie. The TSEs are fatal neurodegenerative diseases that manifest as dementias with varying symptoms, even within syndromes; they occur either sporadically or are also able to be transferred between organisms and in some cases species (Aguzzi, Heikenwalder and Polymeridou, 2007; Hofmann and Vorberg, 2013).

### 1.3.2 Functional amyloid

Historically research was focused on disease-associated amyloid, but in recent years functional amyloid have been discovered, which are now starting to be explored. These functional amyloid aggregates are made intentionally by the cell to fulfil a specific cellular purpose. These range from curli in *E. coli*, HET-s in *Podospora anserina*, Sup35p in *S. cerevisiae* to Pmel17 in humans (Fowler et al., 2007). They have very specific and tight regulation in order to prevent the previously mentioned

toxic potential. *E. coli* uses nucleation-precipitation machinery encoded by the *csgAB* and *csgDEFG* operons to specifically aggregate curli, which then has roles in biofilm formation and structure as well as host invasion (Chapman et al., 2002). HET-s plays a role in regulation of heterokaryon formation (Coustou et al., 1997). Sup35p acts as a translation termination factor, such that when it becomes aggregated in [*PSI*<sup>+</sup>] it reduces the efficiency of translation termination, leading to proteins with extended C-terminal regions, altering the proteome (True and Lindquist, 2000). The amyloid formed by Pmel17 plays roles in the facilitation and regulation of the chemical reactivity of the melanin small molecule quinone precursors during melanin biosynthesis (Fowler et al., 2007). There have also been studies suggesting that peptides and proteins can be stored in an amyloid state in the secretory granules of the endocrine system (Maji et al., 2009).

#### 1.4 The main processes of the amyloid life cycle

##### 1.4.1 Overview

There are four stages to the amyloid life cycle which are primary nucleation (*de novo* formation), elongation and growth, secondary nucleation and fibril fragmentation. These can then be classed into primary and secondary pathways (Fig 1.5), where primary nucleation and elongation are primary pathways and secondary nucleation and fibril fragmentation are secondary pathways. Primary pathways convert monomers into aggregates, but secondary pathways increase the number of fibril ends available for elongation to occur on. All four stages occur in all amyloid but the rate each occurs is connected to its properties. For example, more stable amyloids

would have lower fragmentation rates so could potentially have fewer fibrils that are of high length, while a low stability amyloid could fragment easily leading to a high number of short length fibrils.

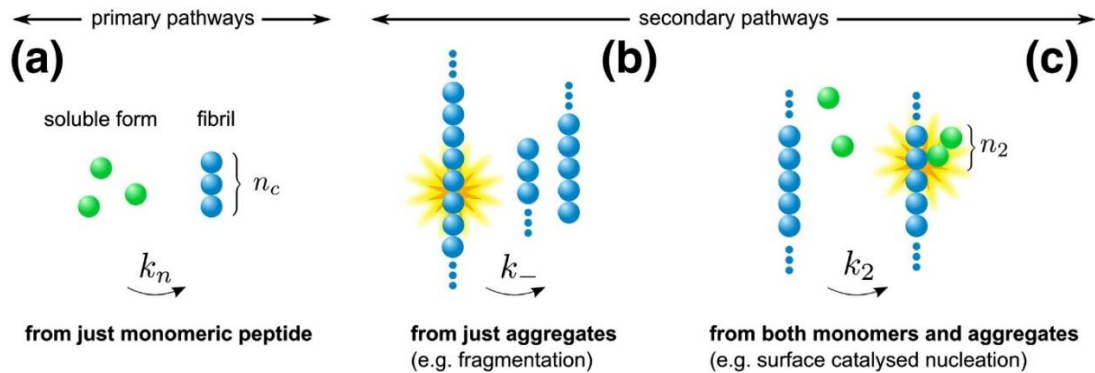


**Figure 1.5- Primary and secondary pathways of the amyloid life cycle.** The primary pathways involve primarily the soluble monomers aggregating to form the fibril, through the stages of nucleation and elongation. The secondary pathways increase the number of fibril ends, thereby increasing the potential rate of growth of amyloid yield. This occurs by the stages of fibril fragmentation and secondary nucleation. Image from Cohen et al., 2012.

#### 1.4.2 Primary processes

The first stage is primary nucleation, also known as *de novo* formation and is the formation of nuclei from monomers (*de novo* meaning “anew” in Latin). The requirement to begin this stage is the formation of a monomer conformation that can form an amyloid core. This means that unless the protein is in an unfolded state, it will require at least partial unfolding to allow these regions to become exposed. Due to help from chaperones and their regions with sequences that promote amyloid formation, functional amyloid form more easily. The initial step of unfolding and folding into an amyloid conformation is reversible and unfavourable, leading to their

kinetic behaviour (see section 1.2.2). While all stages occur at all times normally, during the initial phase where no nuclei have been formed, the other processes are completely suppressed (Arosio, Knowles and Linse, 2015). This means that primary nucleation is required to start the cycle and then the nuclei need to reach a critical size where they become stable. The reversibility and unfavorability of the formation of primary nuclei makes them a significantly smaller number than nuclei formed by secondary processes. Primary nuclei formation is where structural polymorphisms take shape as the amyloid core is formed.

Once the primary nuclei have formed the second stage can begin. This is the extension of the aggregate into fibrils and has been proposed to occur via two models, elongation and assembly of oligomers. Elongation is where monomers are templated by nuclei into joining the aggregate and lead to the nuclei extending into a fibril (Jarrett and Lansbury, 1993). Oligomeric growth is where nuclei grow into helical oligomers that will then associate to form a fibril (Vestergaard et al., 2007). It has been also been suggested that the oligomer will form and then dissociate into dimers which will then lead to polymerisation rather than oligomeric assembly (Ahmad et al., 2003).

#### 1.4.3 Secondary processes

Secondary nucleation is a secondary process that acts to increase the number of fibril ends for elongation, leading to an increase in the rate of increase of amyloid yield. It does this via branching points, where new fibrils will begin growing outwards from a single fibril by templating off it. This has been found to be polymorph

dependent as some polymorphs will undergo secondary nucleation while some will not, leading to it not be a generic amyloid process (Jeong et al., 2013). It has been suggested that a possible unravelling of the fibril, leading to an exposed protofilament is what leads to the creation of the branch. This protofilament will mature into a fibril and begin elongation (Andersen et al., 2009).

Fibril fragmentation is another process that increases the number of fibril ends leading to the exponential growth of fibril yield. In contrast to branching, it is the process by which amyloid fibrils are broken down into oligomers and nuclei that will nucleate elongation. Leading to a continuous cycle of elongation and fragmentation. *In vitro*, this fragmentation is usually induced via physical agitation such as sonication. In functional amyloid *in vivo*, however it is often dependent on chaperones, such as Hsp104 for Sup35 (Collins et al., 2004). For prions this is the process that in combination with propagation is the most important for their infective potential. Due to oligomeric species having higher cytotoxic potential than fibrils, fragmentation also plays a role in the increase of an amyloid's cytotoxicity (Xue et al., 2009).

## 1.5 Experimental and modelling approaches to characterise the amyloid life cycle

### 1.5.1 Overview

Since the discovery of amyloid, a wide range of methods have been used to study them, both *in vitro* and *vivo*. While many of these are used to ascertain the biological impacts of such aggregates, there are also a great many techniques that are used to gain information about the aggregates themselves and their life cycle. In the

following section a few of these techniques are described including the ones that were used in this project.

#### 1.5.2 Thioflavin T and Congo red staining

Dyes are of historical importance in the study of amyloid for purposes such as imaging amyloid and monitoring their growth *in vitro*. Congo red has been used as a diagnostic dye for amyloid fibrils since the 1920s as when it binds fibrils it produces a yellow-green birefringence under crossed polarisers. This characteristic has even been used as a part of some of the previous definitions for amyloid (Sipe et al., 2012). It has however been found that the dye is non-specific for amyloid fibrils as has been shown to be able to bind collagen fibres and cytoskeletal proteins, making it a non-specific dye for amyloid fibrils (Khurana et al., 2001). Another dye often used is Thioflavin T (ThT), a benzothiazole dye that on binding to amyloid fibrils exhibits fluorescence. It has been shown to be superior to previously used dyes such as Congo red in the sense of binding more specifically to amyloid in lower pH conditions (Khurana et al., 2005). This property has made it an attractive dye for use in various different methodologies including fluorescence imaging of fibrils as well as being used to measure aggregate yield over time via measurement of fluorescence intensity. This then allows the creation of ThT fluorescence curves (see Fig 1.4). These curves can then be used to give various details about the mechanisms of the amyloid life cycle and their kinetics as well as allowing the different phases to be visualised and compared between systems. These ThT fluorescence curves will primarily be

used as an indication for fibril growth as well as being used for optimisation of the methodology of producing fibrils in relation to this study.

### 1.5.3 Visualising amyloid

While ThT fluorescence curves can produce a wealth of knowledge, they do have their limitations leading to other methods that can explore other aspects of the aggregates in more detail, such the structure of the formed fibrils. Imaging of the fibrils can provide much of this and hence many techniques of doing so have been developed. The previously described dyes of ThT and Congo Red also play a part in certain techniques used for the visualisation of amyloid. An example of this is the use of Total Internal Reflection Fluorometry microscopy which has been used to perform imaging of dye bound fibrils growing over time (Ban et al., 2003). Until relatively recently however fluorescent imaging techniques have been had a lowered resolution in comparison to other imaging techniques due as optical diffraction limits the obtainable resolution significantly making them unsuited for detailed amyloid viewing. The creation of “super-resolution fluorescence” imaging techniques such as stimulated emission depletion (STED) and structured illumination (SIM) has allowed this to be reduced somewhat (Kaminski Schierle et al., 2011). These new techniques are therefore leading to an increase in the usage of fluorescence for amyloid imaging as they become more relevant.



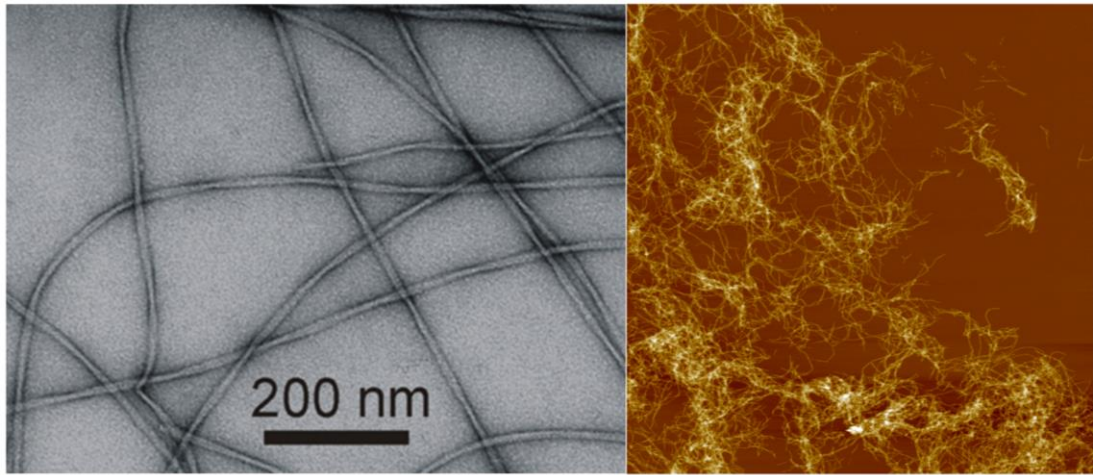


**Figure 1.6- Example TEM and AFM amyloid images.** (Left) Negatively stained transmission electron microscopy (TEM) image of  $A\beta_{1-40}$  fibrils. The scale bar is 200nm. Image from (Paravastu et al., 2008). (Right) Atomic force microscopy (AFM) image of Sup35NM fibrils formed by seeding monomers with a concentration of  $10\mu M$ . The image is  $10\mu M \times 10\mu M$  at a resolution of  $2048 \times 2048$ .

Transmission electron microscopy (TEM) has been in use for a relatively long time due to its high resolution, potentially 1-2nm, allowing it to be used in generating a large amount of structural data. This can include fibril lengths and widths as well as information on the twisting of the fibril such as its periodicity. It can also be used for investigation of other points within the life cycle such as oligomeric stages (Sorci et al., 2009). An important point to note is that TEM requires a vacuum to function as electrons would be scattered by air in present. This will inevitably cause changes in comparison to any native state, creating a need for cryo EM, which can partially resolve this. The sample is rapidly frozen in cryo EM, allowing the native state to be better preserved in comparison to standard TEM. Usually images of multiple structures within a sample will be combined to allow a 3D reconstruction of the overall structure to be made (Sachse, et al., 2008). This works well when a sample is homogeneous but as fibrils show heterogeneity within a single sample, due to

various polymorphisms arising, this means an averaged image such as this will not show the variation in structure within the sample.

Often used alongside TEM is atomic force microscopy (AFM). Unlike most other types of microscopy, AFM physically interacts with the sample it is being used to visualise, which it does through the use of a fine tip in different fashions, depending on the exact methodology being used. It will then measure the height of the sample at that point and by doing this across the surface, create a contour map of the sample. To prepare a sample for AFM it will be deposited onto a surface such as mica and then imaged; this can allow a more native state to be seen even in comparison to cryo EM. While the resolution of the images is not as high as the reconstructions produced by TEM, the ability to visualise particles on an individual level can allow polymorphisms and other structural features to be looked at in more depth. For these reasons, AFM has been used to investigate fragmentation and elongation of different amyloid systems (Nichols et al., 2002; Collins et al., 2004; Marchante et al., 2017).

## 1.6 Model systems for studying amyloid and prions

### 1.6.1 Sup35

Sup35p acts as a subunit of the translation termination factor in yeast and has roles in recognising termination codons and releasing the peptide from the final tRNA, giving it importance in controlling translation termination. The C-terminal domain of Sup35p (Sup35C) is essential for growth and is the section of the protein determined to be responsible for the translation termination function (Ter-Avanesyan et al.,

1993). The N and M domains however are required for the protein to show its characteristic prion-based inheritance. The N domain contains the prion forming domain itself while the M domain links the other two whilst also containing a large number of charged residues which act to increase the solubility of the whole protein (Liu, Sondheimer and Lindquist, 2002). In its prion form the protein will become insoluble and lose its functionality as a part of the translation termination factor, leading to a phenotype of increased readthrough of stop codons of mRNA resulting in protein being synthesised with an extended C-terminal domain. This prion form is known as  $[PSI^+]$ , a biologically functional prion, and the non-prion form is known as  $[psi^-]$ . The  $[PSI^+]$  prion is located in the cytoplasm of the yeast and will be transferred to offspring, bringing the phenotype with it, during mitosis. This prion-based inheritance method was identified due to its associated phenotype undergoing non-Mendelian inheritance (Cox, 1994). Due to its role in yeast biology it is often used as a model system for functional prions.

#### 1.6.2 $\alpha$ -synuclein

Historically  $\alpha$ -synuclein was a little studied protein until the 1990s, which was when it was found that a missense mutation of the protein caused a rare form of Parkinson's disease as well as being found in Lewy bodies of sporadic cases of Parkinson's disease (Polymeropoulos, 1997; Spillantini et al., 1997). These would associate the protein with the disease leading to its study becoming of significant importance. Later the fibrillar aggregates were found to form a cross- $\beta$  sheet conformation that is characteristic of amyloid species (Serpell et al., 2000).  $\alpha$ -synuclein itself is a soluble 140 residue protein, that is highly conserved in

vertebrates and it is intrinsically disordered, meaning it lacks a fixed structure. This latter property is in part why it is able to easily form amyloid species, which is also supported by a 12 residue stretch of hydrophobic amino acids that are prone to forming an amyloid core (Giasson et al., 2000). The function of the protein however is elusive and there have only been suggestions for it, including roles in neurotransmitter release (Snead and Eliezer, 2014). It has been suggested in recent years that  $\alpha$ -synuclein, as well as other neurodegenerative disorders, are able to propagate in a prion-like manner to allow spreading throughout a brain (Marques and Outeiro, 2012). While this prion-like spread has been suggested,  $\alpha$ -synuclein has not been formally classified as a prion due to the uncertain nature of if it can infect another individual (Schwarzman et al., 2019). Due to its biological significance, this protein is highly studied and thus makes it useful as a model disease associated prion-like amyloid.

### 1.7 Concluding remarks: Questions and challenges

Amyloid and prions are important research areas, which with the discovery of functional amyloid has only been growing in attention. Currently there are still many questions left unanswered in the field. An example of this is that research into the effects of altering the sequence of the protein as well as the various types of structural polymorphism they display has barely been only just scratching the surface. There are also many questions relating to the different amyloid systems as well, such as the possibility that the aggregates found in the brains of Parkinson's and

Alzheimer's disease patients are aggregated forms of the oligomers that are inert, acting as a measure to reduce toxicity overall (Congdon and Duff, 2008).

Importantly many of the specifics of the life cycle are still under debate, such as the multiple conflicting models for elongation of fibrils. Rules determining which molecular characteristics give some amyloid prion properties have been suggested but are still a subject of much debate. This also links into how prion-like amyloid arise and if amyloid and prions are ends of a sliding scale or if they are more distinct from each other. It also raises questions about the differences between the properties and life cycle of functional and disease-associated amyloid. While the fibrils and oligomers of disease associated systems will have such a detrimental effect on a cellular level it will affect the whole organism, this is not the case for functional however as they need to exist within a similar environment without having these negative effects. What properties cause the differences between such systems and what does this mean for their life cycles.

The aims and research themes of this study were derived from these questions. In particular, characterising the elongation and fragmentation stages of the model systems of Sup35NM and  $\alpha$ -synuclein through the use of AFM imaging to explore the growth and stability of their respective amyloid fibrils. Allowing a direct comparison to be made between examples of not just functional and disease associated amyloid but also prion and prion-like as well.

## 2. Materials and Methods

### 2.1 Materials

#### 2.1.1 Lysogeny Broth Media

*E. coli* was used to express the two different proteins used, leading to the use of LB media for the expression as well as the buffers required for the further stages as well as for the proteins' purification.

**Table 2.1- Lysogeny Broth (LB) media composition.** LB was the media used for growing cultures of the *E. coli* strains for the expression of  $\alpha$ -synuclein and Sup35NM. LB Agar was used for making plates that the strain was initially streaked onto before individual colonies were added to the liquid media for the growth and expression. Prior to use, media was sterilised using a Prestige Medical Desktop autoclave.

Substance	Amount (per 100ml)
Tryptone	1 g
Yeast Extract	0.5 g
NaCl	1 g
Distilled H <sub>2</sub> O	100ml
Agar	2g (for LB Agar)

### 2.1.2 Sup35NM Protein Purification Buffer Composition

**Table 2.2- Composition of the buffers used in the purification of Sup35NM prior to size exclusion chromatography.** 1.0M Tris HCl was a component used in making each of the buffers. The buffers used were: Melki lysis buffer (MLB), Melki lysis buffer denaturing (MLBG) and Melki lysis buffer elution (MLBGE).

Substance	1.0M Tris HCl	MLB	MLBG	MLBGE
Tris HCl	78.8g	-	-	-
1.0M Tris HCl pH 8.0	-	20ml	20ml	2ml
NaCl	-	58.3g	58.3g	5.84g
Imidazole	-	1.35g	1.35g	1.7g
Guanidine HCl	-	-	573g	57.3g
Water quality	Mili Q	Mili Q	Mili Q	Mili Q
pH	8.0	-	-	-
Total volume	500ml	1000ml	1000ml	100ml

### 2.1.3 Sup35NM AKTA Buffer Composition

**Table 2.3- The buffers used for the equilibration of the size exclusion chromatography column and then to elute the Sup35NM from the column. The 1.0M Tris HCl pH 8.0 was made as in Table 2. The buffers were filtered using a 0.2µm SFCA membrane filter and a vacuum, the buffer was then degassed using a vacuum pump before use on the column.**

<b>Substance</b>	<b>Equilibration Buffer</b>	<b>Elution G Buffer</b>
<b>1.0M Tris HCL pH 8.0</b>	20ml	20ml
<b>NaCl</b>	29.1g	29.1g
<b>Guanidine HCl</b>	-	573g
<b>Water quality</b>	HPLC grade	HPLC grade
<b>Total volume</b>	1000ml	1000ml



### 2.1.4 Sup35NM Fibril Formation Buffer

**Table 2.4- Sup35NM Fibril Formation Buffer (SFFB) composition.** SFFB was the buffer the Sup35NM was buffer exchanged into, used to dilute the protein to the correct concentrations and to perform the fibril formation assays. After the buffer was produced it was filtered using a 0.2 $\mu$ m SFCA membrane filter and a vacuum, this was then degassed using a vacuum pump before its use.

Substance	1M Na <sub>2</sub> HPO <sub>4</sub> (Per 100ml)	1M NaH <sub>2</sub> PO <sub>4</sub> (Per 100ml)	0.1M PO <sub>4</sub> (Per 100ml)	SFFB (per 1000ml)
Na <sub>2</sub> HPO <sub>4</sub>	14.2g	-	-	-
NaH <sub>2</sub> PO <sub>4</sub>	-	12.0g	-	-
1M Na <sub>2</sub> HPO <sub>4</sub>	-	-	7.74ml	-
1M NaH <sub>2</sub> PO <sub>4</sub>	-	-	2.26ml	-
0.1M PO <sub>4</sub>	-	-	-	200ml (20mM)
NaCl	-	-	-	2.9g (50mM)
Water quality	HPLC	HPLC	HPLC	HPLC
pH	-	-	7.4	7.4

### 2.1.5 $\alpha$ -synuclein Protein Purification Buffer Composition

**Table 2.5- Composition of buffers used in the purification of  $\alpha$ -synuclein prior to ion exchange chromatography.** As well as the Lysis buffer, Melki lysis buffer was also used with the same composition as in section 2.1.2.

Substance	Lysis Buffer (200ml)
Tris (hydroxymethyl) methylamine	0.48g
NaCl	1.17g
Water quality	HPLC
pH	7.5

### 2.1.6 $\alpha$ -synuclein AKTA Buffer Composition

**Table 2.6- The buffers used for the equilibration of the Ion exchange column and then to elute the  $\alpha$ -synuclein from the column.** The buffers were filtered using a 0.2 $\mu$ m SFCA membrane filter and a vacuum, the buffer was then degassed using a vacuum pump before use on the column.

Substance	20mM Tris (1L)	20mM Tris 1M NaCl (1L)
Tris (hydroxymethyl) methylamine	2.42g	2.42g
NaCl	-	58.44
Water quality	HPLC	HPLC
pH	7.5	7.5

### 2.1.7 $\alpha$ -synuclein Fibril Formation Buffer

**Table 2.7-  $\alpha$ -synuclein Fibril Formation Buffer ( $\alpha$ FFB) composition.**  $\alpha$ FFB was the buffer the  $\alpha$ -synuclein was buffer exchanged into via gel filtration chromatography, used to dilute the protein to the correct concentrations and to perform the fibril formation assays. The components of the buffer are also listed here. After the buffer was produced it was filtered using a 0.2 $\mu$ m SFCA membrane filter and a vacuum, this was then degassed using a vacuum pump before its use.

Substance	1M Na <sub>2</sub> HPO <sub>4</sub> (Per 100ml)	1M NaH <sub>2</sub> PO <sub>4</sub> (Per 100ml)	0.1M PO <sub>4</sub> (Per 100ml)	$\alpha$ FFB (per 1000ml)
Na <sub>2</sub> HPO <sub>4</sub>	14.2g	-	-	-
NaH <sub>2</sub> PO <sub>4</sub>	-	12.0g	-	-
1M Na <sub>2</sub> HPO <sub>4</sub>	-	-	7.74ml	-
1M NaH <sub>2</sub> PO <sub>4</sub>	-	-	2.26ml	-
0.1M PO <sub>4</sub>	-	-	-	250ml (25mM)
NaCl	-	-	-	8.8g (150mM)
NaN <sub>3</sub>	-	-	-	3.1ml
Water quality	HPLC	HPLC	HPLC	HPLC
pH	-	-	7.4	7.4

## 2.1.8 Sup35NM C-terminal Hexa-His *E. coli* strain

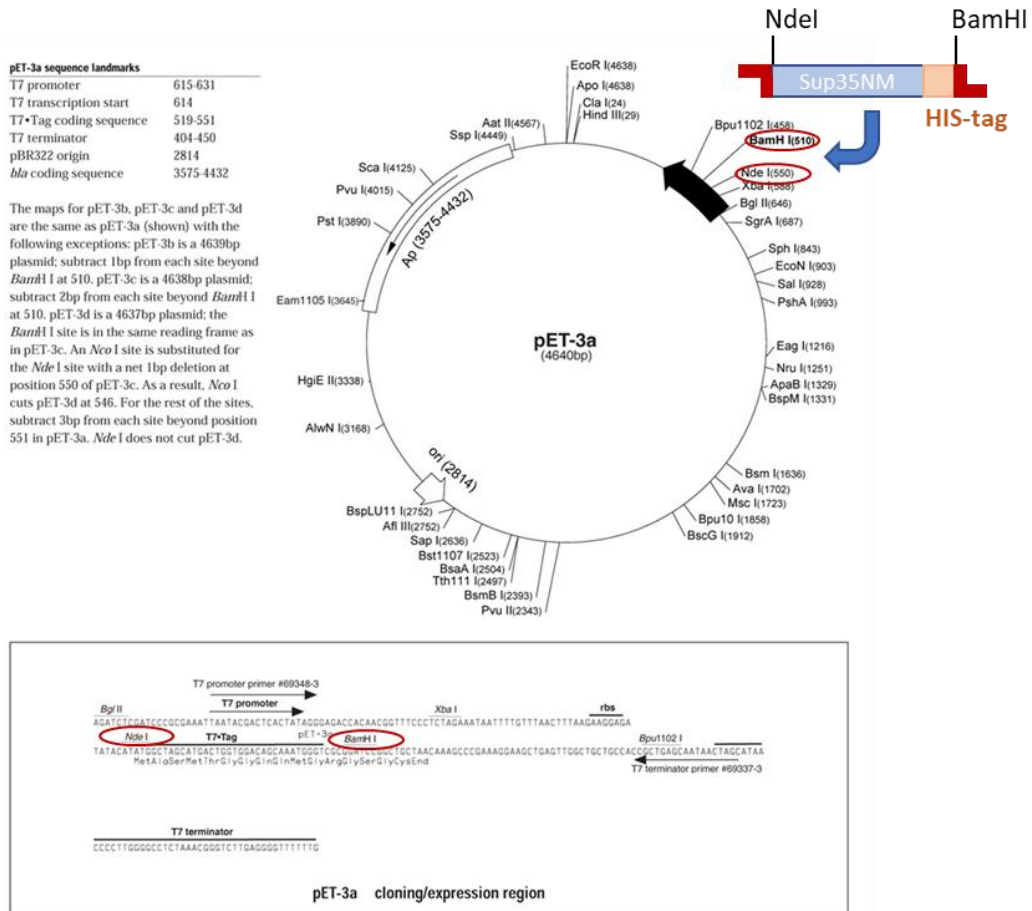


**Figure 2.1-** Map of the plasmid containing the gene for Sup35NM C-terminal Hexa-His. The corresponding plasmid was inserted into *E. coli* to generate the Sup35NM C-terminal Hexa-His producing strain used in 2.2.1. The Sup35NM fragment was amplified from *pet15b* (N-term HIS-tag+Sup35NM) using Sup35NM forward (*Nde*I site containing) and Sup35NM Cterm His (containing *Bam*HI, stop codons and 9 His-encoding codons) primers and inserted into *pet3a*.

### 2.1.9 $\alpha$ -synuclein *E. coli* strain

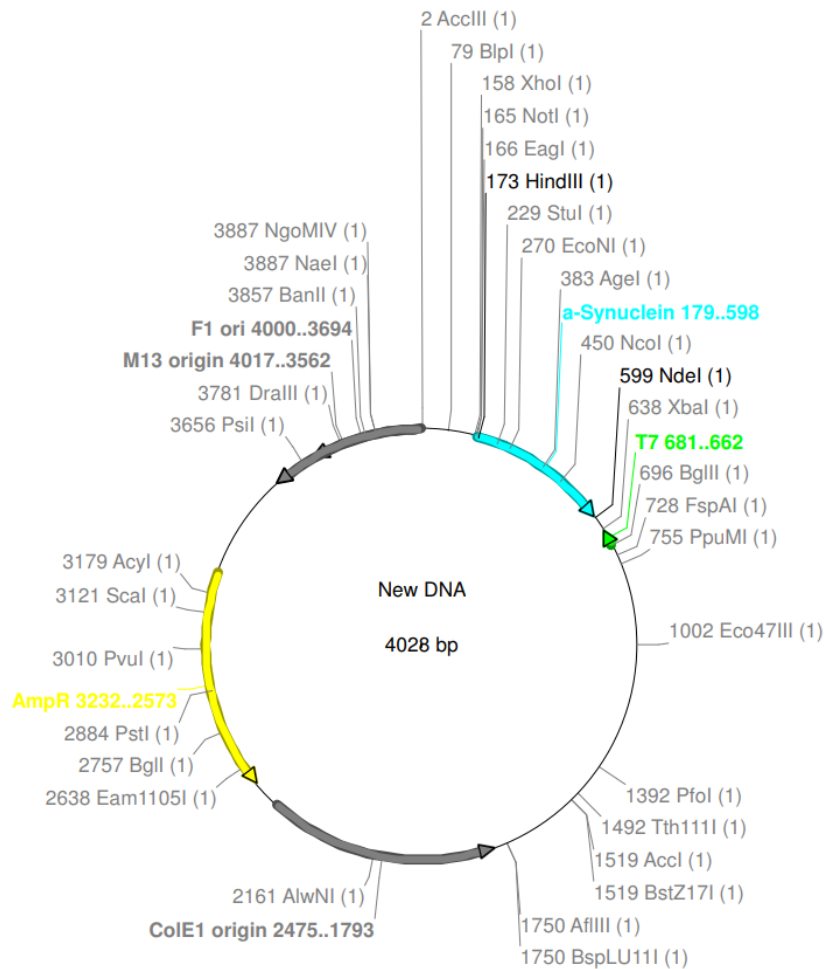


**Figure 2.2-** Map of the plasmid containing the gene for  $\alpha$ -synuclein. The corresponding plasmid was inserted into *E. coli* to generate the  $\alpha$ -synuclein producing strain used in 2.2.2.

## 2.2 Protein expression

### 2.2.1 Sup35NM C terminal hexa-His expression

*E. coli* were modified with the plasmid shown in Fig 2.1, to allow them to produce Sup35NM, and streaked onto two plates of LB agar media containing 25 $\mu$ g/ml chloramphenicol and 100 $\mu$ g/ml ampicillin sodium salt and incubated at 37°C

overnight. Once grown, individual colonies were used to inoculate 4x100ml of LB, selecting with chloramphenicol (25µg/ml) and ampicillin sodium salt (100µg/ml), which were then incubated overnight again at 37°C. These overnight cultures were spun down at 4000rpm for 5 minutes and the resulting supernatant was then discarded. The pellets were resuspended in LB which was added to 4x1 litre LB, selecting with chloramphenicol (25µg/ml) and ampicillin sodium salt (100µg/ml), in baffled flasks. These were incubated at 37°C until an OD600 of 0.6 was reached. 1ml of IPTG was added to each to induce Sup35NM expression and they were incubated for 4 hours. These cells were harvested by centrifugation at 4000rpm for 10 minutes and the supernatant was discarded. The pellets were resuspended in 20ml of MLB buffer and spun down at 4000rpm for 5 minutes. The final pellets were then stored at -80°C for a couple of days at most before purification began.

#### 2.2.2 $\alpha$ -synuclein expression

*E. coli* were modified with the plasmid shown in Fig 2.2, to allow them to produce  $\alpha$ -synuclein, and were then streaked onto two plates of LB agar media containing 25µg/ml chloramphenicol and 100µg/ml ampicillin sodium salt and incubated at 37°C overnight. Once grown, individual colonies were used to inoculate 4x100ml of LB, selecting with chloramphenicol (25µg/ml) and ampicillin sodium salt (100µg/ml), which were then incubated overnight again at 37°C. These overnight cultures were spun down at 4000rpm for 5 minutes and the resulting supernatant was then discarded. The pellets were resuspended in LB which was added to 4x1 Litre LB, selecting with chloramphenicol (25µg/ml) and ampicillin sodium salt (100µg/ml), in

baffled flasks. These were incubated at 37°C until an OD600 of 0.6 was reached. 1ml of IPTG was added to each to induce  $\alpha$ -synuclein expression and they were incubated for 4 hours. These cells were harvested by centrifugation at 4000rpm for 10 minutes and the supernatant was discarded. The pellets were resuspended in 20ml of MLB buffer and spun down at 4000rpm for 5 minutes. The final pellets were then stored at -80°C for a couple of days at most before purification began.

### 2.3 Protein purification

#### 2.3.1 Sup35NM C terminal hexa-His purification

The pellets produced in 2.2.1 were resuspended using 20ml of MLB each and then placed in ice to cool. Once cooled they were lysed by sonication at 18 $\mu$ m amplitude for 3x30 second bursts, with a minute interval back on ice between each burst. These were centrifuged at 12000rpm for 30 minutes remove the cell debris. In preparation for the next stage a Ni-NTA column was prepared using 6ml of chelating sepharose, which was made up to 50ml with HPLC water and spun at 3000rpm for 3 minute and the pellet was then discarded. This wash was then repeated with NiCl<sub>2</sub>, MLB and then finally MLBG. The Ni-NTA pellet was resuspended with 2ml of MLBG and half was added to each half of the supernatant from the 12000rpm centrifugation. These were incubated on a tube roller for 1 hour. The mixtures were centrifuged at 3000rpm for 3 minutes and the supernatant discarded. Each of the two pellets was made up to 50ml with MLBG and centrifuged again at 3000rpm for 3 minutes. The pellets were placed in a poly-prep column and the liquid that flowed through was discarded. 4.5ml of MLBGE was added to this column and the resulting eluate underwent size

exclusion chromatography via an ÅKTA prime using a Superdex™ 200 Increase 10/300 GL column equilibrated with equilibration buffer and the protein was eluted with Elution G buffer leading to the fractions corresponding to Sup35NM being collected. These fractions were “pooled”, and this was snap frozen using liquid nitrogen into 0.5ml and 1ml aliquots.

### 2.3.2 $\alpha$ -synuclein purification

The pellets produced in 2.2.2 were thawed slowly in ice and then resuspended in 20ml of lysis buffer each and 1 protease inhibitor tablet was added. These were sonicated at 20 $\mu$ m amplitude in 10 second bursts for a total of 110 seconds with 10 seconds of resting on ice between each burst. The cell debris was then removed by centrifugation at 13000rpm for 30 minutes. The resulting supernatant was acidified to pH3.5 using 1M HCl and incubated on a tube roller at 4°C for 30 minutes. It was then neutralised to pH7.5 using NaOH and cooled on ice. This was treated with  $(\text{NH}_4)_2\text{SO}_4$  to give a 30% solution, which was incubated at 4°C for 20 minutes on a tube roller. It was then centrifuged at 13000rpm for 20 minutes and the supernatant was treated with  $(\text{NH}_4)_2\text{SO}_4$  again giving a 50% solution this time and incubated at 4°C on a tube roller for 20 minutes. This was then centrifuged for 30 minutes at 13000rpm and the resulting 2 pellets had 2ml of 20mM tris pH7.5 added to dissolve them. These were added to a PD10 column that had been equilibrated with 20mM tris pH7.5 and after a void volume of 1.5ml approximately 4.5ml of eluate was collected and underwent Ion Exchange chromatography via an ÅKTA prime using a HiTrap™ 5ml Q FF column equilibrated with 20mM Tris buffer and the protein was



then eluted with 20mM Tris 1M NaCl buffer. The fractions corresponding to the peak were collected and pooled, split into 0.5 ml aliquots and snap frozen using liquid nitrogen before being stored at -80°C.

## 2.4 Thioflavin T assays

### 2.4.1 Sup35NM well and assay preparation

Starting with a 96 well plate (Corning Assay Plate, 96 wells, Non-Binding surface), all outside wells were filled with 100µl of water, to act as a temperature buffer for the samples that be on the outside edges otherwise. 1µl of thioflavin T (ThT) was then added to any wells that were to be measured for fluorescence intensity, which was used to monitor the growth of amyloid fibrils. Control wells containing 100µl Sup35NM fibril formation buffer (SFFB) would then be made up, with some containing ThT. A PD-10 buffer exchange column was equilibrated with ~25ml of stereo filtered SFFB, produced using a Minisart Syringe Filter 0.2µm, before 1ml of the Sup35NM pool was thawed and added to the column. Once the protein had fully entered the column another 1.5ml of SFFB was allowed to fully enter the column. The protein was then eluted with another 3.5ml of SFFB and 0.5ml fractions were collected, the protein would usually come out in 2 fractions giving 1ml of protein with a concentration of ~35µM. This was calculated using the formula below (Note: if the absorbance was over 1.0 a dilution to 1/10 was performed prior to reading):

$$\text{Molar concentration } (\mu\text{M}) = \frac{A_{280}}{\frac{0.971}{30.69}} \times 1000$$

	1	2	3	4	5	6	7	8	9	10	11	12
A												
B		20 $\mu$ M	20 $\mu$ M	SFFB	SFFB	SFFB	SFFB	SFFB	SFFB	20 $\mu$ M	20 $\mu$ M	
C		10 $\mu$ M	10 $\mu$ M	10 $\mu$ M	10 $\mu$ M	10 $\mu$ M	SFFB	10 $\mu$ M	10 $\mu$ M	10 $\mu$ M	10 $\mu$ M	
D		5 $\mu$ M	5 $\mu$ M	5 $\mu$ M	5 $\mu$ M	5 $\mu$ M	SFFB	5 $\mu$ M	5 $\mu$ M	5 $\mu$ M	5 $\mu$ M	
E		2.5 $\mu$ M	2.5 $\mu$ M	2.5 $\mu$ M	2.5 $\mu$ M	2.5 $\mu$ M	SFFB	2.5 $\mu$ M	2.5 $\mu$ M	2.5 $\mu$ M	2.5 $\mu$ M	
F		1.25 $\mu$ M	1.25 $\mu$ M	1.25 $\mu$ M	1.25 $\mu$ M	1.25 $\mu$ M	1.25 $\mu$ M	1.25 $\mu$ M	1.25 $\mu$ M	1.25 $\mu$ M	1.25 $\mu$ M	
G		SFFB	SFFB	SFFB	SFFB	SFFB	SFFB	SFFB	SFFB	SFFB	SFFB	
H												

**Figure 2.3- An example well layout of a 96 well plate for a de novo Sup35NM fibril formation assay.**  $\mu$ M denotes the concentration of protein monomer used. SFFB denotes wells used as SFFB controls. White wells indicate the addition of 1 $\mu$ l Thioflavin T. Red wells indicate lack of Thioflavin T. Blue wells indicate water used as a temperature buffer.

This was then diluted to the concentrations required for the assay using SFFB and 100µl of this was added to the required wells. Once the desired layout was complete (example can be seen in Fig. 2.3.), the plate would then be sealed with StarSeal Advanced Polyolefin Film before the assay was started.

The protein not used in the plates was incubated in LoBind Eppendorfs (Eppendorf tubes Protein LoBind Tube 1.5ml) at 10µM placed inside a 50ml falcon tube which was rotated on a tube roller at 30rpm. 500µl *de novo* samples of these were then used for the fragmentation and quantifiable seed production and consequently to seed the time-dependent assays.

#### 2.4.2 Sup35NM ThT kinetic assay

The fibril growth assay was performed using a BGM labtech CLARIOstar. Prior to the plate being placed in the CLARIOstar its temperature was set to 30°C and left to reach this temperature. Once the plate was fully prepared, it was placed in the machine and the appropriate protocol run. This protocol scanned using top optics and measured fluorescence intensity using the ThT pre-sets with excitation set to 440-12, dichroic at auto 460 and emission at 480-12. Before it performs the scan, the plate was shaken using the double orbital mode at a frequency of 700rpm for 2 seconds. The scanning itself took 2 minutes in total to read the whole plate, excluding the water temperature buffer wells. After a reading at time 0 minutes, this protocol was repeated after 900 seconds (15 minutes). This produced the ThT traces used to construct the Sup35NM fibril ThT fluorescence curves. If it were required, at certain time points the protocol was stopped, the plate removed, and samples were

extracted either for AFM imaging or for storage in a 37°C incubator in LoBind Eppendorfs.

#### 2.4.3 $\alpha$ -synuclein well and assay preparation

Starting with a 96 well plate (Corning Assay Plate, 96 wells, Non-Binding surface), all outside wells were filled with 100 $\mu$ l of water, to act as a temperature buffer for the samples that would have been on the outside. 1 $\mu$ l of thioflavin T (ThT) was then added to any wells that were to be measured for fluorescence intensity, which was used to monitor the growth of amyloid fibrils. Control wells containing 100 $\mu$ l  $\alpha$ -synuclein fibril formation buffer ( $\alpha$ FFB) would then be made up, with some containing ThT. A HiLoad™ 16/600 Superdex™ 200pg column was equilibrated with  $\alpha$ FFB (that had been filtered using a 0.2 $\mu$ m SFCA membrane filter with a vacuum and then degassing) before using it to perform gel filtration on a thawed aliquot of the protein. The fractions to be used was collected before being diluted to the required concentrations for the assay using  $\alpha$ FFB and the addition of 100 $\mu$ l of this to each well. The concentration was calculated using the formula below:

$$\text{Molar concentration } (\mu\text{M}) = \frac{A_{280}}{5800} \times 1000000$$

Once the desired layout was completed (example can be seen in Fig. 2.4.), the plate would then be seal with StarSeal Advanced Polyolefin Film before the assay was started.

	1	2	3	4	5	6	7	8	9	10	11	12
A												
B		10 $\mu$ M	10 $\mu$ M	10 $\mu$ M	10 $\mu$ M	10 $\mu$ M	10 $\mu$ M	10 $\mu$ M	10 $\mu$ M	10 $\mu$ M	10 $\mu$ M	
C		10 $\mu$ M	10 $\mu$ M	10 $\mu$ M	10 $\mu$ M	10 $\mu$ M	10 $\mu$ M	10 $\mu$ M	10 $\mu$ M	10 $\mu$ M	10 $\mu$ M	
D		20 $\mu$ M	20 $\mu$ M	20 $\mu$ M	20 $\mu$ M	20 $\mu$ M	20 $\mu$ M	20 $\mu$ M	20 $\mu$ M	20 $\mu$ M	20 $\mu$ M	
E		5 $\mu$ M	5 $\mu$ M	5 $\mu$ M	5 $\mu$ M	5 $\mu$ M	5 $\mu$ M	5 $\mu$ M	5 $\mu$ M	5 $\mu$ M	5 $\mu$ M	
F		100 $\mu$ M	100 $\mu$ M	100 $\mu$ M	100 $\mu$ M	100 $\mu$ M	100 $\mu$ M	100 $\mu$ M	100 $\mu$ M	100 $\mu$ M	100 $\mu$ M	
G		$\alpha$ FFB	$\alpha$ FFB	$\alpha$ FFB	$\alpha$ FFB	$\alpha$ FFB	$\alpha$ FFB	$\alpha$ FFB	$\alpha$ FFB	$\alpha$ FFB	$\alpha$ FFB	
H												

**Figure 2.4-** An example well layout of a 96 well plate for a  $\alpha$ -synuclein fibril formation assay.  $x\mu$ M denotes the concentration of protein monomer used.  $\alpha$ FFB denotes wells used as  $\alpha$ FFB controls. White wells indicate the addition of 1 $\mu$ l Thioflavin T. Red wells indicate lack of Thioflavin T. Blue wells indicate water used as a temperature buffer.

$\alpha$ -synuclein has a long lag phase when produced *de novo* leading to its incubation in a LoBind Eppendorf being shaken at 180 rpm at 37°C for the *de novo* assays, where ThT fluorescence curves were not needing to be recorded. Once the fractions were eluted off the column they were kept separated as 0.5ml aliquots, 2 for each 1ml fraction, for this without dilution, but the concentrations were recorded (see results for breakdown of fractions used). These were the fibrils that were later diluted down to 10 $\mu$ M and used for later assays, including the fragmentation and quantifiable seed production assays and consequently to seed the time-dependent assays.

#### 2.4.4 $\alpha$ -synuclein ThT kinetic assay

The fibril growth assay was performed using a BGM labtech CLARIOstar. Prior to the plate being placed in the CLARIOstar its temperature was set to 37°C and left to reach this temperature. Once the plate was fully prepared, it was placed in the machine and the appropriate protocol run. This protocol scanned using top optics and measured fluorescence intensity using the ThT pre-sets with excitation set to 440-12, dichroic at auto 460 and emission at 480-12. Before it performs the scan, the plate is shaken using the double orbital mode at a frequency of 700rpm for 2 seconds. The scanning itself took 2 minutes in total to read the whole plate, excluding the water temperature buffer wells. After a reading at time 0 minutes, this protocol was repeated after 900 seconds (15 minutes). In between the cycles of the reading protocol the plate was shaken at a frequency of 180rpm using the orbital mode. This produced the ThT traces used to construct the  $\alpha$ -synuclein fibril ThT fluorescence curves. At required points the protocol was stopped, the plate removed, and samples

were extracted either for AFM imaging or for storage in a 37°C incubator in LoBind Eppendorfs.

#### 2.4.5 Thioflavin T analysis

The .csv files produced during 2.4.2 and 2.4.4 were converted into scatter graphs using Microsoft Excel, producing ThT fluorescence curves with Fluorescence intensity as the Y axis. This data was then analysed using the ThT fluorescence curve data analysis software xProThTData Version v3.1 (Nov 2016) produced by Wei-Feng Xue, to normalise the data. Masking of the plateau phase was increased until the calculated curve matched the raw data curve as closely as possible. The normalised data was then exported and used to produce scatter graphs in Microsoft Excel, same as with the raw data.

### 2.5 Seed generation

#### 2.5.1 Sup35NM seed generation

500µl 10µM Sup35NM fibril samples (monomeric concentration) grown in a LoBind Eppendorf tube were used for the fragmentation and quantifiable seed formation assay. This sample was placed in ice and pulse sonicated in 5 second intervals by a Q Sonica Q125 sonicator (frequency of 20kHz), followed by 5 seconds of rest. This was performed additively to reach the required time remaining in the sonication series, giving total times of 20, 40, 80, 160 and 320 seconds (time sonicating) at 20% amplitude. At each point 20µl was taken for producing AFM samples and the 320

second seeds were subsequently used to seed the time-dependent growth assays. Note that for earlier assays before optimisation of seed formation an amplitude of 60% for 20 seconds was used instead.

### 2.5.2 $\alpha$ -synuclein seed generation

500 $\mu$ l 10 $\mu$ M  $\alpha$ -synuclein fibril samples (monomeric concentration) grown in a LoBind Eppendorf tube were used for the fragmentation and quantifiable seed formation assay. This sample was placed in ice and pulse sonicated in 5 second intervals by a Q Sonica Q125 sonicator (frequency of 20kHz), followed by 5 seconds of rest. This was performed additively to reach the required time remaining in the sonication series, giving total times of 20, 40, 80, 160, 320, 640, 1280, 2560 and 5120 seconds (time sonicating) at 20% amplitude. At each point 20 $\mu$ l was taken for producing AFM samples and the 5120 second seeds were subsequently used to seed the time-dependent growth assays.

## 2.6 Seeded Thioflavin T assays

### 2.6.1 Sup35NM seeded growth assays

After generating seeds using previously formed fibrils as detailed in 2.5.1 and a desired well layout as in 2.4.1, an additional final step was completed. This was the addition of a small quantity of seeds to give the desired percentage of monomer in seeds. If varying seed or monomer concentrations were used, the order of seed addition was lowest concentration to highest concentration to minimise the loss of time for the faster reactions. The assay was then carried out the same as *de novo*



assays, using the same protocol (see section 2.4.1 and 2.4.2). Also, for the time-dependent assays all timings are based off the moment the seed is added to the monomer.

#### 2.6.2 $\alpha$ -synuclein seeded growth assays

After generating seeds using previously formed fibrils as detailed in 2.5.2 and a desired well layout as in 2.4.3, an additional final step was completed. This was the addition of a small quantity of seeds to give the desired percentage of monomer in seeds. If varying seed or monomer concentrations were used, the order of seed addition was lowest concentration to highest concentration to minimise the loss of time for the faster reactions. The assay was then carried out the same as *de novo* assays, using the same protocol (see section 2.4.3 and 2.4.4). Also, for the time-dependent assays all timings are based off the moment the seed is added to the monomer.

### 2.7 Time-dependent growth assays

#### 2.7.1 Sup35NM time-dependent growth imaging assay

As stated in 2.4.1 and 2.5.1 the fibrils used for the seeding of this assay was grown *de novo* at 10 $\mu$ M in LoBind Eppendorfs while undergoing a rotation of 30rpm. The fibrils were subjected to 5 second pulse sonication at an amplitude of 20% for a total of 320 seconds sonicating to produce the seeds. 25 $\mu$ l of seed would then be added to 475 $\mu$ l of 10 $\mu$ M monomeric protein in a LoBind Eppendorf, giving a seed

percentage of 5% and be allowed to grow at 30°C without and disturbance. After 5 minutes 20µl was taken from the solution diluted 1:4 with SFFB and used to produce AFM samples. This is to reduce the high density of the Sup35NM images to allow easier analysis. The AFM sample preparation requires 5 minutes of deposition before being washed while on the mica. This gives the sample 5 minutes more than when it was in the Eppendorf, giving a total time of 10 minutes after the addition of the seed to the monomer. These images were used to measure and the length of the fibrils in comparison to the seeds that were used and identify their elongation rate.

To measure elongation and fragmentation at the same time, the above protocol was repeated but with the addition of sonication. The sonication rate that was chosen was 1 second pulses every 30 seconds (1 second pulse, 29 seconds of rest) for the entire time the sample was in the Eppendorf. These samples were also used to produce images at the same time points to allow comparison of the effect of fragmentation on the growth.

#### 2.7.2 $\alpha$ -synuclein time-dependent growth imaging assay

As stated in 2.4.3 and 2.5.2 the fibrils used for the seeding of this assay was grown *de novo* at the highest concentration possible, post gel filtration, in LoBind Eppendorfs while undergoing shaking at 180 rpm at a temperature of 37°C. The fibrils were subjected to 5 second pulse sonication at an amplitude of 20% for a total of 5120 seconds sonicating to produce the seeds. 25µl of seed would then be added to 475µl of 10µM monomeric protein in a LoBind Eppendorf, giving a seed percentage of 5% and be allowed to grow at 30°C without and disturbance. After 5 minutes 20µl

was taken from the solution and used to produce AFM samples, which requires 5 minutes of deposition before being washed while on the mica. This gives the sample 5 minutes more than when it was in the Eppendorf, giving a total time of 10 minutes after the addition of the seed to the monomer. These images were used to measure and the length of the fibrils in comparison to the seeds that were used and identify their elongation rate.

To measure elongation and fragmentation at the same time, the above protocol was repeated but with the addition of sonication. The sonication rate that was chosen was 1 second pulses every 30 seconds (1 second pulse, 29 seconds of rest) for the entire time the sample was in the Eppendorf. These samples were also used to produce images at the same time points to allow comparison of the effect of fragmentation on the growth.

## 2.8 Atomic force microscopy imaging

### 2.8.1 Mica disk preparation

An Agar Scientific 9.9mm Mica Disk was attached to an Agar Scientific 15mm SPM Specimen Disk using double sided tape and then pressed together to ensure they were as flat as possible. PVC tape was then used to cleave the exposed layer of mica to ensure the surface is clean before sample preparation.

### 2.8.2 Sup35NM sample preparation

20 $\mu$ l of sample was pipetted onto the newly exposed mica surface and then placed mica side face up in a petri dish with the bottom covered by clean filter paper. This was incubated as such for 5 minutes before washing with 1ml of stereo-filtered water, produced using a Minisart Syringe Filter 0.2 $\mu$ m, and drying with a gentle steam of nitrogen gas. This prepared disk would then be stored in a Petri dish in the same way as in the incubation step, until imaging. For the fragmentation, elongation and combined assays the sample was diluted to 1 in 5 using SFFB to decrease the density of the images.

### 2.8.3 $\alpha$ -synuclein sample preparation

20 $\mu$ l of sample was pipetted onto the newly exposed mica surface and then placed mica side face up in a petri dish with the bottom covered by clean filter paper. This was incubated as such for 5 minutes before washing with 1ml of stereo-filtered water, produced using a Minisart Syringe Filter 0.2 $\mu$ m, removal of excess liquid with filter paper before drying with a very gentle steam of nitrogen gas. This prepared disk would then be stored in a Petri dish in the same way as in the incubation step, until imaging.

### 2.8.4 AFM imaging

Samples were imaged using a Bruker MultiMode Atomic Force Microscope with a NanoScope V controller. The ScanAsyst mode of the Nanoscope software was used

together with Bruker SCANASYST-AIR model AFM probes (Silicon Tip on Nitride Lever). Images were captured at a size of 10 $\mu$ m with a resolution of 2048 by 2048 pixels (pixel width 4.88nm) and analysed using the Nanoscope Analysis software and saved as .png file, alongside the processed .000 file.

#### 2.8.5 AFM image analysis

The Nanoscope Analysis software was used to process and analyse the data collected from the AFM. Firstly, the .000 data was flattened by 1<sup>st</sup> order correction, without thresholding to remove tilt. This was repeated using a threshold value depending on the image to further flatten the image. This flattened image would then be exported as a .png file, examples of these images of which can be seen in section 3. Results.

The .000 files and Nanoscope Analysis were also used to measure fibril width. This was achieved using the section tool, which shows the profile of the surface. A section was made perpendicular to the direction of the fibril, so that its profile is captured. The width was then identified using the height of the fibril from the section, with the average baseline considered. These would then be collected for use in 3.3.

### 3. Results

#### 3.1 Sup35NM C terminal Hexa-His tag

##### 3.1.1 Protein expression and purification

Before any assays involving fibril formation could be carried out the first stage was to obtain the protein that was used as the stock of monomeric protein. For Sup35NM, this involved growing an *E. coli* strain modified with the plasmid shown in 2.1.8 and expressing the protein, before purification.

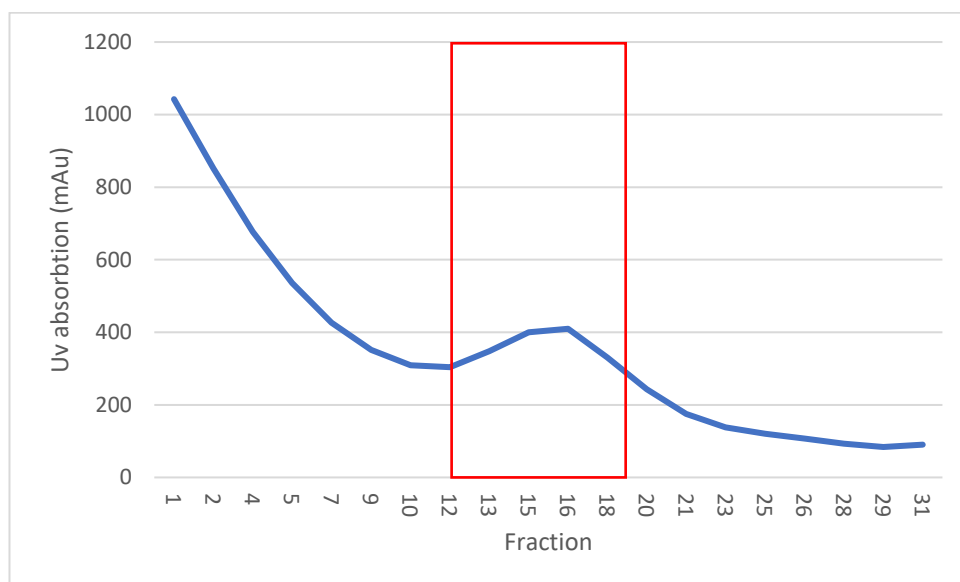


**Figure 3.1- Sup35NM size exclusion chromatography.** UV absorption trace of the fractions produced by performing size exclusion chromatography on the Sup35NM eluate. The region selected for collection to produce the Sup35NM pool is highlighted with a red box and corresponds to fractions 12-19.

The output of the ÅKTA used in the final step of this expression and purification of Sup35NM C terminal hexa-His is shown in Fig 3.1. Fractions 12-19 were determined to be the fractions that made up the peak corresponding to the expected Sup35NM peak, leading to these being collected and converted into the pool that was used as

the source of monomeric protein for later growth assays. Once the pool was generated, it was snap frozen as 1ml aliquots to allow for storage until required.

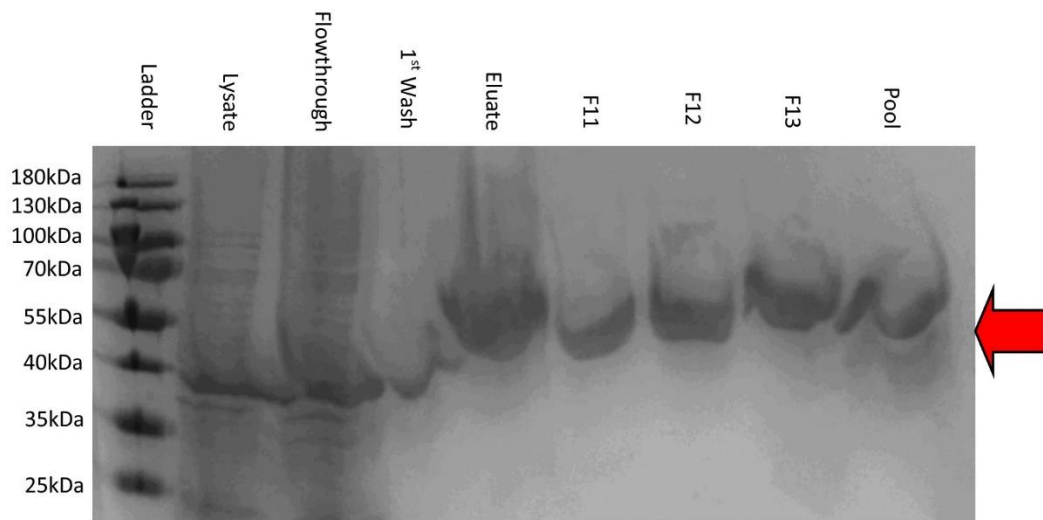


**Figure 3.2- Sup35NM SDS PAGE gel.** These are the results of running a 12% SDS PAGE gel on samples collected from across the purification of Sup35NM. The samples are: Ladder, Lysate, Flowthrough, 1<sup>st</sup> wash, Eluate, Fraction 11, Fraction 12, Fraction 13 and Pool. The highlighted band corresponds to the Sup35NM purified.

To confirm the presence of Sup35NM at all stages of the purification, a 12% SDS PAGE gel was ran using samples collected at key points, with the results of this being shown in Fig 3.2. The samples collected were: Lysate was collected after sonication of the sample initially, Flowthrough was the supernatant left over from the Ni-NTA column, 1<sup>st</sup> wash was the result of the first wash of the Ni-NTA pellet, eluate was the sample eluted from the Ni-NTA pellet that was added to the ÅKTA for size exclusion chromatography, F11, 12 and 13 were fractions corresponding to the start of the peak from Fig 3.1, Pool was the final stock of Sup35NM. While Sup35NM actually has a weight of ~30kDa it comes off at ~40kDa due to the guanidine salt present in the sample, which also distorts the bands. At each stage the purity of the Sup35NM

increased, leading to the purified protein in the collected fractions (12 and 13) and the pool, showing that a purified sample of Sup35NM C-terminal Hexa-His had been collected.

### 3.1.2 *De novo* fibril formation

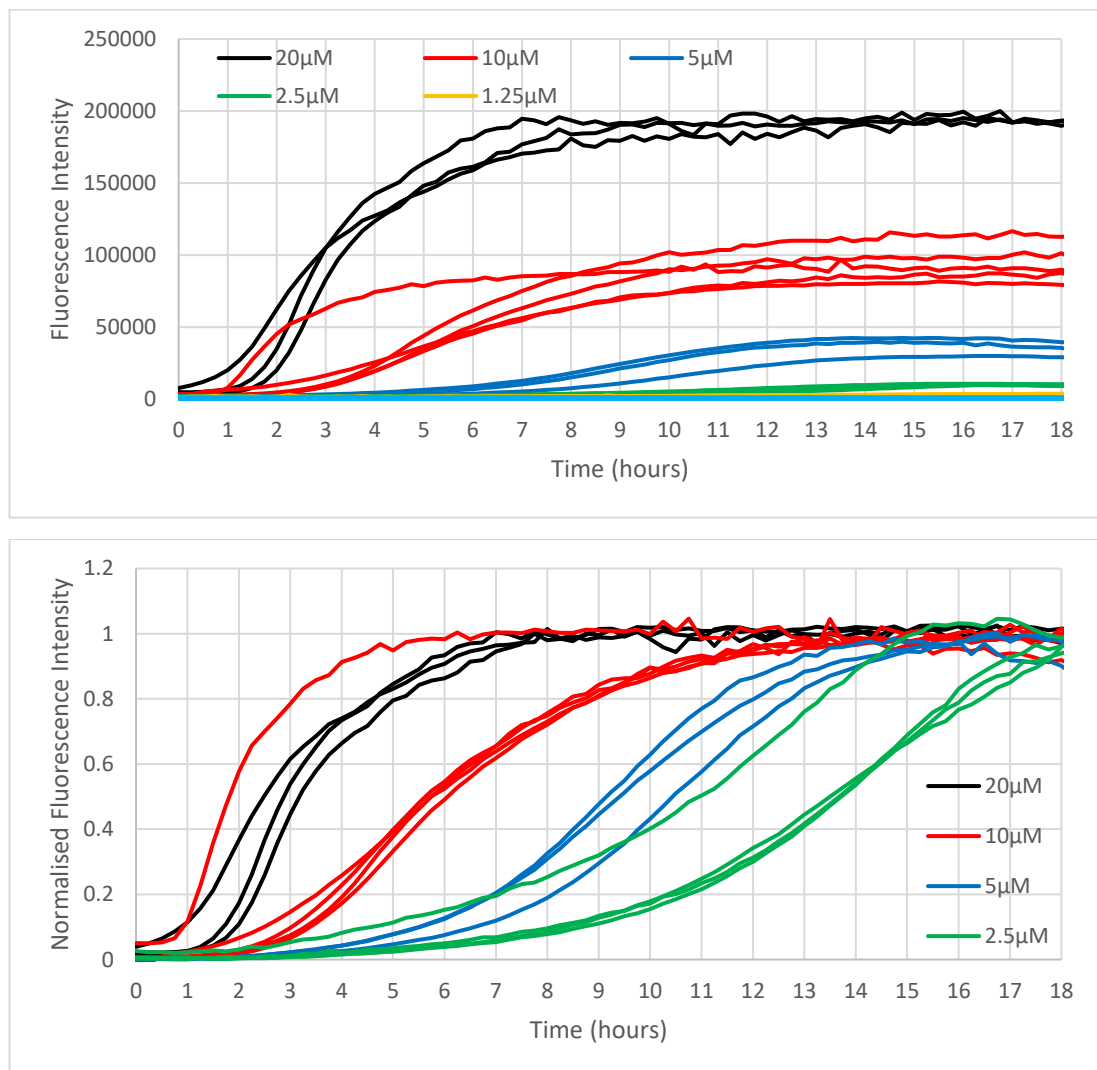


**Figure 3.3-Varying Sup35NM monomeric concentration in *de novo* fibril formation.** (Top) ThT fluorescence curves showing the effects of varying Sup35NM monomer concentration on *de novo* fibril formation and elongation as well as the same curves after being normalised (Bottom). Repeats were made of the SFFB control (cyan) as well as monomeric concentrations of 20 μM (black), 10 μM (red), 5 μM (blue), 2.5 μM (green) and 1.25 μM (orange)



Once Sup35NM had been confirmed to have been produced, the next stage was to form generation 1 (G1) fibrils, which are formed *de novo*, without seeding. The methodology for this is detailed in 2.4.1 and 2.4.2 with a series of concentrations being examined, which were 20 $\mu$ M, 10 $\mu$ M, 5 $\mu$ M, 2.5 $\mu$ M and 1.25 $\mu$ M. A SFFB and ThT control was used alongside these and the results of this assay can be seen in Fig 3.3. Each concentration in the assay produced a sigmoidal ThT fluorescence curve, but with varying characteristics. A major effect of halving the starting monomeric concentration was an approximately 50% reduction in the peak fluorescence intensity ~190000 for 20 $\mu$ M, ~90000 for 10 $\mu$ M and ~40000 for 5 $\mu$ M, indicating a 50% reduction in the total yield of final aggregated material for each successive reduction in monomer. The lag time was also extended by a reduction in monomeric concentration with the lag phase of 20 $\mu$ M lasting up to 1 hour, 10 $\mu$ M lasting until 1 to 3 hours and 5 $\mu$ M taking between 4 and 8 hours, showing that this not only increases the lag phase, but consequently increasing the variation in the length of it. The slope of the curves during the elongation phase was also reduced, indicating a reduction in the rate the aggregated material is being produced. The length of the elongation phase however was not extended much by the reduction in concentration, with the length of this staying between approximately 5 and 7 hours for each concentration. Due to the very low signal values of 1.25 $\mu$ M, it was chosen not to be normalised as this would lead to a very high signal to noise ratio.

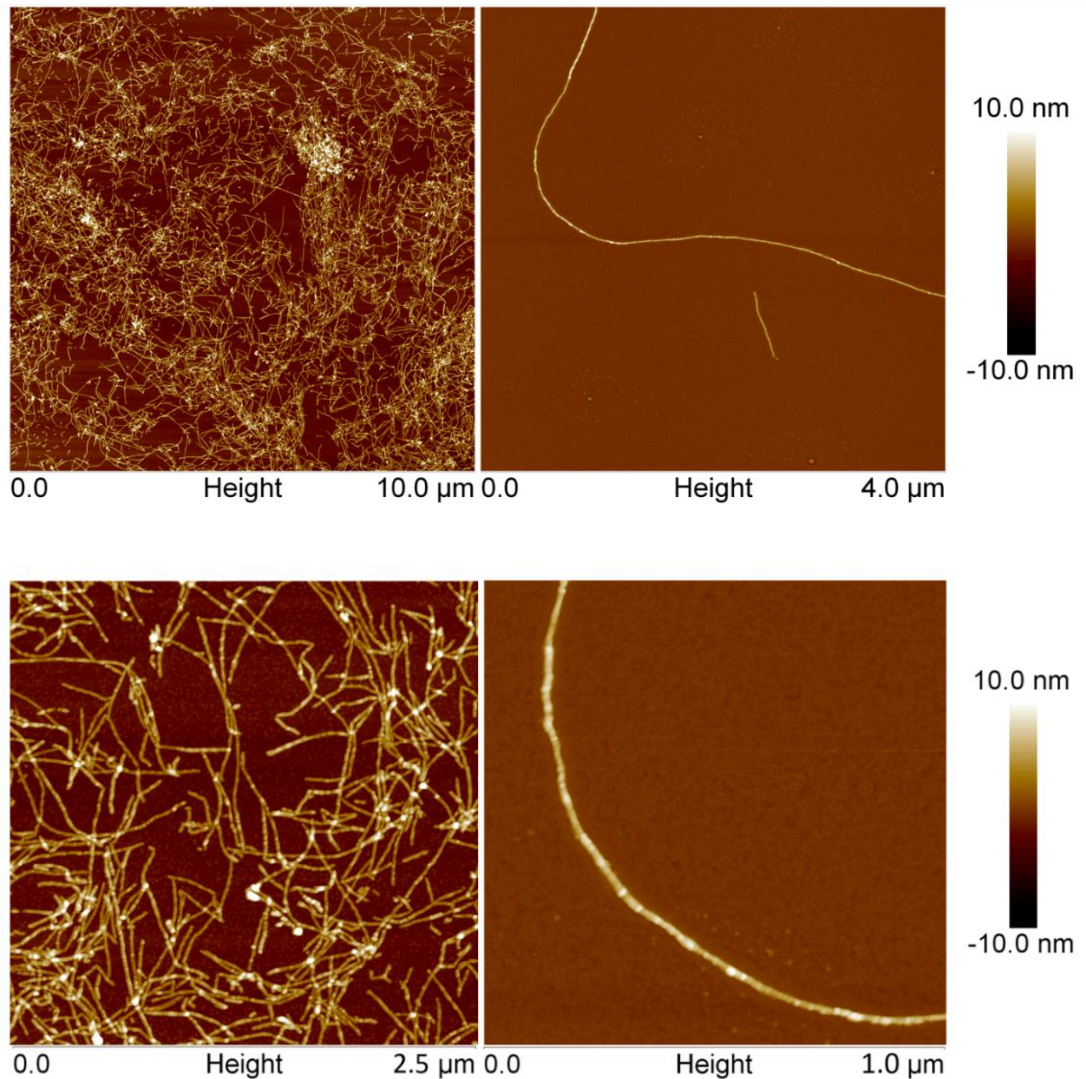


**Figure 3.4- AFM images of Sup35NM fibrils in the plateau phase.** These samples were produced *de novo* from 10 $\mu$ M of monomer. The top left image is 10 $\mu$ m x 10 $\mu$ m at a resolution of 2048 x 2048, whilst the top right is 4 $\mu$ m x 4 $\mu$ m with a resolution of 2048 x 2048, the scale bar shows this size and the height bar shows a range of 20nm from -10nm to +10nm in relation to the mica surface. The bottom images are 4x magnifications of the top images giving sizes of 2.5 $\mu$ m x 2.5 $\mu$ m and 1.0 $\mu$ m x 1.0 $\mu$ m for the left and right images respectively, with their resolutions being 512 x 512.

10 $\mu$ M was chosen to be used as the standard concentration from now on, this was due to the amount of aggregated material produced being relatively high and the fact that the lag phase, while varying, will last a couple of hours, giving more control over

seeding growth. AFM images were then produced using 10 $\mu$ M samples once they had fully reached the plateau phase, two of which can be seen in Fig 3.4. The lengths of the fibrils varied a high amount, possibly due to variation in the time taken for their primary nuclei to form, alternatively they could also have fragmented to some degree over the time they were growing. The formed fibrils clustered together to produce large aggregates (Fig 3.4 left image) that were impossible to analyse and would need to be fragmented significantly to produce the G1 seeds.

### 3.1.3 Fragmentation and quantifiable seed production

As a monomeric concentration of Sup35NM protein had been decided, the next stage was to produce seeds that would allow seeded assays to be performed. These seeds would have to create a large number of fibril ends, that elongation can occur from, to allow elongation to be measured while also allowing a controlled beginning of the elongation phase. The method used to produce these seeds is detailed in 2.5.1, whereby seeds were produced by pulse sonication, 5 seconds of sonication followed by 5 seconds of rest, at a set amplitude for a set time period. Initially, a high amplitude of 60% was chosen to fragment the fibrils (Fig 3.5), requiring a 20 second sonication to fragment the fibrils into particles with low sizes. These fibrils were then used to perform many of the seeding assays to optimise the conditions required for the time-dependent growth assays, the results of which are shown in 3.1.4

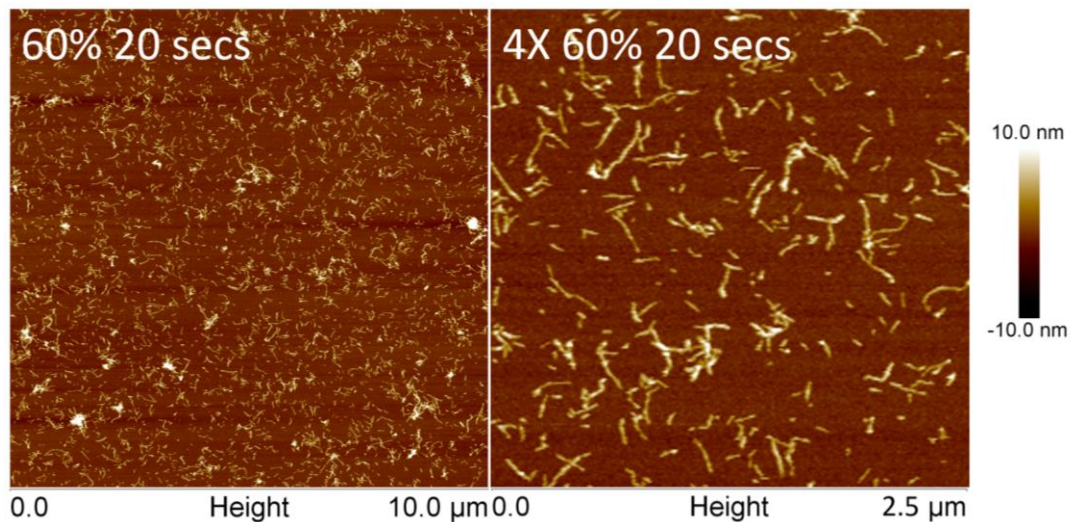


**Figure 3.5- AFM image of undiluted Sup35NM de novo fibrils after undergoing fragmentation at 60% amplitude for 20 seconds.** The left image is  $10\mu\text{m} \times 10\mu\text{m}$  at a resolution of  $1024 \times 1024$  and the right is a 4x magnification giving a  $2.5\mu\text{m} \times 2.5\mu\text{m}$  at a resolution of  $512 \times 512$ , the scale bar shows these, and the height bar shows a range of 20nm from -10nm to +10nm in relation to the mica surface.

As will be noted later in 3.1.4, problems were found to occur from the use of the low time and high amplitude strategy of seed production that had been used previously. Namely, seeds produced by this method varied in size dramatically, leading to issues caused by the varying number of particles that will be able to seed elongation. Even more importantly, variation in the starting size of seeds makes any subsequent measuring of elongation rates less accurate. This was shown to be an issue by the varying fibril lengths at all timepoints, as will be seen in 3.1.4. More disperse fibril samples could be made by growing the fibrils in a rotating lo-bind Eppendorf (see appendices 1. & 2.), which aided both in imaging and fragmentation.

For the above reasons the method needed to be modified, leading to the conclusion that a slower and longer fragmentation would give more control and fragment the fibrils more evenly over time, leading to particles of more similar sizes.

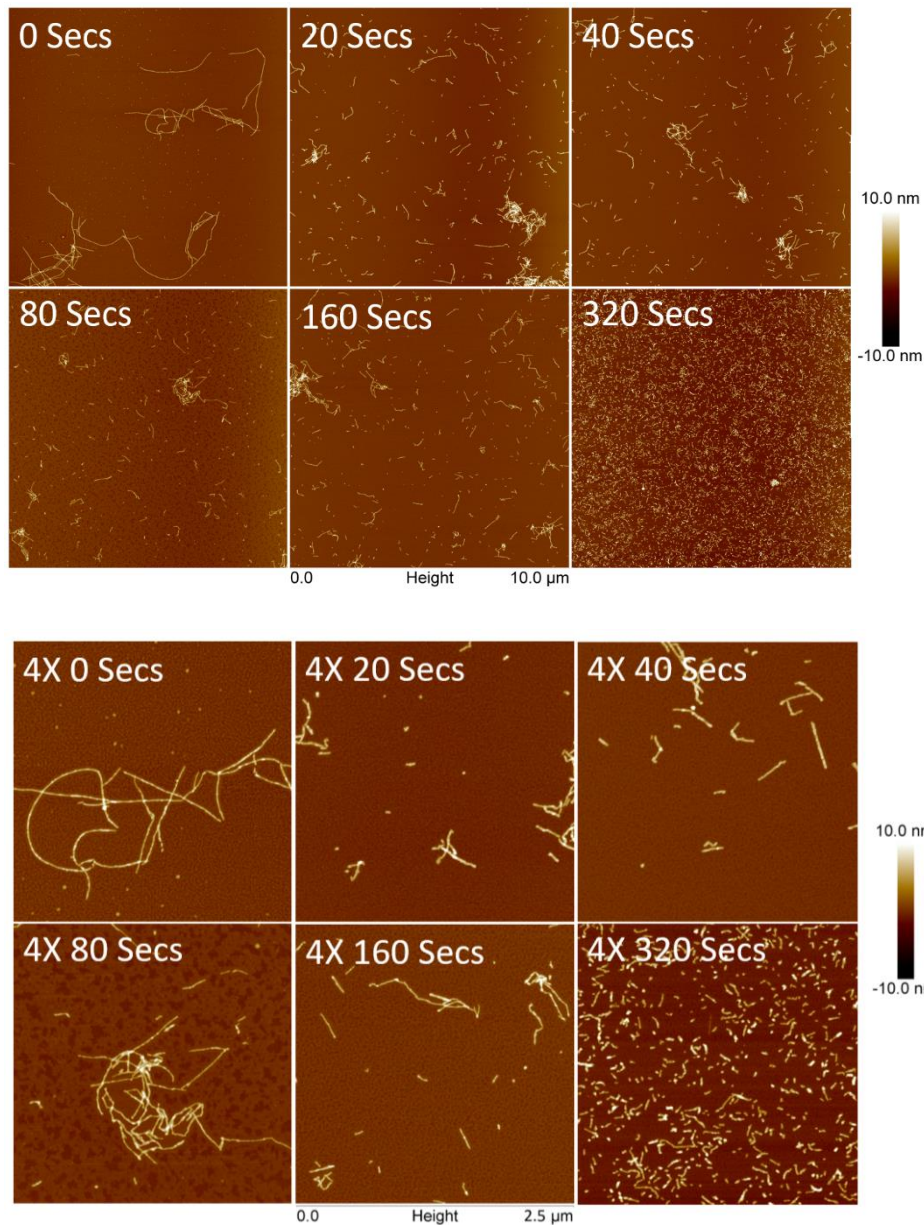


**Figure 3.6- Sup35NM fragmentation assay.** This series of AFM images shows Sup35NM de novo fibrils after undergoing successive fragmentation at an amplitude of 20%. The time points imaged at were after 0, 20, 40, 80, 160 and 320 seconds of pulse sonication (5 seconds on and 5 seconds off, the time is total time and not including resting time). Due to the high density of the particles, the samples were diluted to 1 in 5 prior to being prepared for AFM imaging. The top series of images are 10 $\mu$ m x 10 $\mu$ m at a resolution of 2048, the scale bar shows this size and the height bar shows a range of 20nm from -10nm to +10nm in relation to the mica surface. The bottom series are a 4x magnification of the top series, giving sizes of 2.5 $\mu$ m x 2.5 $\mu$ m at a resolution of 512 x 512.

A methodology which was combined with the more dispersed fibrils produced in a lo-bind Eppendorf. This led to lowering the sonication amplitude to the lowest amplitude of 20% and producing a sonication series where the fibrils were subjected to a doubling time of sonication. The results of this are shown in Fig 3.6. At the lower timepoints the aggregated material varied in size significantly but progressively were reduced in size, causing them to become similar in size over time. The result was that by 320 seconds, a very large number of small seeds were produced with the variation in their sizes being reduced. This was found to be repeatable and due to this consistency was chosen as the method of seed production for the time-dependent assays measuring elongation (results can be seen in 3.1.5).

#### 3.1.4 Use of seeding to explore elongation

Produced by the initial seed forming methodology of 60% amplitude for 20 seconds, 1 $\mu$ l of seeds with a monomeric concentration of 5 $\mu$ M were added to 100 $\mu$ l of varying monomer concentration. The results of this can be seen in Fig 3.7. Similarly to the *de novo* fibril formation assays, halving the monomeric concentration lead to an approximately 50% reduction in final fibril yield. The addition of the seeds removed the lag phases of each concentration leading to their plateau phases beginning at similar times of ~5 hours for 20 $\mu$ M and 10 $\mu$ M, with the remainder being slightly longer. This gave elongation phases approximately equal to those seen in the *de novo* assays. While the elongation phases were a similar length, the initial rate followed the 50% reduction shown by the fibril yield. This assay lead to the continuation of 10 $\mu$ M as the standard concentration for both *de novo* and seeded assays for

Sup35NM. Due to the very low signal values of 1.25 $\mu$ M, it was chosen not to be normalised as this would lead to a very high signal to noise ratio.

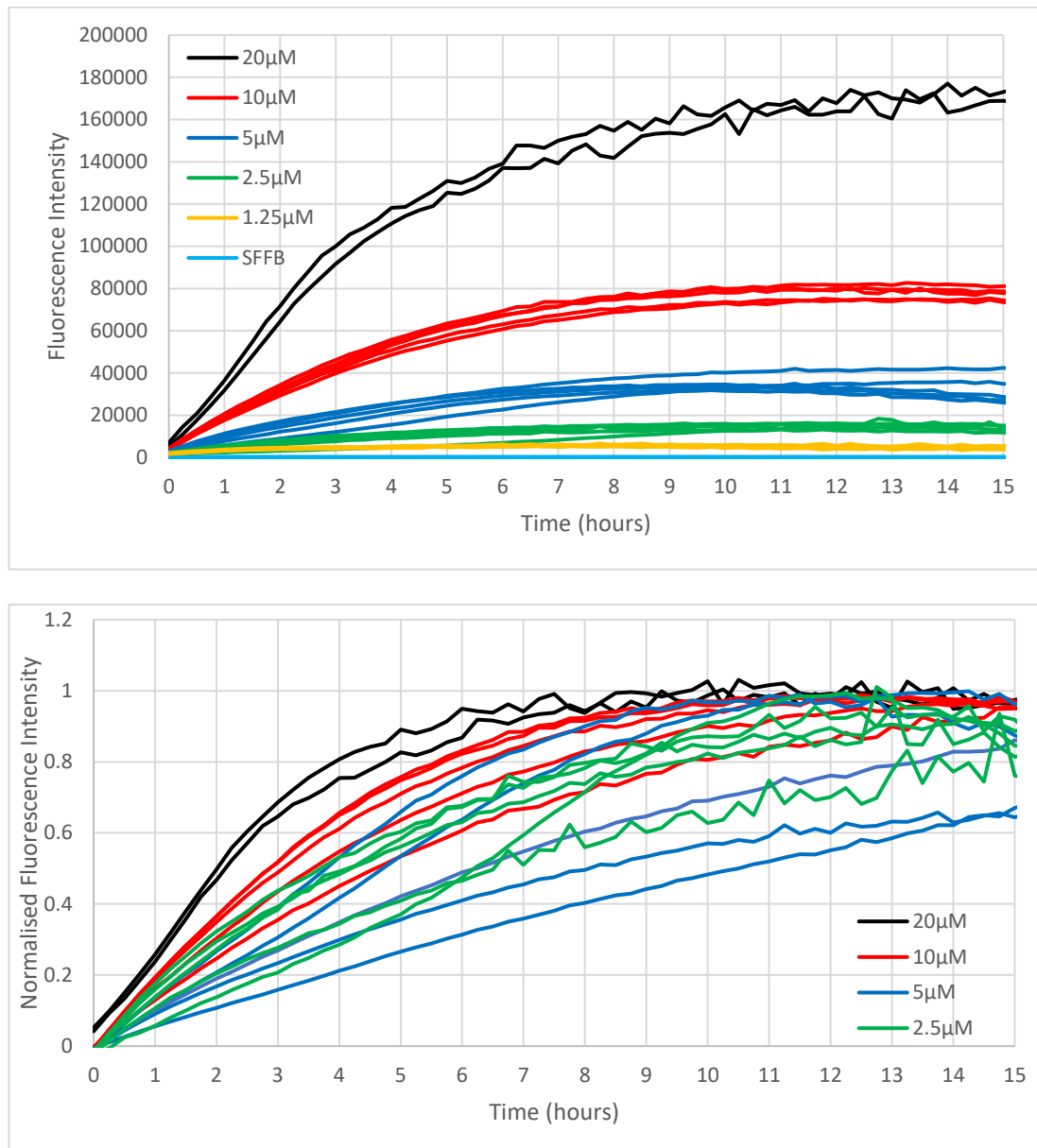


**Figure 3.7- Varying Sup35NM monomeric concentration in seeded fibril formation.** (Top) ThT fluorescence curves showing the effects of varying Sup35NM monomer concentration on seeded fibril formation and elongation as well as the same curves after normalisation (Bottom). Growth was seeded by the addition of 1 $\mu$ l of seeds with a monomeric concentration of 5 $\mu$ M. Repeats were made of the SFFB control (cyan) as well as monomeric concentrations of 20 $\mu$ M (black), 10 $\mu$ M (red), 5 $\mu$ M (blue), 2.5 $\mu$ M (green) and 1.25 $\mu$ M (orange).

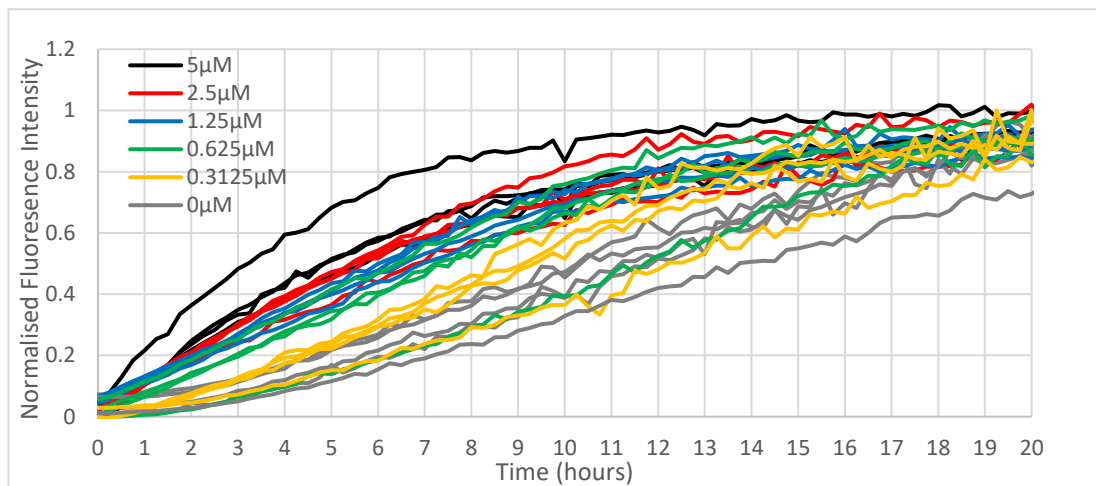
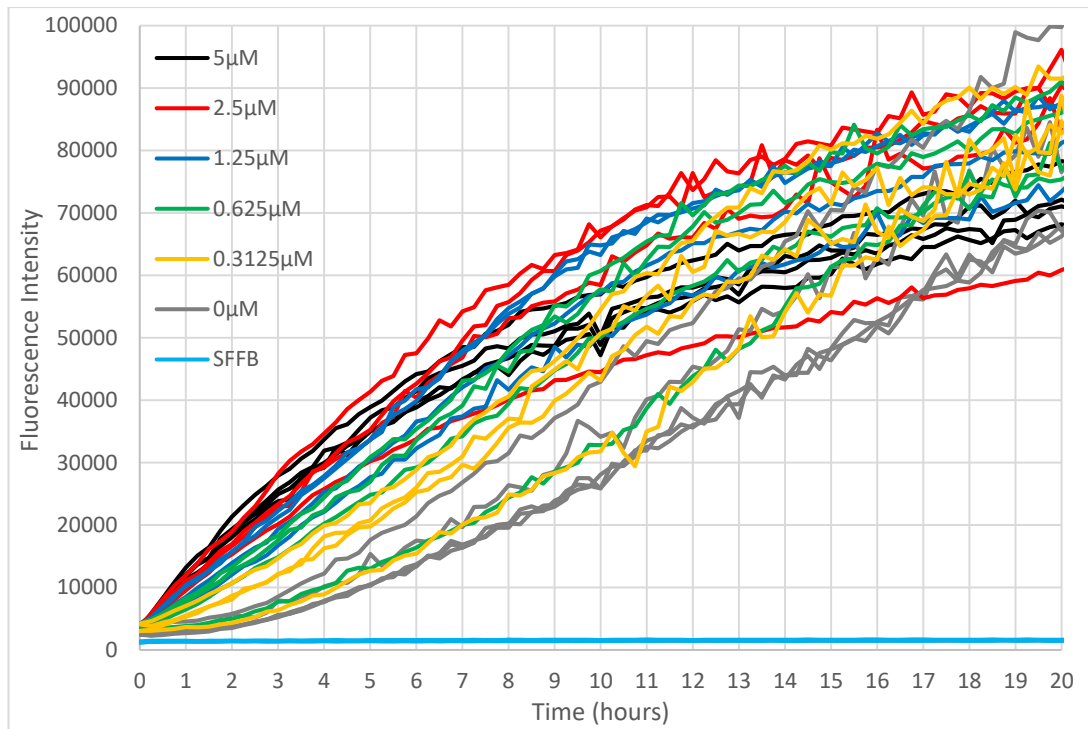


**Figure 3.8- Effects of varying Sup35NM seed concentration.** (Top) ThT fluorescence curves showing the effects of varying Sup35NM seed concentration on fibril formation and elongation as well as the same curves after being normalised (Bottom). Growth was seeded by the addition of  $1\mu\text{l}$  of seeds with a varying monomeric concentration to  $100\mu\text{l}$  of  $10\mu\text{M}$  monomeric protein. Repeats were made of the SFFB control (cyan) as well as seeds with monomeric concentrations of  $5\mu\text{M}$  (black),  $2.5\mu\text{M}$  (red),  $1.25\mu\text{M}$  (blue),  $0.625\mu\text{M}$  (green),  $0.3125\mu\text{M}$  (orange) and  $0\mu\text{M}$  (grey).

To measure the initial elongation rate in the time-dependent assays, the lag phase must be completely eliminated. This led to varying the seed concentration to



ascertain what range of concentrations fulfilled this condition. Increasing the monomeric concentration of the seeds increases the initial growth rate (Fig 3.8). The lowest seed concentration of  $0.3125\mu\text{M}$  was only slightly faster initially than the *de novo*, giving while reduced a definite lag phase. This would continue to improve with every doubling concentration. The lag phase was eliminated by  $5\mu\text{M}$ , with the initial rates suggesting the start of the elongation phase at time 0. Due to this reason  $5\mu\text{M}$  ( $\sim 0.5\%$  of total monomers) was chosen to be a minimum for eliminating lag phase in later assays.

Now that ranges of seeds and monomeric concentration had been established, the next stage was to find a timeframe after seeding to allow imaging of elongation over time. 4 and 8 hours were chosen based on the seeded assays shown in Fig 3.7 & 3.8. The AFM images shown in Fig 3.9 are the results of stopping elongation at 4 and 8 hours. Even after 4 hours, fibrils of increased lengths were present. To image these fibrils in their entirety would require a significant increase in the size of the sample area which would lead to a loss of resolution of the image. By 8 hours the numbers of these increased length fibrils had increased significantly as expected for the start of the plateau phase. These images highlighted three problems with the current methodology. Firstly, the fibril lengths were significantly too long to be used for elongation assays at 4 hours, as to maintain resolution sample size should be kept at  $10\mu\text{M}$ . Secondly, the number of fibrils per image was extremely low, reducing the validity of data obtained from the pictures. Finally, fibril length while high, also varied drastically.

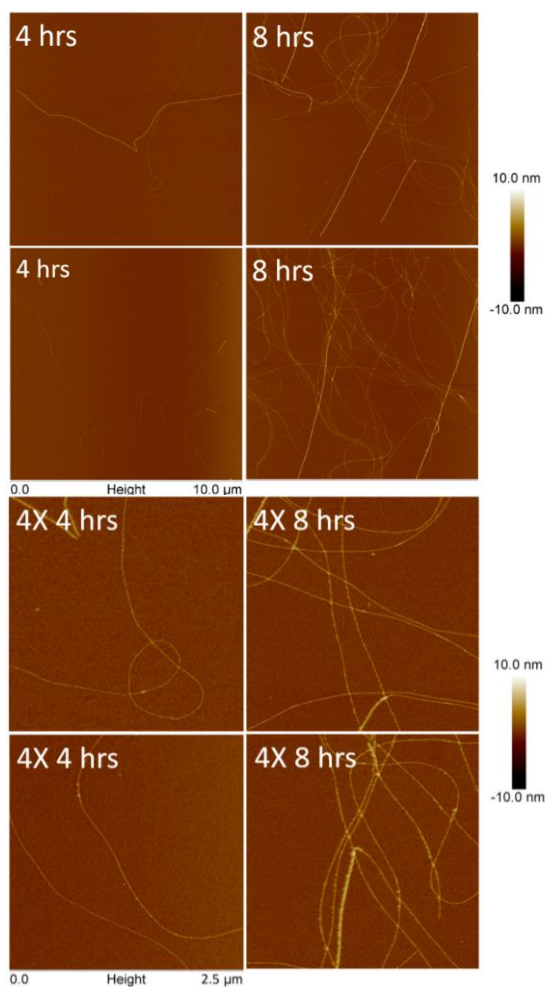


**Figure 3.9- Elongation of Sup35NM after 4 and 8 hours.** AFM images of two undiluted Sup35NM seeded fibril samples (top and bottom) formed using  $10\mu\text{M}$  monomer and  $1\mu\text{l}$  of  $5\mu\text{M}$  monomeric concentration seeds at 4 and 8 hours after seeding. The top four images are  $10\mu\text{m} \times 10\mu\text{m}$  at a resolution of  $1024 \times 1024$ , the scale bar shows this size and the height bar shows a range of  $20\text{nm}$  from  $-10\text{nm}$  to  $+10\text{nm}$  in relation to the mica surface. The bottom four are a 4x magnifications of the top four, giving sizes of  $2.5\mu\text{m} \times 2.5\mu\text{m}$  at a resolution of  $512 \times 512$ .

To resolve the time issue, an earlier time point was decided to be used and as elongation can be seen in the fluorescence curves very early it was decided 10 minutes would be trialled. The other two issues were results of the seed production method, namely the fast 60% amplitude one. There needed to be more seeds to increase the numbers of fibrils and the seeds also needed to be of a more similar

length to reduce the effect their variation has on fibril length. This led to the refinement of the seeding methodology (section 3.1.3), whereby a smaller amplitude over a longer time leads to more controlled fragmentation and increases the particle number as they will be more consistently of a small size. Also, these images showed two distinct widths of fibrils which could potentially be separated protofilaments and fibrils, which was not present in the *de novo* assays. This is described in more detail in section 3.3 below. Due to their varying lengths this could suggest that elongation can occur in both separated protofilaments, that will subsequently associate together to form fibrils, as well as by fibrils extending themselves.

Using the refined seeding methodology, the effect of varying seed concentration was investigated again with higher concentrations being used to further increase the number of particles able to be imaged. Instead of using concentrations a ratio of monomers in seeds to monomers was used to allow a standard volume of 100 $\mu$ l to be used. In Fig 3.10, similar to the results shown in Fig 3.8, increasing the ratio of the seeds increased the initial growth rate. All seeded assays had a significantly increased rate of elongation in comparison to unseeded, giving a range of 2-5 hours depending on the ratio used. Even at 1% there were sufficient seeds to eliminate the lag phase, as was suggested in the previous assay. 5% was only slightly lower than 10% in the normalised curves suggesting that a seeding limit had been reached by 10% and that 5% may be just below this limit. For this reason, alongside completely eliminating the lag phase and having a high number of particles, 5% was chosen to be the seeding percentage to be used in elongation assays. A lower percentage could have been used for Sup35NM, but there are limitations on this system caused by  $\alpha$ -synuclein that will be elaborated on in 3.2.5.

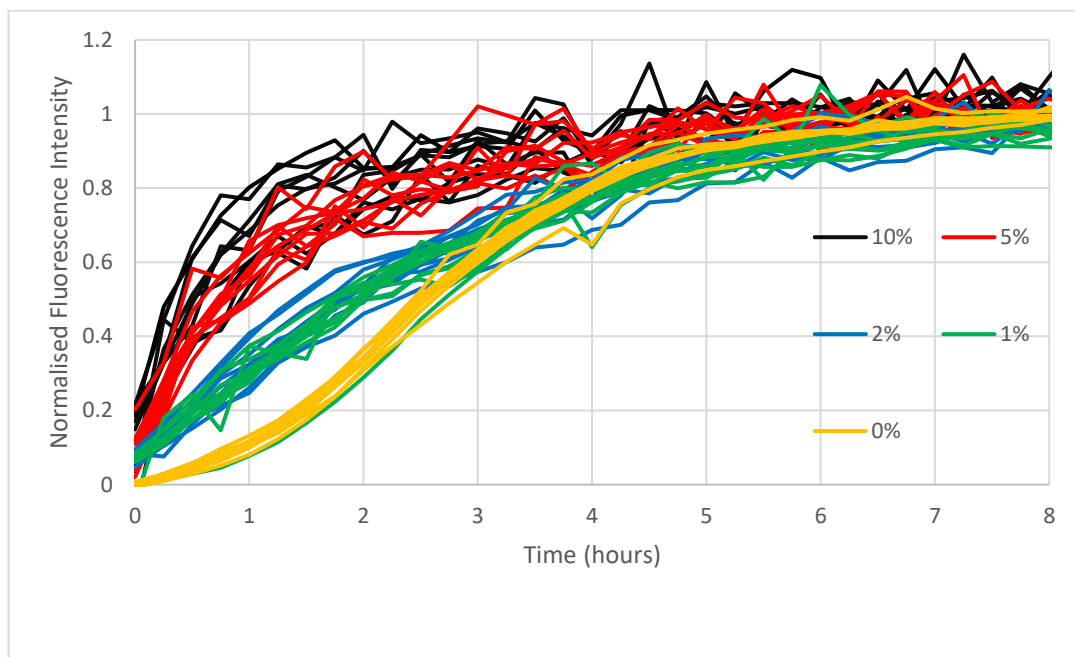
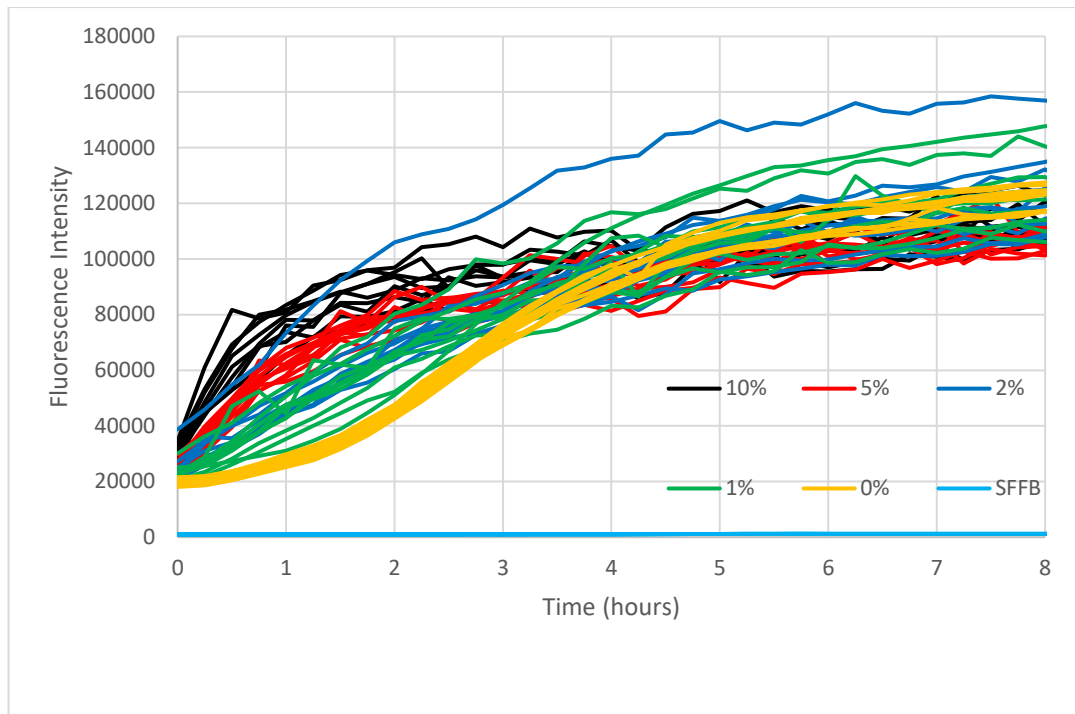


**Figure 3.10- Seeding Sup35NM with high seed percentages.** (Top) ThT fluorescence curves showing the effects of varying Sup35NM seed concentration on fibril formation and elongation as well as the same curves after being normalised (Bottom). Growth was seeded by the addition of  $10\mu\text{M}$  seeds with varying volume to make the desired ratio of seeds to monomeric protein, total volume is the same. Repeats were made of the SFFB control (cyan) as well as seeds with ratios of 10% (black), 5% (red), 2% (blue), 1% (green) and 0% (orange).

### 3.1.5 Time-dependent imaging assay

Given the results of the seeded assays in 3.1.4, a monomeric concentration of  $10\mu\text{M}$  was chosen with seeds making up 5% of the total, with the seeds being generation 1 (G1) fibrils that were fragmented by pulse sonication for 320 seconds at an amplitude of 20%. As mentioned in 3.1.4, this seed to monomer ratio was chosen due to the limitations caused by  $\alpha$ -synuclein that will be explained in 3.2.5. The time frame chosen for measuring elongation was 10 minutes, as it was determined to be an early time where elongation can be seen clearly. Due to the high particle density this produces, the samples were diluted to 1 in 5 using SFFB prior to deposition on the mica for AFM imaging.

The results of these conditions are shown in Fig 3.11, with the seeds produced in the fragmentation assay in 3.1.3 being used to seed the reaction. Even after 10 minutes, elongation had occurred to varying degrees. In the centre of each of the seeded systems there was a region of increased height, likely being the seeds, as this is where the fibrils seem to originate. The fact that each of these sections is producing multiple fibrils suggests either that multiple seeds were aggregating together prior to seeding fibrils or seeds are able to seed multiple fibrils at a time. Regarding the fibrils' length distribution, the majority were approximately  $\sim 1\mu\text{m}$  in length or less, assuming an origin at the region of increased height. Some of the fibrils however do have a length significantly longer, at up to approximately  $2.5\mu\text{m}$ , with a rare few going even further. There were additionally some smaller species that can either be fragments of newly formed fibrils or seeds that have not elongated or are just elongating slower.

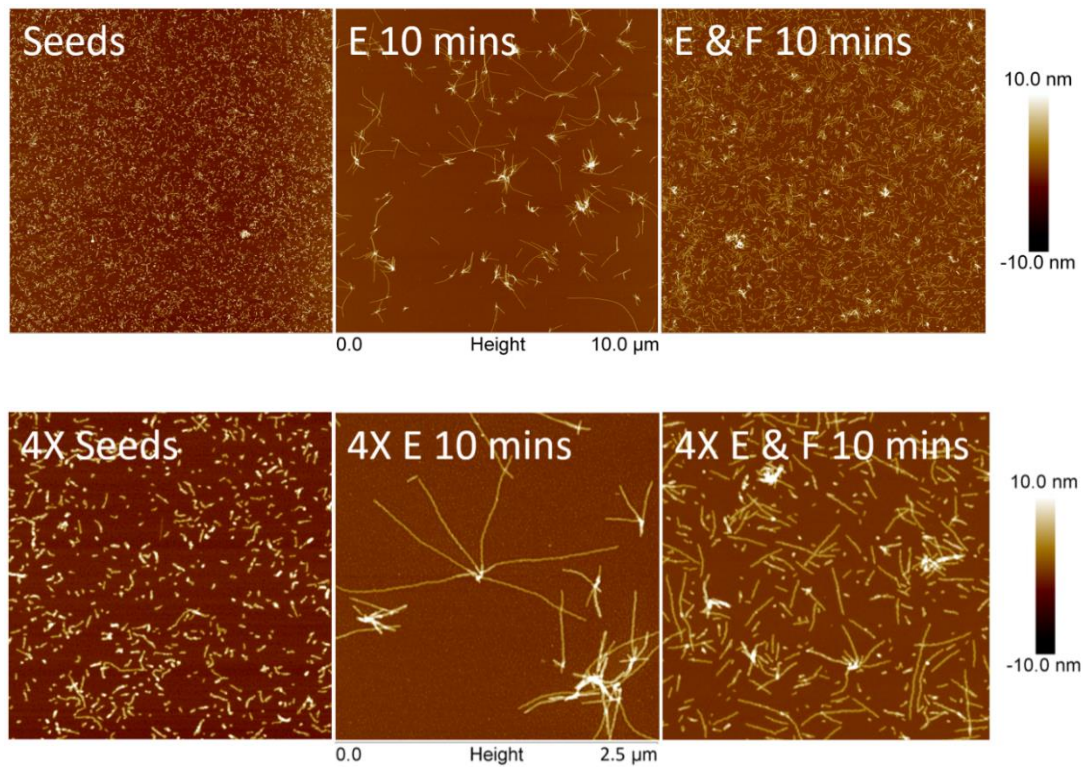


**Figure 3.11- Sup35NM time-dependent elongation assay.** This series of AFM images shows Sup35NM generation 1 (G1) seeds at different timepoints. The seeds were prepared for AFM imaging prior to addition of monomer and the elongation (E) and elongation and fragmentation (E & F) were diluted and deposited onto the mica 5 minutes after the seeds were added to the monomer and were washed 5 minutes later. Sample E was left undisturbed during the 10 minutes while the E & F sample was sonicated for a 1 second pulse every 30 seconds (29 seconds of rest) prior to deposition. Due to the high density of the particles, the samples were diluted to 1 in 5 prior to being deposited for AFM imaging. The top series of images are 10μm x 10μm at a resolution of 2048, the scale bar shows this size and the height bar shows a range of 20nm from -10nm to +10nm in relation to the mica surface. The bottom series are a 4x magnification of the top series, giving sizes of 2.5μm x 2.5μm at a resolution of 512 x 512.

To explore the effects of fragmentation alongside elongation, the time-dependent assay was repeated with the addition of a relatively low amount of sonication during the first 5 minutes, until deposition. The sample was pulse sonicated at a rate of 1 second out of every 30 with an amplitude of 20%. This led to a total of 10 seconds of

20% amplitude sonication during the first 5 minutes after seeding. The effects of this are shown in sample E & F of Fig 3.11. The particle density, even with 5 times dilution, was very high. While these particles were smaller than those produced by just elongation, there was a much higher yield of aggregated material due to their very high numbers. The actual sizes of the particles appeared to be of a range between the majority of the elongation only samples ( $\sim 1\mu\text{m}$ ) and the original seeds.

## 3.2 $\alpha$ -synuclein

### 3.2.1 Protein expression and purification

Similarly to Sup35NM, before any assays involving fibril formation could occur, the protein that was used as the stock of monomeric protein had to be generated. For  $\alpha$ -synuclein, this involved growing the *E. coli* strain shown in 2.1.9 and expressing the protein, before purification.

The output of the first Äkta stage used in the later stages of the expression and purification of  $\alpha$ -synuclein, where it was purified using ion exchange chromatography are shown in Fig 3.1. The fractions selected for the peak were 16-21, leading to these being collected and combined to form the protein pool, which was then used as the source of monomeric protein for the growth assays. The pool was snap frozen as 1ml aliquots to allow for storage until required.

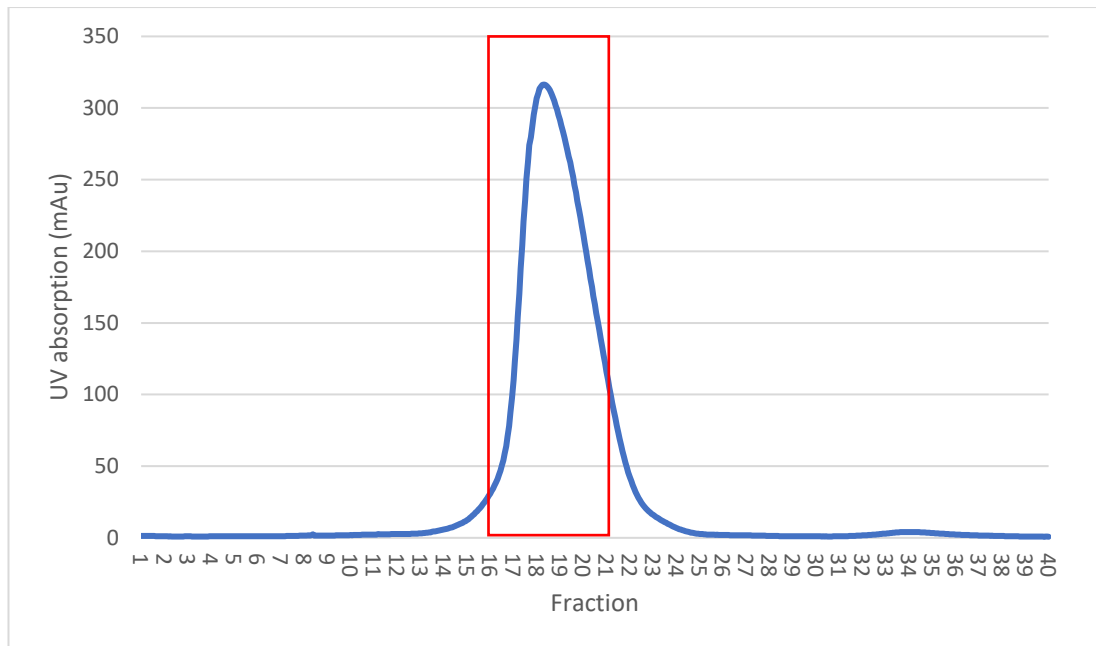


**Figure 3.12-  $\alpha$ -synuclein ion exchange chromatography.** UV absorption trace of the fractions produced by performing ion exchange chromatography on the  $\alpha$ -synuclein eluate. The region selected for collection to produce the  $\alpha$ -synuclein pool is highlighted with a red box and corresponds to fractions 16-21.

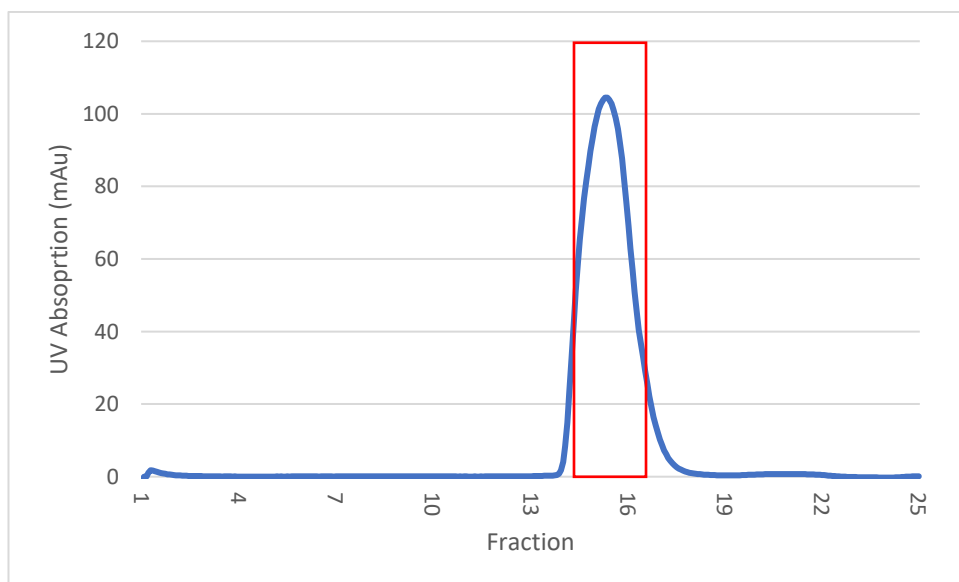


**Figure 3.13-  $\alpha$ -synuclein gel filtration chromatography.** UV absorption trace of the fractions produced by performing gel filtration chromatography on the  $\alpha$ -synuclein eluate. Fraction 15 was the fraction that would be used for the growth assays, but fraction 16 and 17 were also collected and used separately.



When monomeric protein was required for growth assays it was thawed and prepared for a second ÄKTA controlled column, in the final step of the purification. Results of one of the gel filtrations are shown in 3.13, with the collected peaks being shown. Fraction 15 of this specific peak corresponds to the monomer that was added to the seeds to run the elongation assay in 3.2.5. Fractions 15, 16 and 17 were chosen to be used separately due to the shoulder on the peak as well as the fact that only fraction 15 formed fibrillar aggregates in the *de novo*, with the other two forming amorphous aggregates.

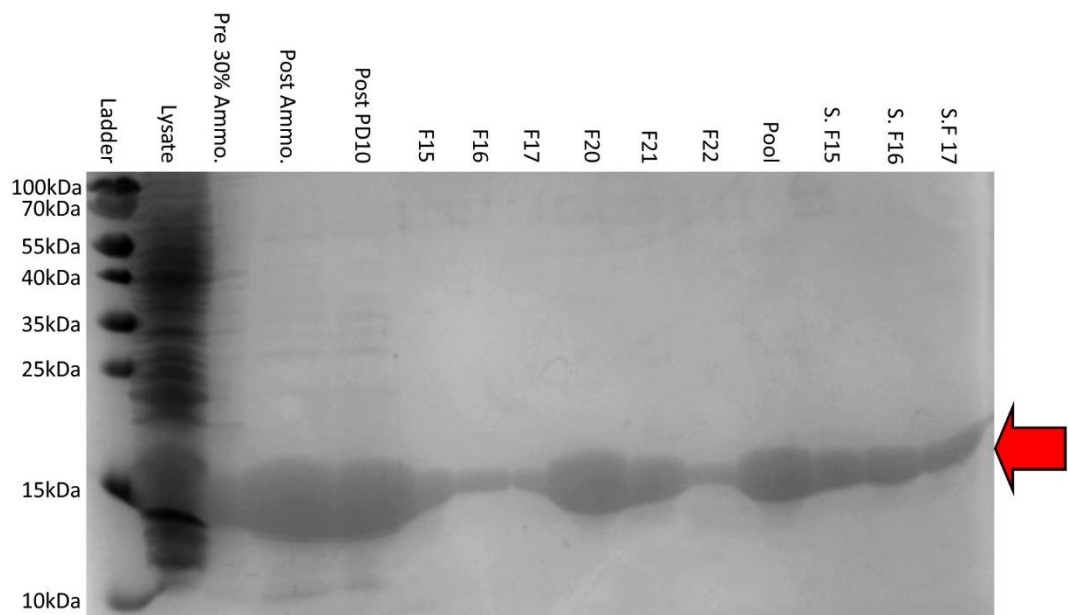


**Figure 3.14-  $\alpha$ -synuclein SDS PAGE gel.** These are the results of running a 15% SDS PAGE gel on samples collected from across the purification of  $\alpha$ -synuclein. The samples are: Ladder, Lysate, Pre 30% Ammonium Sulfate Precipitation, Post Ammonium Sulfate Precipitation, Fraction 15, Fraction 16, Fraction 17, Fraction 20, Fraction 21, Fraction 22, Pool, Second Stage Fraction 15, Second Stage Fraction 16 and Second Stage Fraction 17. The highlighted band corresponds to  $\alpha$ -synuclein.

To confirm the presence of  $\alpha$ -synuclein at all stages of the purification a 15% SDS PAGE gel was ran using samples collected at key points, with the results of this being shown in Fig 3.14. The samples collected were: Lysate was collected after sonication of the sample initially, Pre 30% Ammonium Sulfate Precipitation was the sample prior to the first stage of the ammonium sulfate precipitation, Post Ammonium Sulfate Precipitation was the sample after the final stage of the ammonium sulfate precipitation, Post PD10 was the sample eluted from the PD10 column that was added to the ÅKTA for ion exchange chromatography, F15, 16, 17, 20, 21 and 22 were fractions corresponding to the peak from the ion exchange chromatography (Fig 3.12); Pool was the stock of  $\alpha$ -synuclein frozen before gel filtration, Second stage Fractions 15, 16 and 17 were the collected fractions from the gel filtration stage (Fig 3.13). The molecular weight of  $\alpha$ -synuclein is  $\sim 15$ kDa, which corresponds to the most prominent band shown by the samples from across the purification methodology performed. All other proteins present in the early stages of the purification were removed before the collection of fractions to make the pool, showing that  $\alpha$ -synuclein had been purified significantly before this stage.

### 3.2.2 De novo fibril formation

Similar to with Sup35NM in 3.1.2, once the protein had been purified the next stage was to form *de novo* G1 fibrils. Due to the large lag time of  $\alpha$ -synuclein, as high a concentration of monomer as possible was used, i.e.  $60\mu\text{M}$ , which formed fibrils after approximately 2 weeks. The resulting fibrils were then diluted down to the standard monomeric concentration of  $10\mu\text{M}$  for use in the seeding assays. This allowed

comparisons to be made with Sup35NM, and AFM images of these are shown in Fig 3.15. When diluted to 10 $\mu$ M, the density of aggregated material was significantly lower than the same concentration of Sup35NM *de novo*. The lengths varied somewhat, but on average they were significantly shorter than those formed by Sup35NM. They also clustered together, but instead of forming very large networks like Sup35NM, the fibrils bundled together leading to multiple smaller aggregates being produced. The fibrils were also relatively straight, suggesting they are less flexible than those produced by Sup35NM. There was also potentially some twisting that can be seen in Fig 3.15 (right), but if so is of a very large periodicity of approximately 1 $\mu$ m.

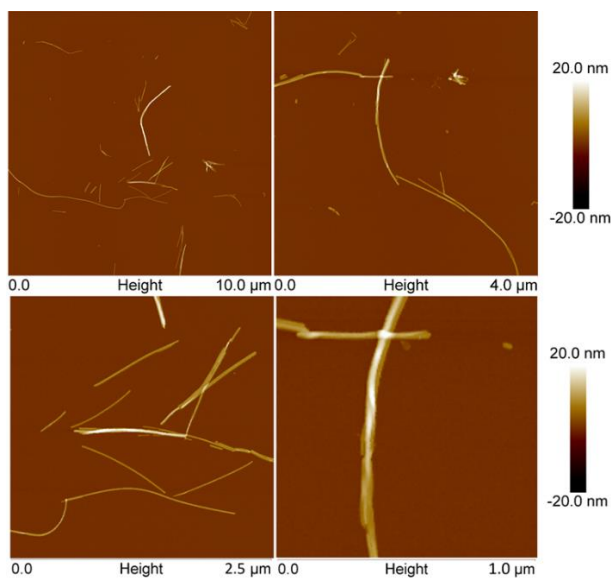


**Figure 3.15- AFM images of  $\alpha$ -synuclein fibrils in the plateau phase.** The samples were produced *de novo* from 60 $\mu$ M of monomer before being diluted to 10 $\mu$ M once fibrils were formed. The top left image is 10 $\mu$ m x 10 $\mu$ m at a resolution of 2048 x 2048, whilst the top right is 4 $\mu$ m x 4 $\mu$ m with a resolution of 2048 x 2048, the scale bar shows this size and the height bar shows a range of 20nm from -10nm to +10nm in relation to the mica surface. The bottom images are 4x magnifications of the top images giving sizes of 2.5 $\mu$ m x 2.5 $\mu$ m and 1.0 $\mu$ m x 1.0 $\mu$ m for the left and right images respectively, with their resolutions being 512 x 512.

### 3.2.3 Fragmentation and quantifiable seed production

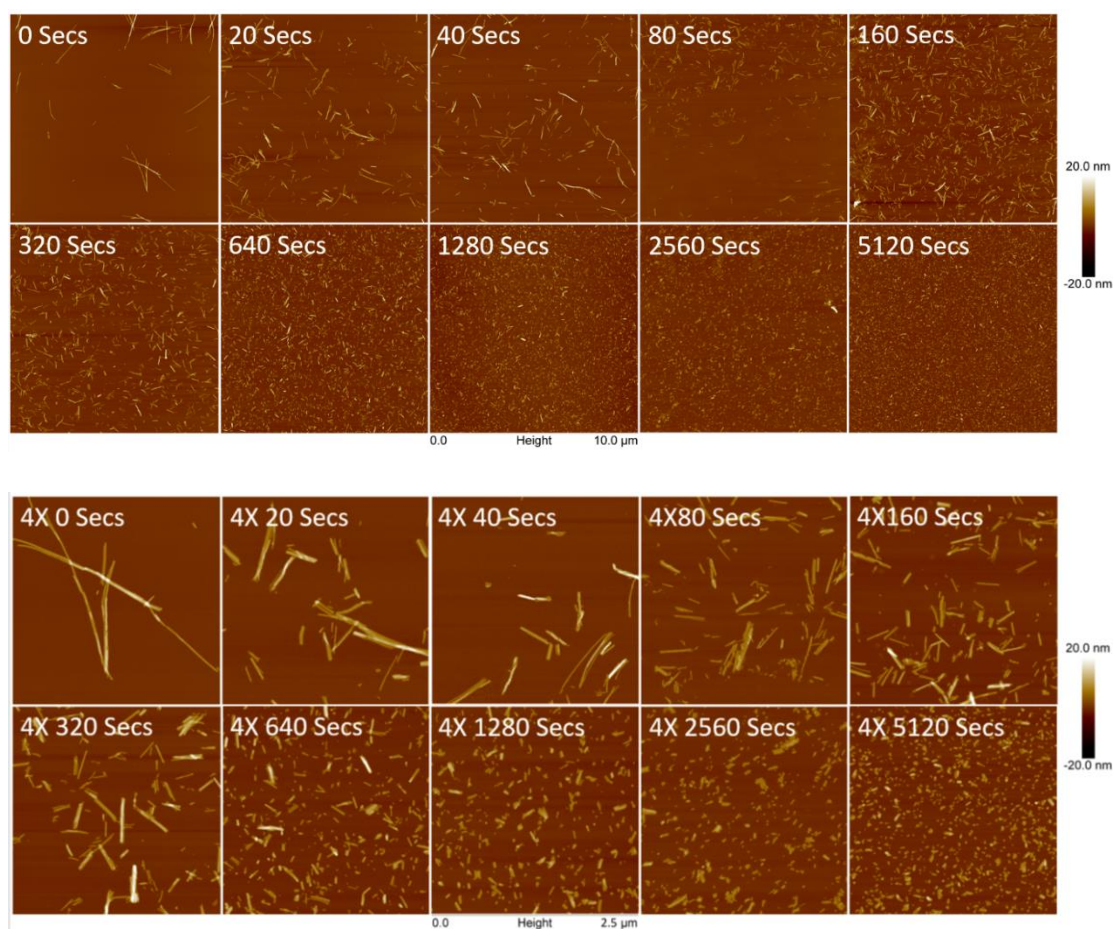


**Figure 3.16-  $\alpha$ -synuclein fragmentation assay.** This series of AFM images showing  $\alpha$ -synuclein *de novo* fibrils after undergoing successive fragmentation at an amplitude of 20%. The time points imaged at were after 0, 20, 40, 80, 160, 320, 640, 1280, 2560 and 5120 seconds of pulse sonication (5 seconds on and 5 seconds off, the time is total time and not including resting time). The top series of images are 10 $\mu\text{m}$  x 10 $\mu\text{m}$  at a resolution of 2048, the scale bar shows this size and the height bar shows a range of 20nm from -10nm to +10nm in relation to the mica surface. The bottom series are a 4x magnification of the top series, giving sizes of 2.5 $\mu\text{m}$  x 2.5 $\mu\text{m}$  at a resolution of 512 x 512.

As with Sup35NM, the next stage after attaining *de novo* fibrils was the production of seeds that would allow for seeded growth to be performed. Using the method detailed in 2.5.2, the 10 $\mu\text{M}$  monomeric concentration fibrils were fragmented by pulse sonication, 5 seconds sonicating followed by 5 seconds of rest, at an amplitude

of 20% for a doubling length of time beginning with 20 seconds of total time sonicating. This method was chosen to allow a direct comparison of the ease of fragmentation of Sup35NM to  $\alpha$ -synuclein. The sonication series resulting from this can be seen in Fig 3.16. At lower timepoints there is significant heterogeneity in the sizes of the particles, which is gradually reduced as their sizes became more uniform later in the series. By 5120 seconds nearly every particle is of a similarly small size, reducing the possibility of the issues seen with the Sup35NM seeds formed by 60% amplitude sonication. This series highlights that  $\alpha$ -synuclein takes significantly longer to fragment under the same conditions from shorter starting fibrils to a similar size to the seeds that were produced by Sup35NM after only 320 seconds of sonication.

#### 3.2.4 Seeded assay

Once seeds had been produced, identifying a suitable seed monomeric percentage was required. This led to seeding 10 $\mu$ M monomer with a range of seed concentrations, where the seeds were produced by 5120 seconds of sonication as in 3.2.3. The results of this can be seen in Fig 3.17. Even a ratio with 1% seeds is sufficient to eliminate the lag time seen in the *de novo* fibril formation, which in combination with the long lag time of the *de novo* means the start of the elongation phase can be easily controlled. This suggests that the ratio required to eliminate the lag phase is lower than this. Increasing the ratio of seeds to monomers causes the initial rate of increase of fluorescence intensity to rise, with them all following an approximately proportional increase in rate and percentage. While the initial rates and the time to reach the plateau phase vary, the plateau phase begins when a

fluorescence intensity of  $\sim 2 \times 10^5$  is reached, suggesting this is nearing the peak fibril yield. These results suggest an elongation phase time range between 8 and 40 hours in length depending on the seed ratio used.

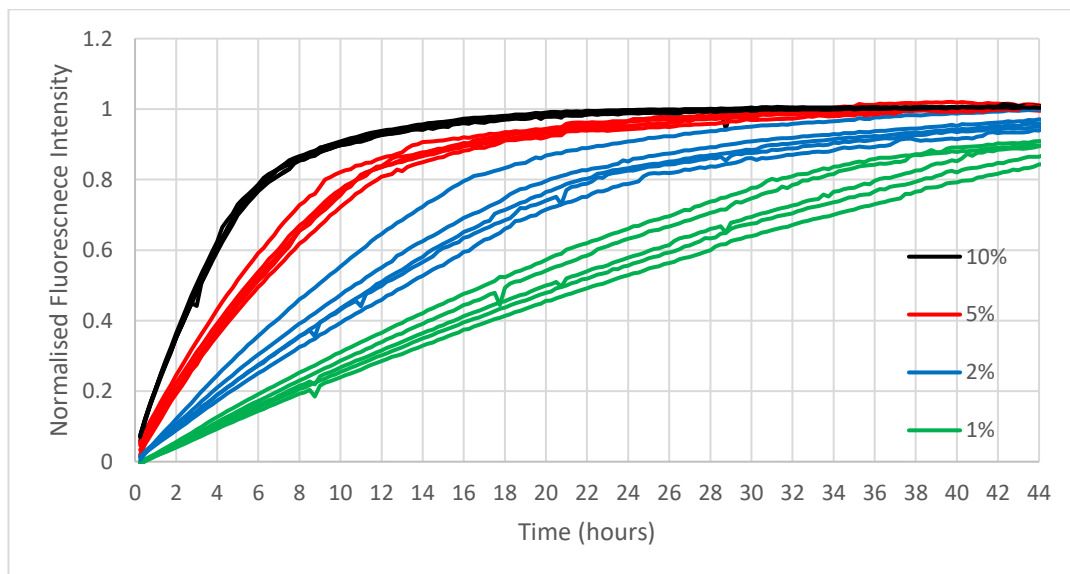
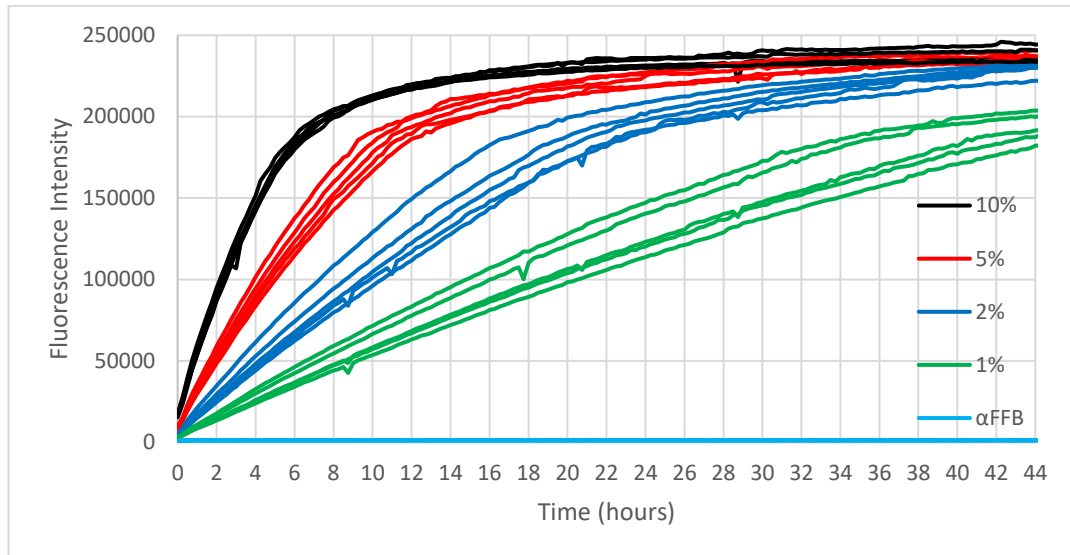


**Figure 3.17- Effect of varying  $\alpha$ -synuclein seed monomeric percentage on fibril formation.** (Top) ThT fluorescence curves showing the effects of varying  $\alpha$ -synuclein seed concentration on fibril formation and elongation as well as the same curves after being normalised (Bottom). Growth was seeded by the addition of  $10\mu\text{M}$  seeds with varying volume to make the desired ratio of seeds to monomeric protein, total volume is the same. Repeats were made of the  $\alpha$ FFB control (cyan) as well as seeds with ratios of 10% (black), 5% (red), 2% (blue) and 1% (green).

### 3.2.5 Time-dependent imaging assay

Given the results of the seeded assay in 3.2.4,  $\alpha$ -synuclein can be grown in comparable conditions and concentrations to Sup35NM. The chosen concentration of monomer of 10 $\mu$ M works for both systems and seeding can be used to completely end the lag phase and start the elongation phase. Together, these allowed the elongation rate of the two systems to be compared via a time-dependent assay, with a time frame of 10 minutes. However, the fibrils of  $\alpha$ -synuclein fragment at a much lower rate than those of Sup35NM, leading to seed production requiring 5120 seconds of sonication compared to the 320 seconds the Sup35NM fibrils needed. Due to the low concentration of particles when the  $\alpha$ -synuclein particles are diluted to seeding concentrations, an increased monomeric ratio of 5% seeds was chosen to allow an increased number of particles to be imaged at a time. While 10% would have potentially been possible for  $\alpha$ -synuclein, 5% was determined to be close to or above the limit for maximum effect of seeding for Sup35NM. Also due to Sup35NM having a much higher particle density at this concentration it required dilution to enable imaging, which is why this was the condition used in 3.1.5.

The results of using the seeds produced during the fragmentation assay in 3.2.3 and the conditions specified above are shown in Fig 3.18. Any elongation that occurred in the elongation only sample, was to a very low extent, with the majority of the particles being similar to the sizes of the starting seeds or slightly larger. To show elongation was occurring over time, another image of the same sample was produced 15 hours after seeding, which was suggested to be the beginning of the plateau phase by Fig 3.17. In this case fibrils had formed, although of a shorter length

than the *de novo* formed fibrils with lengths similar to the Sup35NM fibrils after 10 minutes. The addition of fragmentation had little effect in the first 10 minutes due to the low rate of increase in fibril yield, with the particles remaining a similar size to those produced in the elongation only assay

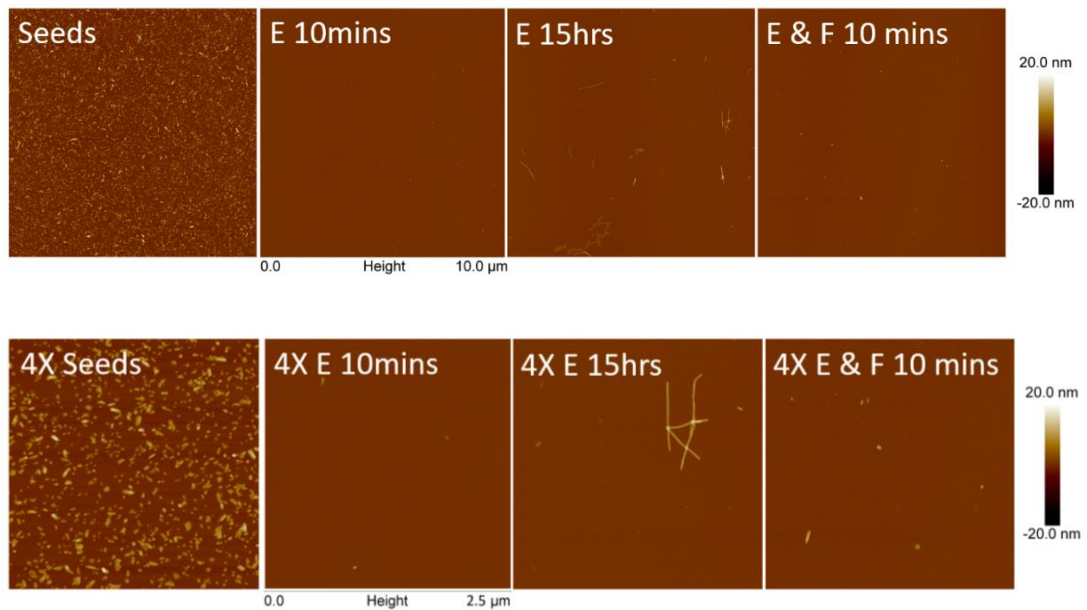


**Figure 3.18-  $\alpha$ -synuclein time-dependent elongation assay.** Series of AFM images showing  $\alpha$ -synuclein G1 seeds at different timepoints. The seeds were prepared for AFM imaging prior to addition of monomer and the elongation (E) and elongation and fragmentation (E & F) were diluted and deposited onto the mica 5 minutes after the seeds were added to the monomer and were washed 5 minutes later. Both elongation only samples (E) were left undisturbed during the 10 minutes and 15 hours respectively while the E & F sample was sonicated for a 1 second pulse every 30 seconds (29 seconds of rest) prior to deposition. The top series of images are  $10\mu\text{m} \times 10\mu\text{m}$  at a resolution of 2048, the scale bar shows this size and the height bar shows a range of 20nm from -10nm to +10nm in relation to the mica surface. The bottom series are a 4x magnification of the top series, giving sizes of  $2.5\mu\text{m} \times 2.5\mu\text{m}$  at a resolution of 512 x 512.



### 3.3 Fibril morphology

#### 3.3.1 Fibril width

During image collection it was observed that there were various difference in the morphology shown by the different fibrils generated. This was not just between Sup35NM and  $\alpha$ -synuclein, but within samples themselves.

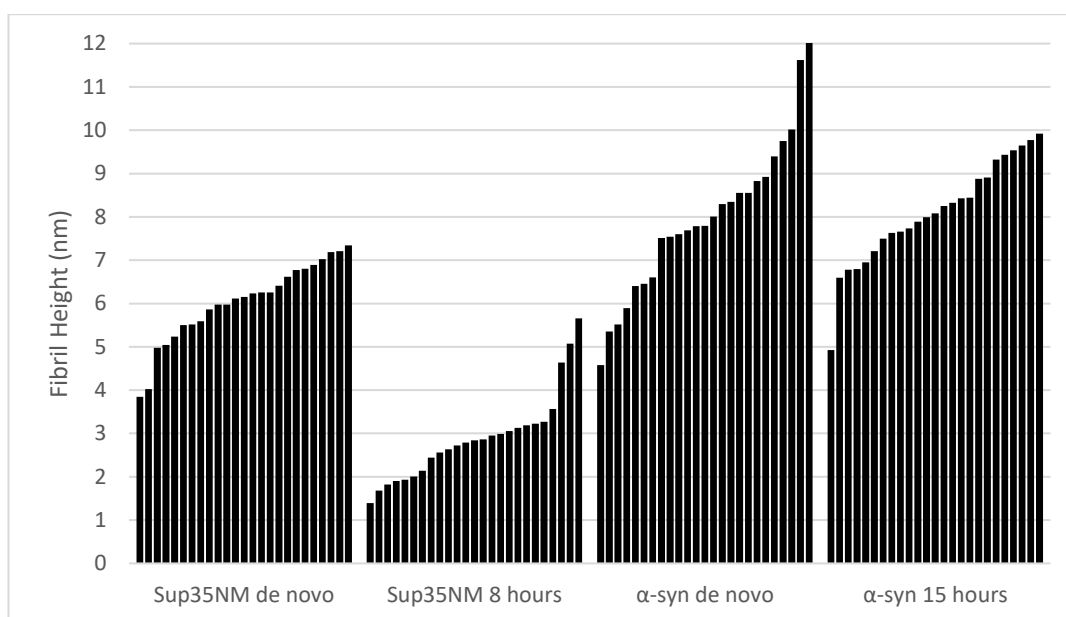


**Figure 3.19- Comparison of Sup35NM and  $\alpha$ -synuclein fibril widths.** AFM images Bar graph showing the measured heights of 10 repeats of fibrils from samples of interest. The images the data was taken from were: Fig 3.4 left (Sup35NM de novo); Fig 3.9 8hrs bottom (Sup35NM Seeded 8 hrs); Fig 3.15 left ( $\alpha$ -synuclein de novo); Fig 3.18 E 15hrs ( $\alpha$ -synuclein Seeded 15hrs). Note the final point of  $\alpha$ -syn de novo is  $\sim 25$ nm and is cut off to increase the visibility of the other values.

One such feature that was observed to vary was the width of the fibrils, leading to the analysis of this. Samples of the plateaued *de novo* fibrils and fibrils at the start of the plateau phase for G2 were chosen and 25 fibrils were randomly selected from each of these, with their measured heights (and widths) being compiled in Fig 3.19.

Examples of sections taken to measure widths are shown in Appendix 3. For Sup35NM *de novo*, nearly all samples fitted within a range of 5-7.5nm while in the G2 sample collected 8 hours after seeding only 3 of the samples collected were in a similar range to this, in a range of 4.5-5.5nm, with the other 23 laying in the range of 1-3.5nm. This lower band is significantly lower than those of the *de novo*, with the majority being 2-3 times less.

In comparison, for  $\alpha$ -synuclein the trend seen in Sup35NM was reversed. Nearly all fibrils chosen for the G2 15 hours sample were in the upper band of 6.5-10nm. In the *de novo*, while the upper band is still prevalent with approximately two thirds laying within it, there are significantly more of the lower band of 4.5-6.5nm. Two of the fibrils were outside this range with one having a width of approximately 11.5nm, making it only slightly wider than normal. The other however is  $\sim$ 25nm (limit of 12 shown in graph) and appears to consist of fibrils bundling together.

While upper and lower bands are suggested to be present in both samples of each system, this trend was reversed with the upper sample dominating Sup35NM *de novo* and  $\alpha$ -synuclein G2 15 hours, and the lower band having an increased presence in  $\alpha$ -synuclein *de novo* and Sup35NM G2 8 hours.

### 3.3.2 Morphology observations

Many observations on characteristics of the fibrils of the two systems can be made from the images produced during the refinement of the TDA. It was noted that while fibril lengths vary drastically across every sample, generally the fibrils formed by

Sup35NM were 1-5 $\mu$ m in length for the *de novo* in the majority of samples. It was however not uncommon to see samples where every fibril is of a length larger than the size of the sample are, which was especially true for the G2 fibrils in the elongation and early plateau phase. This suggests that a length of over 10 $\mu$ m is a common occurrence. However, this high number of increased length fibrils appeared to decrease over time as the fibrils started to fragment (see appendix 4). For  $\alpha$ -synuclein on the other hand lengths were typically less than 3 $\mu$ m with the majority being about 1.5 $\mu$ m. This was not always the case as there are some cases of longer fibrils appearing, but these appeared very infrequently in the samples (see appendix 5.).

Twists are easily visible in certain Sup35NM samples, an example of which is highlighted in appendix 6. In contrast, any twisting in  $\alpha$ -synuclein fibrils was less obvious but there were a few instances with potential twisting (Fig 3.15 right). Alternatively this could be an effect of the fibrils bundling together. The  $\alpha$ -synuclein fibrils also appeared to be more rigid than those of Sup35NM, which seemed to be significantly more flexible. Sup35NM fibrils also form large networks unlike  $\alpha$ -synuclein which appears to prefer bundling, which many of its fibrils are in some form of as can be seen in figures 3.1 and 3.15, as well as appendices 1, 4 and 5.

## 4. Discussion

### 4.1 *De novo* growth

*De novo* growth of amyloid varies dramatically not just between different protein systems but also within a single one depending on the conditions used, such as salt concentrations and addition of shaking. This leads to slight changes in conditions having large effects on an amyloid's life cycle, especially the lag phase. In this study, the main factor explored in relation to this was concentration of starting monomer, leading to lag phases for Sup35NM ranging from 1 hour to 6 hours for 20 $\mu$ M to 5 $\mu$ M respectively. However, under different conditions such as those employed by Kinoshita et al., (2017), the lag phase of even 5 $\mu$ M could be reduced to a time of 1 hour. The change in conditions employed here was increasing the NaCl concentration from 50mM to 100mM and the addition of mechanical perturbation by a stirrer bar rotating at a rate of 800rpm. These conditions also had the effect of reducing the elongation phase, potentially by the increased numbers of primary nuclei being generated by the salt as well as allowing fragmentation to occur, increasing the rate further. This shows that to allow comparisons of ThT fluorescence curves to be made, as many of the conditions as possible should be kept the same, as each one can have a significant effect.

$\alpha$ -synuclein only formed *de novo* fibrils after a two week incubation period under conditions of 180rpm shaking, increased concentrations in comparison to Sup35NM (60 $\mu$ M vs 10 $\mu$ M), increased temperature (37°C vs 30°C) and significantly increased salt concentrations (25mM PO<sub>4</sub> and 150mM NaCl vs 20mM PO<sub>4</sub> and 50mM NaCl). The increase in these conditions suggests that formation of primary nuclei occurs less

readily and takes a lot longer for  $\alpha$ -Synuclein in comparison to Sup35NM. Attempts at forming *de novo* fibrils in conditions more comparable to those used for Sup35NM were unsuccessful. Due to Sup35NM's functional role as a prion it could be suggested that it has been evolutionarily optimised to more readily aggregate than the disease associated  $\alpha$ -synuclein. Like with Sup35NM, changing the conditions can allow a reduction in  $\alpha$ -synuclein's lag phase to within a range of 20-40 hours. The conditions employed in one such case (Wördehoff and Hoyer, 2018) are somewhat similar to those used here, with concentrations of PO<sub>4</sub> at 25mM and 100mM Cl but with alterations in the perturbation method to non-continuous shaking but with a higher speed being used of 400rpm instead of 180rpm.

#### 4.2 Seeded growth

Through the use of seeding, the lag phases of both systems explored were eliminated completely. While the initial seed formation methodology was revised for the later assays it was useful in producing ranges of seeds to use later on as well as highlighting issues that needed to be dealt with before elongation could be measured. Using a fixed seed concentration and altering monomeric concentration (Fig 3.7) allowed comparisons to be drawn directly between seeded and unseeded growth. The result of this assay was that addition of seeds allowed the ThT fluorescence curve to behave similar to those of the *de novo* assay (Fig 3.3) with the only exception being the removal of the lag phase. This suggests that that is the only effect of adding seeds in this manner. Having seeds with some variation in their length potentially mimics a *de novo* system better than those of a close size would as primary nuclei would form at

different times, leading to some variation in the length of fibrils they form. Maintaining a single monomeric concentration whilst altering the concentration of seeds (Fig 3.8) allowed the effect of seeds on the initial rate to be shown, and that increasing the concentration of seeds reduces the lag phase until it was removed. This suggested a minimum concentration of seeds that was used for later seeding assays. It also gave some level of control over the length of the elongation phase as increasing the initial rate allowed the final yield to be achieved faster. This information was then used to perform the first trials of measuring the elongation rate of Sup35NM over time and hence identify a timeframe suited to this.

Once the revised methodology of seed formation was in place and seeds had been generated for both Sup35NM and  $\alpha$ -synuclein, finding a final ratio of seeds to monomeric protein was required, in order to allow the final elongation assay to be performed. In tandem with early attempts at the elongation assay, the final monomeric ratio of 5% seeds was chosen due to the low size and particle count of  $\alpha$ -synuclein as well as the fact the growth assays had shown this to be a suitable percentage for growth of both systems. This was because it eliminated the lag phase completely, while not over saturating the sample so that monomer becomes rate limiting within the time frame that was measured. As this was a limitation caused by  $\alpha$ -synuclein, it could not be reduced, leading to some modifications of the Sup35NM imaging conditions, due to its high size and particle number. Seeding the growth of the systems also allowed the differences in their elongation phases to be shown. While Sup35NM's elongation phase usually lasted a maximum of 7 hours, with it potentially dropping to under 2 hours at high seed percentages,  $\alpha$ -synuclein's lasted

significantly longer at a minimum of 7 or 8 hours at high seed percentages, with it becoming even longer for the lower percentages.

#### 4.3 Fragmentation and stability

The stability of the fibrils and hence their tendency to fragment was analysed through mechanical perturbation via sonication at a frequency of 20kHz and an amplitude of 20% for exponentially increasing periods of time. This was to control the fragmentation so that it could be compared between the systems. Looking at the fragmentation series for Sup35NM (Fig 3.6) and  $\alpha$ -synuclein (Fig 3.16), the difference in rate of their breakdown was immediately apparent. Sup35NM started as significantly larger fibrils that are converted into the smallest size of particle after only 320 seconds of sonication, while  $\alpha$ -synuclein started as smaller fibrils that take 5120 seconds to reach a similar size. This immediately suggests that  $\alpha$ -synuclein fibrils are likely more stable than those of Sup35NM and hence Sup35.

There are two explanations for stability based on the functions of the systems. The first is disease association vs functionality, a possibility would be that functional amyloid would be more stable than disease associated ones. This is due to the fact that functional amyloid have purposes that require a stable form such as Curli in biofilms and for storage of hormones and the loss of this would lead to a decrease in their functionality. This could also lead to an increase in oligomeric species or increase the number of fibrils leading to potential negative effects on a cell's proteostasis. The second aspect to be considered is the matter of their transmissibility.  $\alpha$ -synuclein is a prion-like system, with the potential to be

transferred into neighbouring cells, while Sup35 is a prion, meaning it will be highly transmissible. As suggested by the potential rules of what makes a prion transmissible (see 1.1.7), a high fragmentation rate is important to maximise the number of potential seeds that can be generated. Sup35 is actually a functional prion, where the transmissible aspect of a prion is required as part of its function, meaning that its functionality would further decrease this stability rather than increasing like amyloid with structural or storage roles, meaning that it being functional also may play a part in lowering stability. On the other hand,  $\alpha$ -synuclein is a disease-associated prion-like system. Its biological role is not to act as a prion and potentially not even to form an amyloid, which could promote selection for its stability in amyloid forms to be raised once they have formed to prevent its propagation. These factors in combination could be one potential reason as to why the fragmentation rates of these two systems are so dramatically distinct from each other, but it does not explain how this is physically achieved.

#### 4.4 Elongation and growth

Apart from fragmentation, the other main aim of this study was the characterisation of the growth of fibrils. The resulting method for this was to use AFM images to compare the seeds generated prior to addition of monomeric protein and then to compare it to those seeds after supplying them with monomer for a short period of time. This allowed the initial elongation rate of the seeds, and hence the system, to be assessed. Due to prior tests using Sup35NM a suitably low time of 10 minutes was chosen as the timepoint after which to image the effect of combine the seeds and



monomers (Fig 3.11). Even after a relatively short time period fibrils of  $1\mu\text{M}$  in length and above can be seen, assuming the point of increased height is the seed the fibrils are originating from. This point of increased height is likely to be multiple seeds that have aggregated together before or potentially during elongation. Multiple fibrils resulting from a single of these origins supports this. In contrast to the definite growth shown by Sup35NM, the seeds of  $\alpha$ -synuclein are approximately the same size they were prior to the addition of monomer. This suggests their rate of elongation is very low or that elongation has not started yet. The same sample was left 15 hours, which would place the sample close to the end of the elongation phase according to previous results (see Fig 3.17). Elongation has definitely occurred at this point, but the fibrils are still shorter than those produced by Sup35NM after 10 minutes. These two results together show that Sup35NM, and likely Sup35 as well, elongates at a significantly higher rate than  $\alpha$ -synuclein.

This result of Sup35NM having an increased rate of elongation is likely due to similar reasons for the differences in fragmentation rate mentioned in 4.4. The potential rules that determine if a protein forms a prion comes into play here as well. A functional prion will have been selected to rapidly build up a large amount of aggregated material once its fragments come into contact with a new cell, allowing the prion phenotype to rapidly come into effect as the protein is sequestered into the fibrils. These two characteristics will combine to make fibrils that elongate quickly whilst also breaking into potential seeds rapidly to help spread the phenotype as well as allow aggregate yield to grow exponentially within a cell.  $\alpha$ -synuclein in contrast is a disease associated prion-like amyloid, meaning it will be biologically unfavoured for it to rapidly form, grow and transfer. This could potentially mean the reverse is

true for this system, that it is potentially selected to elongate slowly and remain stable to prevent seeding further growth. Interplay between fragmentation and elongation led to the elongation and fragmentation assays, where the elongation assay was repeated but with the addition of mechanical perturbation until deposition of the sample at 5 minutes. As could be expected with  $\alpha$ -synuclein, the low elongation rate meant there was no new material to break into seeds and the seeds that were already present are of a size that appears to be relatively stable, even in comparison to the starting fibrils. This is likely due to them becoming less likely to break further as they get smaller. For Sup35NM the addition of fragmentation led to a significantly higher yield of aggregated material. Likely due to the high elongation rate rapidly producing more material for seeds to be formed from, which in turn elongate and start an exponential growth cycle. While this level of perturbation is unlikely *in vivo*, whether it be by chaperones or by some mechanical process, fragmentation will be occurring alongside elongation, showing how rapidly a prion system can increase its yield of aggregated material.

#### 4.5 Morphology

A point of interest arose when imaging Sup35NM fibrils during early stages of the plateau phase (Fig 3.9). Two distinct widths of fibril appeared to be present and with further investigation (Fig 3.19), this was found to not be the case in the *de novo* fibrils that had fully entered the plateau phase. A possible explanation for having two different widths of fibril at this timepoint but not later could be that they only exist in this form during elongation. Which could be a hint towards the mechanism that

elongation occurs by. Having these thinner fibrils present during elongation could suggest that elongation occurs in protofilaments prior to them aggregating together to form “mature” fibrils. The variations in lengths of these “mature” fibrils suggest either some form of fragmentation is occurring or that elongation is also occurring in fibrils of this form as well. This potentially could suggest both mechanisms are at play at the same time. Interestingly, an almost reversed trend occurred in the  $\alpha$ -synuclein fibrils, with the lower band containing an increased proportion of the fibrils during the plateau phase, approximately one third, of the *de novo* which fell dramatically by the early plateau phase of G2 fibrils, where the lower band dropped to just one fibril out of the 25 sampled. This could suggest that for  $\alpha$ -synuclein, the two widths are actually indicative of different polymorphs of fibril rather than being caused by elongation mechanisms.

The average fibril width of Sup35NM was also found to be lower than that of  $\alpha$ -synuclein, at an approximate range of 1-5.5nm in comparison to 4.5-10nm, when both bands of each are included. This is spite of  $\alpha$ -synuclein being a smaller protein at ~14.5kDa to ~30kDa for Sup35NM. This high width of fibrils from a smaller protein could go some way to explain the lowered elongation rate, as significantly more monomers may be required to elongate the same distance as a few monomers of Sup35NM. This increased width may potentially play a part in the fragmentation rate as well as this increased width could be one of the factors contributing to the high stability of the fibrils.

It was also observed that the fibrils of Sup35NM tend to be longer at all stages with the majority of the *de novo* fibrils being a length of 1-5 $\mu$ m, while those of  $\alpha$ -synuclein

were usually less than 3 $\mu$ m. While this is not true for all of the fibrils the systems produced, with large numbers of Sup35NM fibrils reaching lengths of over 10 $\mu$ m, as well as a few  $\alpha$ -synuclein, the majority of the fibrils seem to lay in these ranges. The way the fibrils themselves behave also varied between the two systems. Sup35NM formed large networks of criss-crossing fibrils, while those of  $\alpha$ -synuclein formed relatively long and thick bundles. These bundle structures have been shown previously and some of these have been suggested to be a ribbon like structure (Makky et al., 2016). There is potentially twisting shown in Fig 3.15 (right) that is also similar to those shown by the suggested ribbon structures, but this could also just be caused by fibril overlap in the bundles. The twisting shown by Sup35NM however is of a much lower periodicity and appears to be more consistent, making it relatively easier to be certain of.

## 5. Conclusions and Further research

**Table 5.1- Table summarising key results found for Sup35NM and  $\alpha$ -synuclein.** Generations 1 and 2 are separated for each because of the effects of seeding. The results summarised are: typical length range of fibrils (some fibrils of each system are outside this range); typical width; if the fibrils display twisting; the length of their lag phase; length of their elongation phase; time frame to fragment with a set amplitude; their rate of elongation comparatively.

	$\alpha$ -synuclein G1	$\alpha$ -synuclein G2	Sup35NM G1	Sup35NM G2
<b>Length</b>	1-5 $\mu$ m	10 $\mu$ m	<3 $\mu$ m	<3 $\mu$ m
<b>Width</b>	4.5-10nm	4.5-10nm	1-5.5nm	1-5.5nm
<b>Twists</b>	Unsure	Unsure	Yes	Yes
<b>Lag phase</b>	~2 weeks	0 secs	1-3 hours	0 secs
<b>Elongation phase</b>	-	8-40 hours	5-7 hours	2-5 hours
<b>Fragmentation time</b>	5120 secs	-	320secs	-
<b>Elongation rate</b>	-	Very low	-	High

Amyloid and prions are a research area that has only been growing in size in recent years, due to their association with various devastating diseases such as Alzheimer's and Parkinson's diseases. This is further compounded by the discovery of functional amyloid, those that will have an intended biological function as well as research into potential uses of amyloid as nano materials. Even with the rapid growth of this field,

there are many questions that need to be answered. One such question led to the main subject of this study, which was to establish how the varying characteristics of different systems interplays with their life cycles. The main characteristics of interest were if they are prions or prion-like amyloid as well as if they are biologically functional or disease associated. This subject led to the selection of two models of amyloid forming protein in Sup35NM and  $\alpha$ -synuclein to directly compare the changes in these characteristics. Sup35NM is a functional prion while  $\alpha$ -synuclein has been suggested to be a prion-like amyloid that is associated with Parkinson's disease.

Before any work could be made with the fibrillar forms of the proteins, first the protein itself needed to be prepared. The monomeric protein of each was produced by inducing expression in *E. coli* modified for production of these respectively. Once expressed the protein required purification, which finally led to the production of the protein pools of each. Once the protein had been confirmed to be purified, via gels, the next stage was to find conditions that can be used to form amyloid fibrils in a *de novo* fashion. After fibrils were attained using these conditions, their stability was tested by inducing the fibrils' fragmentation through use of sonication. This process of fragmentation also served the additional purpose of generating seeds that would allow for generation 2 seeded assays. In these seeded assays various conditions were tested to find those that not only allowed the visualisation of the elongation of fibrils of each systems, but also so that the two systems could be compared. This eventually led to conditions under which the elongation rate could be shown as well as a timeframe over which to allow this to take place.

This all led to the final results of Sup35NM being suggested to elongate and fragment at a higher rate than  $\alpha$ -synuclein, a summary of this and other results can be found in table 5.1. One proposed reason for this is that due to Sup35's role as a functional prion, it will have been selected to produce a high aggregate yield quickly, while also producing high numbers of small seeds, that can be transmissible. This would allow a rapid shift in phenotype as the monomeric form of the protein will be rapidly sequestered from the protein pool, by the rapidly growing aggregates, while also allowing propagation to occur easier, further spreading the phenotype. In comparison there is no such drive for  $\alpha$ -synuclein to have these properties due to its disease association and these characteristics could even potentially be negatively favoured due to their detriment to the host, potentially leading to it having a life cycle that reflects this. Also, while there already has been a high amount of research into  $\alpha$ -synuclein, its biological function is still partially unknown, meaning that associating the life cycle to its function is only based on the current knowledge, which will change. This could provide more insight into the results attained here, once more is known.

The most important direction for future work would be to attempt comparisons with more systems, as would allow more generalised rules to be identified than is possible in just two systems, while also increasing their validity. Direct comparisons between functional and disease associated prions could be used to explore how biological adaptations affect their characteristics and comparing functional or disease associated prions, prion-like and amyloid to each other would provide more information about how transmissibility arise. Also, a comparison between Sup35NM and Sup35 itself would also be interesting as would show what effects the C terminal domain has on the protein.

Another piece of important future work would be to use tracing software to quantify the rates of elongation and fragmentation, as would allow comparisons to be significantly improved especially for when the results are less clear cut and when more systems are introduced. This could also be adapted to attempt to find these rates in terms of monomers, as the two systems may actually have more similar (or more different) rates, when thought of in terms of monomers rather than length. This would also allow width of fibrils to be taken into account as thinner fibrils and thicker fibrils may elongate at a similar rate in terms of length while increasing in terms of aggregate yield at very different speeds.

Effects of varying the conditions used for the formation of fibrils would also be an important avenue of research, such as different salt concentrations and temperatures. In this study the main focus was on using sonication as a form of mechanical perturbation, but there are other types of this such as shaking and stirring that may yield different results as the properties of fibrils may make them more susceptible to some as opposed to others. For example, mechanical perturbation of Sup35NM led to a rapid fragmentation of fibrils when caused by sonication, but even after extended periods of shaking it was suggested that similar fragmentation did not occur (see Appendix 7.).

Increasing the generation of fibrils from G1 to G2 has an obvious effect on their growth due to the addition of seeding, but repeated seeding may lead to its improvement. For example, increasing the generation of fibril from G2 to G3 had a significant effect on the starting growth rate on the fibrils produced. This may be due to slower polymorphs being selected out with each generation, which may mean the



optimum rate of each system is significantly different to those shown by the first two generations of fibrils.

## 6. References

Aguzzi, A., Heikenwalder, M. and Polymenidou, M. (2007). Insights into prion strains and neurotoxicity. *Nature Reviews Molecular Cell Biology*, 8(7), pp.552-561.

Ahmad, A., Millett, I., Doniach, S., Uversky, V. and Fink, A. (2003). Partially folded intermediates in insulin fibrillation. *Biochemistry*, 42(39), pp.11404-11416.

Andersen, C., Yagi, H., Manno, M., Martorana, V., Ban, T., Christiansen, G., Otzen, D., Goto, Y. and Rischel, C. (2009). Branching in amyloid fibril growth. *Biophysical Journal*, 96(4), pp.1529-1536.

Arosio, P., Knowles, T. and Linse, S. (2015). On the lag phase in amyloid fibril formation. *Physical Chemistry Chemical Physics*, 17(12), pp.7606-7618.

Astbury, W., Dickinson, S. and Bailey, K. (1935). The X-ray interpretation of denaturation and the structure of the seed globulins. *Biochemical Journal*, 29(10), pp.2351-2360.1.

Balch, W., Morimoto, R., Dillin, A. and Kelly, J. (2008). Adapting proteostasis for disease intervention. *Science*, 319(5865), pp.916-919.

Ban, T., Hamada, D., Hasegawa, K., Naiki, H. and Goto, Y. (2003). Direct observation of amyloid fibril growth monitored by thioflavin T fluorescence. *Journal of Biological Chemistry*, 278(19), pp.16462-16465.

Bucciantini, M., Giannoni, E., Chiti, F., Baroni, F., Formigli, L., Zurdo, J., Taddei, N., Ramponi, G., Dobson, C. and Stefani, M. (2002). Inherent toxicity of aggregates implies a common mechanism for protein misfolding diseases. *Nature*, 416(6880), pp.507-511.

Caughey, B. and Lansbury, P. (2003). Protofibrils, pores, fibrils and neurodegeneration: separating the responsible protein aggregates from the innocent bystanders. *Annual Review of Neuroscience*, 26(1), pp.267-298.

Caughey, B., Baron, G., Chesebro, B. and Jeffrey, M. (2009). Getting a grip on prions: oligomers, amyloids, and pathological membrane interactions. *Annual Review of Biochemistry*, 78(1), pp.177-204.

Chapman, M. R., Robinson, L. S., Pinkner, J. S., Roth, R., Heuser, J., Hammar, M., Normark, S., ... Hultgren, S. J. (2002). Role of *Escherichia coli* curli operons in directing amyloid fiber formation. *Science (New York, N.Y.)*, 295(5556), 851-5.

Cohen, S., Vendruscolo, M., Dobson, C. and Knowles, T. (2012). From macroscopic measurements to microscopic mechanisms of protein aggregation. *Journal of Molecular Biology*, 421(2-3), pp.160-171.

Collins, S., Douglass, A., Vale, R. and Weissman, J. (2004). Mechanism of prion propagation: amyloid growth occurs by monomer addition. *PLoS Biology*, 2(10), p.e321.

Congdon, E. and Duff, K. (2008). Is tau aggregation toxic or protective?. *Journal of Alzheimer's Disease*, 14(4), pp.453-457.

Coustou, V., Deleu, C., Saupe, S. and Begueret, J. (1997). The protein product of the het-s heterokaryon incompatibility gene of the fungus *Podospora anserina* behaves as a prion analog. *Proceedings of the National Academy of Sciences*, 94(18), pp.9773-9778.

- Cox, B. (1994). Cytoplasmic inheritance: prion-like factors in yeast. *Current Biology*, 4(8), pp.744-748.
- Derdowski, A., Sindi, S., Klaipe, C., DiSalvo, S. and Serio, T. (2010). A size threshold limits prion transmission and establishes phenotypic diversity. *Science*, 330(6004), pp.680-683.
- Dobson, C. (2003). Protein folding and misfolding. *Nature*, 426(6968), pp.884-890.
- Dobson, C. (2017). The amyloid phenomenon and its links with human disease. *Cold Spring Harbor Perspectives in Biology*, 9(6), p.a023648.
- Eisenberg, D. and Jucker, M. (2012). The amyloid state of proteins in human diseases. *Cell*, 148(6), pp.1188-1203.
- Fernández, M., Batlle, C., Gil-García, M. and Ventura, S. (2017). Amyloid cores in prion domains: key regulators for prion conformational conversion. *Prion*, 11(1), pp.31-39.
- Fowler, D., Koulov, A., Alory-Jost, C., Marks, M., Balch, W. and Kelly, J. (2005). Functional amyloid formation within mammalian tissue. *PLoS Biology*, 4(1), p.e6.
- Fowler, D., Koulov, A., Balch, W. and Kelly, J. (2007). Functional amyloid – from bacteria to humans. *Trends in Biochemical Sciences*, 32(5), pp.217-224.
- Giasson, B., Murray, I., Trojanowski, J. and Lee, V. (2000). A hydrophobic stretch of 12 amino acid residues in the middle of  $\alpha$ -Synuclein is essential for filament assembly. *Journal of Biological Chemistry*, 276(4), pp.2380-2386.

Graña-Montes, R., Marinelli, P., Reverter, D. and Ventura, S. (2014). N-terminal protein tails act as aggregation protective entropic bristles: The SUMO case. *Biomacromolecules*, 15(4), pp.1194-1203.

Greenwald, J. and Riek, R. (2010). Biology of amyloid: structure, function, and regulation. *Structure*, 18(10), pp.1244-1260.

Harper, J. and Lansbury, P. (1997). Models of amyloid seeding in Alzheimer's disease and Scrapie: mechanistic truths and physiological consequences of the time-dependent solubility of amyloid proteins. *Annual Review of Biochemistry*, 66(1), pp.385-407.

Hofmann, J. and Vorberg, I. (2013). Life cycle of cytosolic prions. *Prion*, 7(5), pp.369-377.

Hu, K., McGlinchey, R., Wickner, R. and Tycko, R. (2011). Segmental polymorphism in a functional amyloid. *Biophysical Journal*, 101(9), pp.2242-2250.

Iadanza, M., Jackson, M., Hewitt, E., Ranson, N. and Radford, S. (2018). A new era for understanding amyloid structures and disease. *Nature Reviews Molecular Cell Biology*.

Irvine, G., El-Agnaf, O., Shankar, G. and Walsh, D. (2008). Protein aggregation in the brain: the molecular basis for Alzheimer's and Parkinson's diseases. *Molecular Medicine*, 14(7-8), p.1.

Jarrett, J. and Lansbury, P. (1993). Seeding "one-dimensional crystallization" of amyloid: a pathogenic mechanism in Alzheimer's disease and scrapie?. *Cell*, 73(6), pp.1055-1058.

Jaunmuktane, Z., Mead, S., Ellis, M., Wadsworth, J., Nicoll, A., Kenny, J., Launchbury, F., Linehan, J., Richard-Loendt, A., Walker, A., Rudge, P., Collinge, J. and Brandner, S. (2015). Evidence for human transmission of amyloid- $\beta$  pathology and cerebral amyloid angiopathy. *Nature*, 525(7568), pp.247-250.

Jeong, J., Ansaloni, A., Mezzenga, R., Lashuel, H. and Dietler, G. (2013). Novel mechanistic insight into the molecular basis of amyloid polymorphism and secondary nucleation during amyloid formation. *Journal of Molecular Biology*, 425(10), pp.1765-1781.

Kaminski Schierle, G., van de Linde, S., Erdelyi, M., Esbjörner, E., Klein, T., Rees, E., Bertocini, C., Dobson, C., Sauer, M. and Kaminski, C. (2011). *In situ* measurements of the formation and morphology of intracellular  $\beta$ -amyloid fibrils by super-resolution fluorescence imaging. *Journal of the American Chemical Society*, 133(33), pp.12902-12905.

Khurana, R., Uversky, V., Nielsen, L. and Fink, A. (2001). Is congo red an amyloid-specific dye?. *Journal of Biological Chemistry*, 276(25), pp.22715-22721.

Khurana, R., Coleman, C., Ionescu-Zanetti, C., Carter, S., Krishna, V., Grover, R., Roy, R. and Singh, S. (2005). Mechanism of thioflavin T binding to amyloid fibrils. *Journal of Structural Biology*, 151(3), pp.229-238.

Kinoshita, M., Lin, Y., Nakatsuji, M., Inui, T. and Lee, Y. (2017). Kinetics and polymorphs of yeast prion Sup35NM amyloidogenesis. *International Journal of Biological Macromolecules*, 102, pp.1241-1249.

Laganowsky, A., Liu, C., Sawaya, M., Whitelegge, J., Park, J., Zhao, M., Pensalfini, A., Soriaga, A., Landau, M., Teng, P., Cascio, D., Glabe, C. and Eisenberg, D. (2012). Atomic view of a toxic amyloid small oligomer. *Science*, 335(6073), pp.1228-1231.

Linse, S. (2019). Mechanism of amyloid protein aggregation and the role of inhibitors. *Pure and Applied Chemistry*, 91(2), pp.211-229.

Liu, J., Sondheimer, N. and Lindquist, S. (2002). Changes in the middle region of Sup35 profoundly alter the nature of epigenetic inheritance for the yeast prion [PSI<sup>+</sup>]. *Proceedings of the National Academy of Sciences*, 99(Supplement 4), pp.16446-16453.

Lutter, L., Serpell, C., Tuite, M. and Xue, W. (2019). The molecular lifecycle of amyloid – mechanism of assembly, mesoscopic organisation, polymorphism, suprastructures, and biological consequences. *Biochimica et Biophysica Acta (BBA) - Proteins and Proteomics*, 1867(11), p.140257.

Maji, S., Perrin, M., Sawaya, M., Jessberger, S., Vadodaria, K., Rissman, R., Singru, P., Nilsson, K., Simon, R., Schubert, D., Eisenberg, D., Rivier, J., Sawchenko, P., Vale, W. and Riek, R. (2009). Functional amyloids as natural storage of peptide hormones in pituitary secretory granules. *Science*, 325(5938), pp.328-332.

Makky, A., Bousset, L., Polesel-Maris, J. and Melki, R. (2016). Nanomechanical properties of distinct fibrillar polymorphs of the protein  $\alpha$ -synuclein. *Scientific Reports*, 6(1).

Marchante, R., Beal, D., Koloteva-Levine, N., Purton, T., Tuite, M. and Xue, W. (2017). The physical dimensions of amyloid aggregates control their infective potential as prion particles. *eLife*, 6.

Marques, O. and Outeiro, T. (2012). Alpha-synuclein: from secretion to dysfunction and death. *Cell Death & Disease*, 3(7), pp.e350-e350.

Modler, A., Gast, K., Lutsch, G. and Damaschun, G. (2003). Assembly of amyloid protofibrils via critical oligomers—a novel pathway of amyloid formation. *Journal of Molecular Biology*, 325(1), pp.135-148.

Nelson, R., Sawaya, M., Balbirnie, M., Madsen, A., Riek, C., Grothe, R. and Eisenberg, D. (2005). Structure of the cross- $\beta$  spine of amyloid-like fibrils. *Nature*, 435(7043), pp.773-778.

Nichols, M., Moss, M., Reed, D., Lin, W., Mukhopadhyay, R., Hoh, J. and Rosenberry, T. (2002). Growth of  $\beta$ -amyloid (1–40) protofibrils by monomer elongation and lateral association. Characterization of distinct products by light scattering and atomic force microscopy†. *Biochemistry*, 41(19), pp.6115-6127.

Paravastu, A., Leapman, R., Yau, W. and Tycko, R. (2008). Molecular structural basis for polymorphism in Alzheimer's  $\beta$ -amyloid fibrils. *Proceedings of the National Academy of Sciences*, 105(47), pp.18349-18354.

Polymeropoulos, M. (1997). Mutation in the  $\alpha$ -Synuclein gene identified in families with Parkinson's disease. *Science*, 276(5321), pp.2045-2047.

Prusiner, S. (1982). Novel proteinaceous infectious particles cause scrapie. *Science*, 216(4542), pp.136-144.



Prusiner, S. (1998). Nobel lecture: prions. *Proceedings of the National Academy of Sciences*, 95(23), pp.13363-13383.

Sabate, R. (2014). When amyloids become prions. *Prion*, 8(3), pp.233-239.

Sabate, R., Rousseau, F., Schymkowitz, J., Batlle, C. and Ventura, S. (2015). Amyloids or prions? That is the question. *Prion*, 9(3), pp.200-206.

Sachse, C., Fandrich, M. and Grigorieff, N. (2008). Paired  $\beta$ -sheet structure of an A (1-40) amyloid fibril revealed by electron microscopy. *Proceedings of the National Academy of Sciences*, 105(21), pp.7462-7466.

Sawaya, M., Sambashivan, S., Nelson, R., Ivanova, M., Sievers, S., Apostol, M., Thompson, M., Balbirnie, M., Wiltzius, J., McFarlane, H., Madsen, A., Riek, C. and Eisenberg, D. (2007). Atomic structures of amyloid cross- $\beta$  spines reveal varied steric zippers. *Nature*, 447(7143), pp.453-457.

Schwarzman, A., Senkevich, K., Emelyanov, A. and Pchelina, S. (2019). Prion Properties of Alpha-Synuclein. *Molecular Biology*, 53(3), pp.335-341.

Serpell, L., Berriman, J., Jakes, R., Goedert, M. and Crowther, R. (2000). Fiber diffraction of synthetic alpha-synuclein filaments shows amyloid-like cross-beta conformation. *Proceedings of the National Academy of Sciences*, 97(9), pp.4897-4902.

Shewmaker, F., McGlinchey, R., Thurber, K., McPhie, P., Dyda, F., Tycko, R. and Wickner, R. (2009). The functional curli amyloid is not based on in-register parallel  $\beta$ -sheet structure. *Journal of Biological Chemistry*, 284(37), pp.25065-25076.

Silveira, J., Raymond, G., Hughson, A., Race, R., Sim, V., Hayes, S. and Caughey, B. (2005). The most infectious prion protein particles. *Nature*, 437(7056), pp.257-261.

Sipe, J., Benson, M., Buxbaum, J., Ikeda, S., Merlini, G., Saraiva, M. and Westermark, P. (2012). Amyloid fibril protein nomenclature: 2012 recommendations from the Nomenclature Committee of the International Society of Amyloidosis. *Amyloid*, 19(4), pp.167-170.

Sipe, J. and Cohen, A. (2000). Review: History of the amyloid Fibril. *Journal of Structural Biology*, 130(2-3), pp.88-98.

Snead, D. and Eliezer, D. (2014). Alpha-Synuclein function and dysfunction on cellular membranes. *Experimental Neurobiology*, 23(4), p.292.

Sorci, M., Grassucci, R., Hahn, I., Frank, J. and Belfort, G. (2009). Time-dependent insulin oligomer reaction pathway prior to fibril formation: Cooling and seeding. *Proteins: Structure, Function, and Bioinformatics*, 77(1), pp.62-73.

Soto, C. (2012). Transmissible proteins: expanding the prion heresy. *Cell*, 149(5), pp.968-977.

Spillantini, M., Schmidt, M., Lee, V., Trojanowski, J., Jakes, R. and Goedert, M. (1997).  $\alpha$ -Synuclein in Lewy bodies. *Nature*, 388(6645), pp.839-840.

Ter-Avanesyan, M., Kushnirov, V., Dagkesamanskaya, A., Didichenko, S., Chernoff, Y., Inge-Vechtomov, S. and Smirnov, V. (1993). Deletion analysis of the SUP35 gene of the yeast *Saccharomyces cerevisiae* reveals two non-overlapping functional regions in the encoded protein. *Molecular Microbiology*, 7(5), pp.683-692.

True, H. and Lindquist, S. (2000). A yeast prion provides a mechanism for genetic variation and phenotypic diversity. *Nature*, 407(6803), pp.477-483.

Tuite, M. and Cox, B. (2006). The [PSI<sup>+</sup>] prion of yeast: A problem of inheritance. *Methods*, 39(1), pp.9-22.

Vestergaard, B., Groenning, M., Roessle, M., Kastrup, J., de Weert, M., Flink, J., Frokjaer, S., Gajhede, M. and Svergun, D. (2007). A helical structural nucleus is the primary elongating unit of insulin amyloid fibrils. *PLoS Biology*, 5(5), p.e134.

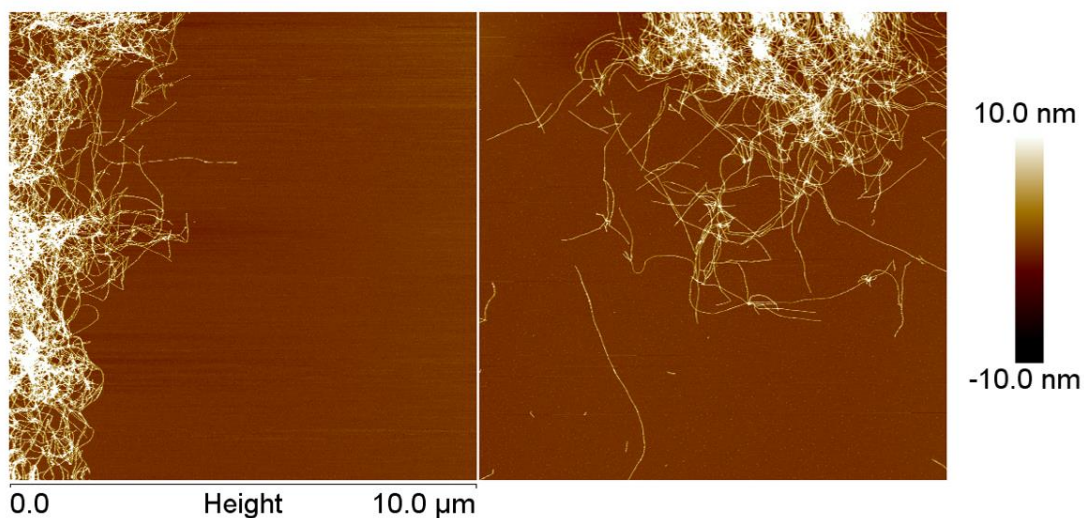
Westermarck, P. (2005). Aspects on human amyloid forms and their fibril polypeptides. *FEBS Journal*, 272(23), pp.5942-5949.

Wetzel, R. (2006). Kinetics and thermodynamics of amyloid fibril assembly. *Accounts of chemical research*, 39(9), pp.671-679.

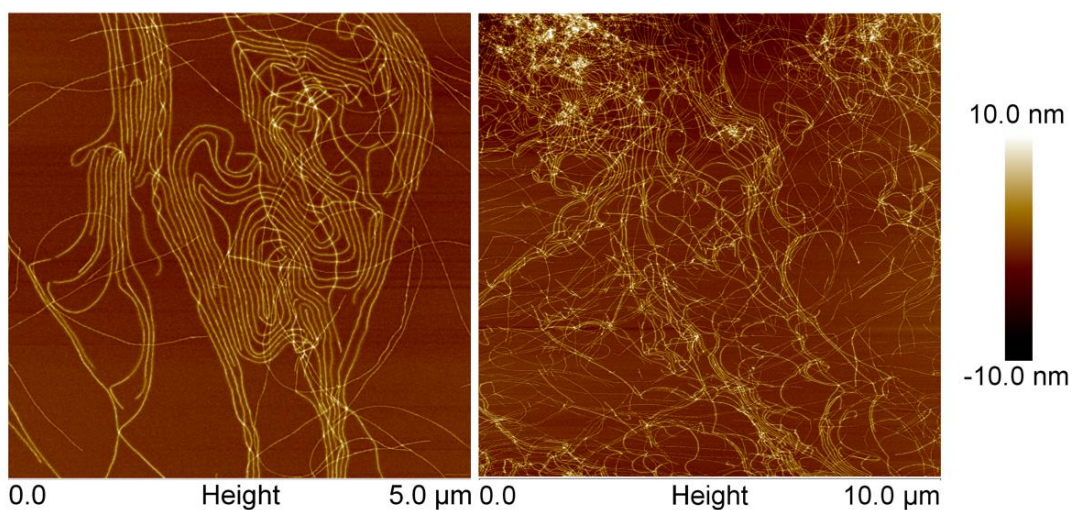
Wördehoff, M. and Hoyer, W. (2018).  $\alpha$ -Synuclein aggregation monitored by thioflavin T fluorescence assay. *Bio-protocol*, 8(14).

Xue, W., Hellewell, A., Gosal, W., Homans, S., Hewitt, E. and Radford, S. (2009). Fibril fragmentation enhances amyloid cytotoxicity. *Journal of Biological Chemistry*, 284(49), pp.34272-34282.

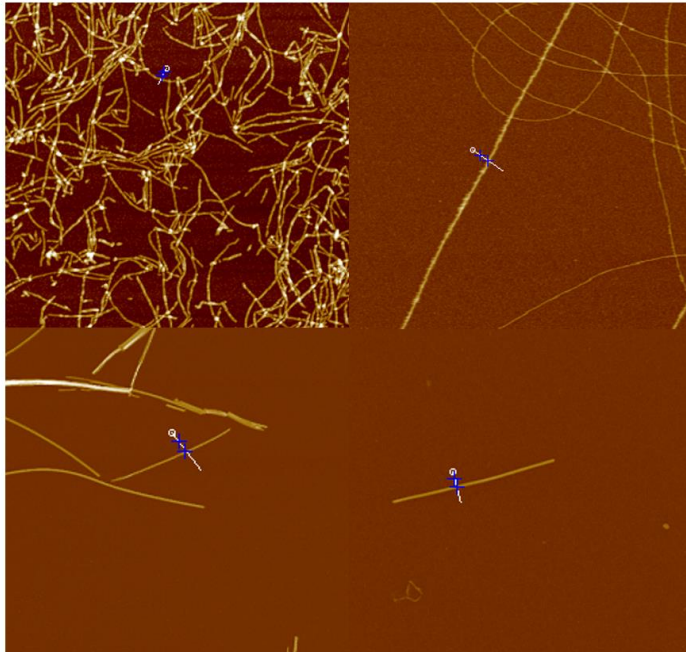
## 7. Appendices



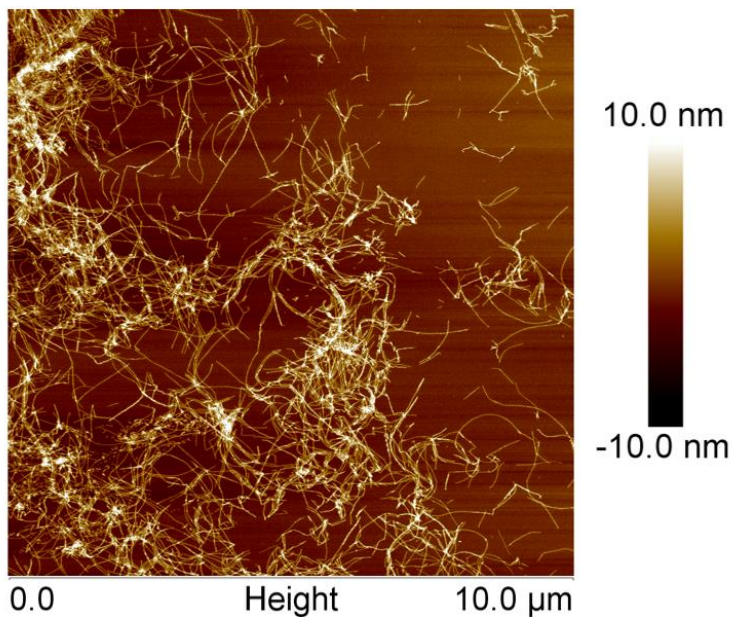
Appendix 1- AFM images of Sup35NM fibrils in the plateau phase, produced de novo in a low bind 96 well plate using a monomer concentration of  $10\mu\text{M}$ . The images are  $10\mu\text{m} \times 10\mu\text{m}$  at a resolution of  $1024 \times 1024$ , the scale bar shows this size and the height bar shows a range of 20nm from -10nm to +10nm in relation to the mica surface.



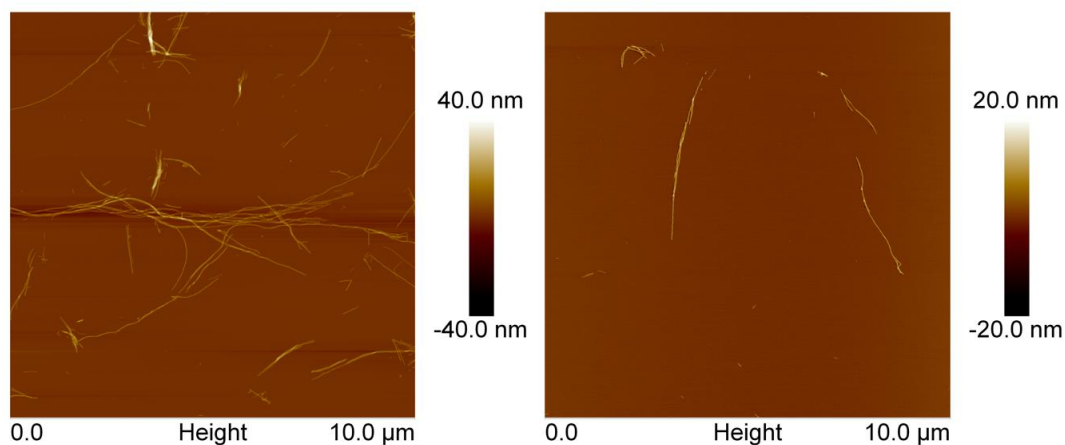
Appendix 2- AFM images of Sup35NM fibrils in the plateau phase, produced de novo in a low bind Eppendorf rotating at 30rpm, using a monomer concentration of  $10\mu\text{M}$ . The left image is  $5\mu\text{m} \times 5\mu\text{m}$  at a resolution of  $2048 \times 2048$  and the right image is  $10\mu\text{m} \times 10\mu\text{m}$  at a resolution of  $2048 \times 2048$ , the scale bar shows this size and the height bar shows a range of 20nm from -10nm to +10nm in relation to the mica surface.



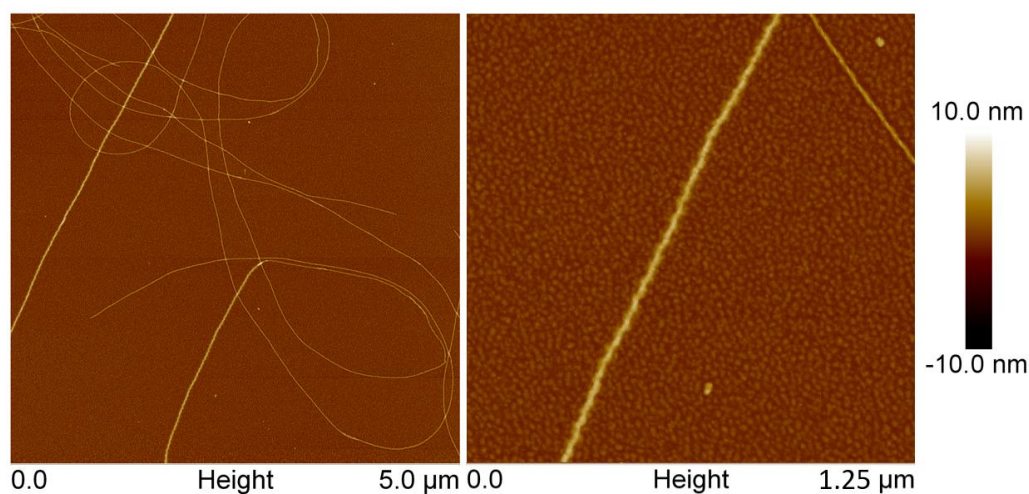
*Appendix 3- Examples of sections taken using Nanoscope Analysis to allow heights and widths of fibrils to be measured. These images are not to scale in comparison to each other.*



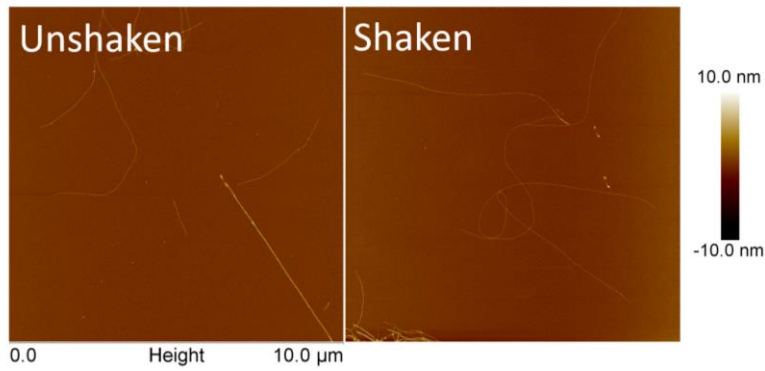
*Appendix 4- AFM images of Sup35NM fibrils 40 hours after entering the plateau phase, produced de novo in a low bind 96 well plate using a monomer concentration of 10 $\mu$ M. The image is 10 $\mu$ m x10 $\mu$ m at a resolution of 1024 x 1024, the scale bar shows this size and the height bar shows a range of 20nm from -10nm to +10nm in relation to the mica surface.*



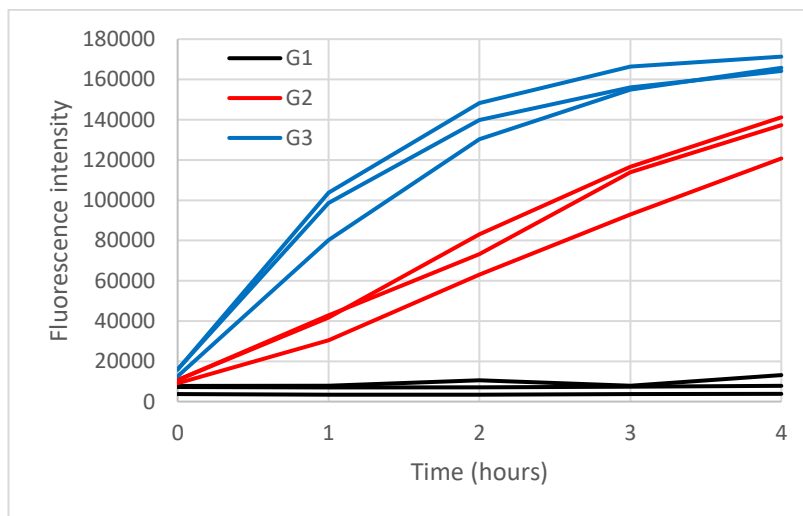
Appendix 5- AFM images of  $\alpha$ -synuclein fibrils in the plateau phase, produced de novo in a lo-bind Eppendorf shaking at 180rpm, using a monomer concentration of  $60\mu\text{M}$ . The images are  $10\mu\text{m} \times 10\mu\text{m}$  at a resolution of  $2048 \times 2048$ , the scale bar shows this size and the height bars shows ranges of  $80\text{nm}$  from  $-40\text{nm}$  to  $+40\text{nm}$  and  $40\text{nm}$  from  $-20\text{nm}$  to  $+20\text{nm}$  in relation to the mica surface for the left and right images respectively.



Appendix 6- AFM images of Sup35NM fibrils after 8 hours, produced de novo in a low bind 96 well plate, using a monomer concentration of  $10\mu\text{M}$ . The image is on the same area of the sample used in Figure 3.9, with a lower sample size allow higher magnification. The region showing twisting is shown in the right image. The left image is  $5\mu\text{m} \times 5\mu\text{m}$  at a resolution of  $2048 \times 2048$  and the right image a  $4\times$  magnification of the left giving a sample area size of  $1.25\mu\text{m} \times 1.25\mu\text{m}$  at a resolution of  $512 \times 512$ , the scale bar shows this size and the height bar shows a range of  $20\text{nm}$  from  $-10\text{nm}$  to  $+10\text{nm}$  in relation to the mica surface.



Appendix 7-- AFM images of Sup35NM fibrils in the plateau phase, produced de novo in low bind 96 well plates using a monomer concentration of  $10\mu\text{M}$ . The right sample was produced with continuous shaking while the left sample was undisturbed. The images are  $10\mu\text{m} \times 10\mu\text{m}$  at a resolution of  $1024 \times 1024$ , the scale bar shows this size and the height bar shows a range of  $20\text{nm}$  from  $-10\text{nm}$  to  $+10\text{nm}$  in relation to the mica surface.



Appendix 8-ThT fluorescence curve showing the effects of increased generation on the fibril formation and elongation of Sup35NM. Growth was seeded by the addition of  $1\mu\text{M}$  seeds produced by sonication of previous generation fibrils for 20 seconds at an amplitude of 60%. Repeats were made of G1 (Black), G2 (Red) and G3 fibrils (Blue).